UNIVERSITAT DE BARCELONA

Computational study of the emergent behavior of micro-swimmer suspensions

Francisco Alarcón Oseguera

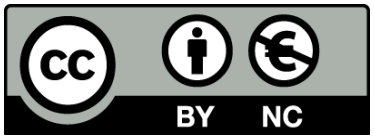

UNIVERSITAT DE BARCELONA

FACULTAT DE FÍSICA
DEPARTAMENT DE FÍSICA FONAMENTAL

MEMÒRIA DE TESI DOCTORAL PRESENTADA PER OPTAR AL TÍTOL DE DOCTOR EN FÍSICA PER LA UNIVERSITAT DE BARCELONA

COMPUTATIONAL STUDY OF THE EMERGENT BEHAVIOR OF MICRO-SWIMMER SUSPENSIONS

Francisco Alarcón Oseguera

Director y Tutor: Dr. Ignacio Pagonabarraga

Barcelona, November 2015

Programa de Doctorat en Física de la Matèria Condensada

Computational study of the emergent behavior of micro-swimmer suspensions

Tesi que presenta Francisco Alarcón Oseguera

per optar al títol de Doctor per la Universitat de Barcelona

Director de Tesi: Dr. Ignacio Pagonabarraga

Universitat de Barcelona

Departament de Física Fonamental, Facultat de Física

Whenever I found out anything remarkable, I have thought it my duty to put down my discovery on paper, so that all ingenious people might be informed thereof.

Anthonie van Leeuwenhoek, (1632 – 1723).

Contents

Outline of the Thesis

The goal of this thesis is to study by numerical simulations, the collective behavior of a model of micro-swimmers. In particular, the squirmer model, where the fluid motion is axisymmetric. Coherent structures emerge from these systems, therefore to try to understand whether coherent structures are generate by the intrinsic hydrodynamic signature of the individual squirmers or by a finite size effect is of paramount importance, we also study the influences of the geometry in the emergence of coherent structures, the direct interaction among particles, concentration, etc.

This thesis report new phases of squirmer suspensions that form a cluster distribution o even suspensions where a macroscopic cluster emerge. An important task of this thesis is to characterize these cluster phases and the morphology of the clusters in order to understand the phenomenology of the system by analogy with cluster distributions and morphological parameters of systems in equilibrium.

The Thesis is organized as follows. We first review in Chapter 1, what are the active systems and the consequence to have a set of active particles. We shall find some examples of active matter under several context. In this chapter we also explain the micro-swimmers and in particular the squirmer motion in a detailed way.

In Chapter 2 we explain the numerical methodology that we use to simulate the fluid that interact with the micro-swimmers. A full review of the method is depicted here.

The Chapter 3 shows that semi-dilute microorganism suspensions in 3D can develop collective motions like polar alignment and giant number fluctuations. We demonstrate that both collective motions depend on the hydrodynamic signature of the particles and systems with giant number fluctuations generate a cluster size distribution where a macroscopic cluster is formed. *This striking phase separation emerges thanks to hydrodynamic interactions that re-orient and align the particles. And not to the reduction of velocity when local density grows. Furthermore, aligned suspension generates a long-time super-diffusive motion after a cross-over from ballistic to diffusive motion generated by the re-orientation of*

the particles. It contains a complete computational study of squirmer suspensions in 3D. We show global measures of the suspension, global parameteres like the number fluctuations, density dependence speed or the mean square displacement give us information of the general behavior of the suspension.

In Chapter 4 we simulate a dilute suspension of attractive self-propelled spherical particles taking into account hydrodynamics interactions. Particles are restricted to move only in a plane. To start with, we observe that depending on the ratio between attraction and propulsion, particles aggregate forming clusters. Next, we analyse their structure, comparing the case when active particles behave either as pushers or pullers (always in the regime where inter-particles attractions competes with self-propulsion). To conclude, we compare the obtained results with a system consisting of self-propelled Brownian disk particles at the same conditions. We have find that hydrodynamics drive the coherent swimming between swimmers while the swimmer direct interactions, modeled by a Lennard-Jones potential, contributes to the swimmersâ$^{\mathrm{TM}}$ cohesion.

In Chapter 5 we developed numerical simulations of squirmer suspensions where particles were confined to move only in a plane but not the solvent. We saw that global polar order of the suspension depend on the hydrodynamic signature and collisions of the particles as in the non-confined case, however due to the geometrical restriction to move in a plane we saw that depending on the hydrodynamic signature particles can align either parallel or perpendicular to the swim plane. When squirmers only are able to re-orient and they are fixed in the plane, we found that polar order disappears for all cases of squirmers, but alignment is still present parallel to the swim plane for pullers, while pusher suspensions are more isotropically stable. This alignment that emerges due to the confinement of fixed particles is studied more systematically by doing simulations of different sizes, we found that this alignment emerges completely due to the confinement restriction and the hydrodynamic interactions among particles and it is not a finite size effect. Due to this geometrical constriction, we also show the eigenvector associated to the nematic order, to analyse if particles re-orient normal or parallel to the confinement plane. Given rise to the fact that pullers with fixed position align parallel to the plane. A systematic study of the cluster size distribution is also showed for this system and contrasted with the case where particles can not re-orient. We found that partial confinement plays a key role in the cluster sizes as well as the hydrodynamic signature.

Finally in Chapter 6 the conclusions and future directions of the research.

Chapter 1

Introduction

In this chapter, we give a general definition of active matter and active particles, we describe the wide range of applications and phenomena where active matter is present. We describe particularly in detail, the theoretical background generated in the recent years for active particles and specially the case of systems with hydrodynamic interactions. Since particles interact with the fluid in order to self-propel we call it micro-swimmers, such active particles and its applications are widely discussed and the model that we used along the computational study presented in this thesis.

1.1 Active systems

Active systems or active matter can be defined as materials which are made of many interacting units, where each unit consume energy and generate motion or mechanical stresses collectively. Given the intrinsic nature of these entities to put/consume energy to/from the system, active matter or active systems are out of equilibrium.

Active systems are found everywhere from the living and nonliving world and they span in a wide range of length scales, from the cytoskeleton to individual living cells, tissues and organisms, animal groups such as bird flocks, fish schools and insect swarms., self-propelled colloids and artificial nanoswimmers. These disparate systems exhibit a number of common mesoscopic to large-scale phenomena, including swarming, non-equilibrium disorder-order transitions, mesoscopic patterns, anomalous fluctuations and surprising mechanical properties. Experiments in this field are now developing at a very rapid pace and new theoretical ideas are needed to bring unity to the field and identify "universal" behavior in these internally driven systems.

It is known that active matter can generate some interesting nonequilibrium features, it gives rise for example to amazing emergent collective motion as swarming or formation of coherent structures [1–5].

Several researchers has been working in understand the fundamental mechanisms that generate the collectivity between particles, like clustering, orientational order or phase separation. They have found that aggregation depends crucially on the particular shape of gliding bacteria or any elongated self-propelled particles in general [6, 7]. But it has been found that spherical particles where nor steric repulsion neither attractive interaction among particles are taking in count also shown aggregation and even phase separation.

Experimentalist has been working with photoactive colloids [8, 9], active emulsion droplets [10] and with spherical swimming bacteria [11]. Motivated by these experiments, people have performed simulations particularly using active brownian particles [12–14].

1.2 Active particles

Simulations have shown a phase-separated liquid state that depend on the density and the activity of the particles. Following this result theoretical advances has been done to understand this phase separation in terms of the density dependent motility [15–17]. Furthermore, they have even derived expressions for the pressure in order to find the equation of state for active systems [18–21]. However, it has been shown that despite that the mechanical pressure can be calculated, an equation of state not necessarily exist [22].

Spherical swimmers is an important case, where an equation of state is less likely to find, since hydrodynamics can cause torques, and torque needs to be negligible under the theoretical framework [22]. Actually, extensions of this theory shows that the interplay of activity and hydrodynamics is highly nontrivial [23].

Regardless of the difficulty to take in count hydrodynamic interactions, several studies in 2D concerning the phase behaviour have been published recently, for example in Ref. [24] simulates 2D swimmers and they found that phase separation is suppressed by hydrodynamic interactions, while in Ref. [25] they simulate swimmers strongly confined by walls in a quasi-2D geometry where a phase separation is found at high concentration. In Ref. [26] shows that squirmers swimming in a plane without walls can indeed form aggregates and orientational order, which is in accordance with a previous result of our group [27].

Ishikawa and Pedley also has carried out simulations in 3D where they have studied the diffusion [28], dispersion [29], and the development of collective motion [30, 31]. Yamamoto's group also studied the diffusion of swimmers [32] and

very recently the swarming formed in 3D suspensions in confinement [33]. Our group, also has contributed in understand the emergence of collective motion in 3D swimmer suspensions [34].

Aside from Ref. [27], swimmers were modelled as squirmers [35, 36] in all the studies mentioned above, which is a standard model for study micro-swimmers.

1.3 Microswimmers

As we have seen in previous section, there are two general kinds of active matter: Living and artificial active matter, and inside of both groups we also found different systems in terms of their interaction with the media. In [4] called dry active matter which are systems that can be described by models with no momentum conservation, while when solvent-mediated hydrodynamic interactions are important, the dynamics of the suspending fluid must be incorporated in the model and one must develop a description of the suspension of active particles and fluid, with conserved total momentum. We refer to systems described by models with momentum conservation, where fluid flow is important, as "wet." In this section, we focus on the wet systems, where we can find several examples and applications either with artificial or living particles suspensions.

In the living world, the main example is the micro-organisms who play a vital role in many biological, medical and engineering phenomena. It has been shown that one important aspect to understand micro-organism behaviours such as locomotion and collective motions of cells are biomechanics. The development of collective motions like the spatio-temporal coherent structures have been studied over the last few years. Among all the research and analysis, one important conclusion about the macroscopic properties of a suspension, it is the strong influence of the interactions between individual microbes on the mesoscale structures generated. Such conclusion were generated by measured macroscopic properties like the rheology and diffusion in the suspension [37].

To study microrganism and biomechanics are key subjects in order to design and optimize micro-robots. Syntethic or artificial micro-swimmers have been made, using a wide variety of materials, from polystyrene spheres coated with platinum, which react with the hydrogen peroxide in the medium, leading to the propulsion of the spheres [38]. Whereas, Thutupalli et al. in [39] have synthesized liquid droplets moving in an oil "background" phase. Propulsion arises due to the spontaneous bromination of mono-olein (racglycerol-1-mono-oleate) as the surfactant.

Zhu et al. in [40] have collected a wide list of natural phenomena where microorganism locomotion is involved:

The physical mechanisms of microorganism locomotion accompany a variety of natural phenomena, including human spermatozoa approaching the ovum in the mammalian female reproductive tract,[41] algal blooms moving to nutrient rich environment in maritime regions,[42, 43] biofilm formation,[44] and paramecia cells escaping from their predators. [45] There are several studies in order to understand the different physical mechanisms at play in the locomotion of microorganisms. In particular, in this thesis we are interested in collective behavior, and hydrodynamic interactions.

To understand the physics of swimming, in other words, the physical mechanism of micro-swimmer locomotion, it is important to take in count that the size of microorganisms are around microns and move at around 10^2 microns per second, thus we have that the Reynolds numbers is less than 10^{-2}. Where the Reynolds number Re is defined in terms of the swimming speed u, the radius of the individual $\sigma/2$ and the kinematic viscosity of the solvent ν as

$$Re = \frac{u\sigma}{2\nu}. \tag{1.1}$$

Therefore, the flow field around a micro-organism is a Stokes flow and hence the inertial force is negligible compared with the viscous force. In the Stokes flow regime, Purcell showed that the reciprocal motion cannot lead to any locomotion; (scallop theorem) [46]. However, for ciliated organisms , the motion of each individual cilium follows an asymmetric pattern. First applies an effective stroke and then a recovery stroke, as we show in figure 1.1-a. The asymetry in the strokes gives to the cilium, the ability to generate a net thrust on the cell body. Cilia are typically short compared with the cell body, and the number of cilia per cell is large. A ciliate swims by synchronizing ciliary motions with slight phase differences, thus generating metachronal waves, as shown in figure 1.1-b. In the next section we shall explain in detail a simple model to take in count the ciliary motion, it is the most popular exact solution and originally due to Lighthill [35] and Blake [36].

1.4 Squirmer Model

The Lighthill [35] and Blake [36] model sometimes is referred as the envelope model, the motion of closely packed cilia tips are modeled as a continuously deforming surface (envelope) over the body of the organism. Basically, this model consider a spherical particle with a fixed director that moves with the particle $\mathbf{e}_1$ and the internal activity of the particle generates an axysimmetric velocity at its surface. This velocity can be written in terms of two independent terms, one ra-

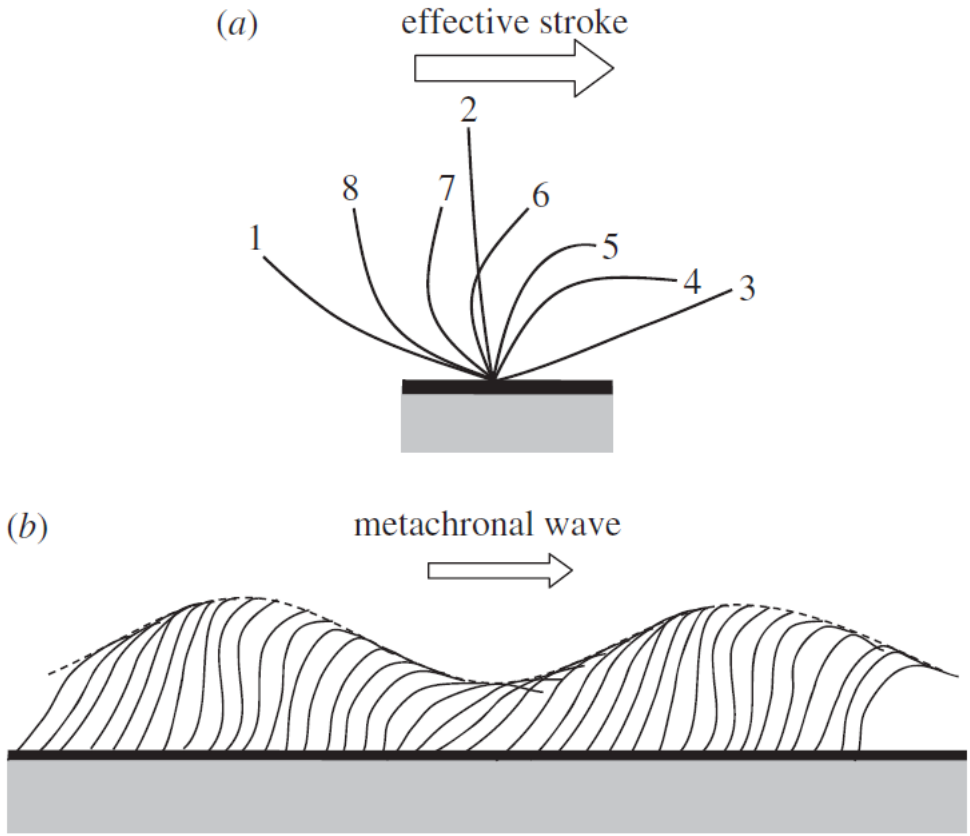

Figure 1.1: Schematic of the motion of an individual cilium and the collective motion of cilia. (a) Effective stroke of an individual cilium. The numbers in the figure indicate the order of the ciliary motion. The effective stroke is defined from 1 to 3. (Reproduced images from Ishikawa in [37].) (b) Metachronal wave generated by cilia (reproduced images from Blake and Sleigh in [47]).

dial v_r and another polar v_θ. Both components can be written in terms of special functions:

$$
\begin{aligned}
u_r|_{r=R_p} &= \sum_{n=0}^{\infty} A_n(t)\, P_n\left(\frac{\mathbf{e}_1\mathbf{r}}{R_p}\right), \\
u_\theta|_{r=R_p} &= \sum_{n=0}^{\infty} B_n(t)\, V_n\left(\frac{\mathbf{e}_1\mathbf{r}}{R_p}\right),
\end{aligned}
\tag{1.2}
$$

where $\mathbf{r}$ represents the position vector with respect to the squirmer's center, which is always pointing the particle surface and thus $|\mathbf{r}| = R_p$, while $\mathbf{e}_1$ describes the intrinsic self-propelling direction, which moves rigidly with the particle and determines the direction along which a single squirmer will displace. P_n stands

for the n-th order Legendre polynomial and V_n is defined as

$$V_n\left(\cos\theta\right) = \frac{2}{n(n+1)}\sin\theta\ P_n'(\cos\theta). \tag{1.3}$$

The amplitudes $A_n(t)$ and $B_n(t)$ determine the flow induced by the beating cilia on the squirmer's surface, both functions are periodic. Since the cilia wave stroke is faster than the squirmer displacement, we can replace the time dependent amplitudes in the boundary conditions, eqn. (1.2), by their effective averaged amplitudes over a stroke period, $B_n(t) = B_n$. Moreover, we will disregard the radial changes of the squirming motion, $A_n(t) = 0$, in this way the velocity field generated by a squirmer will depend only in the polar part of the slip velocity and not in the size of the squirmer. Another feature in this squirmer model is that squirmer swimms in a non inertial medium hence the velocity $\mathbf{u}$ and pressure p of the fluid are given by the Stokes and continuity equations:

$$\begin{aligned} \nabla p &= \nu\nabla^2\mathbf{u}, \\ \nabla\cdot\mathbf{u} &= 0. \end{aligned} \tag{1.4}$$

Solving eqns. (1.4), one can then derive the average fluid flow induced by a squirmer, [48, 49]. Taking in count the boundary conditions specified by the slip velocity in the surface of its body, eqn. (1.2) and the constrains we specified above, we have that the mean fluid flow induced by squirmer is

$$\begin{aligned} \mathbf{u}\left(\mathbf{r}\right) &= B_1\mathbf{e}_1\left(-\frac{1}{3}1 + \frac{\mathbf{rr}}{r^2}\right)\left(\frac{R_p}{r}\right)^3 \\ &+ \sum_{n=2}^{\infty} B_n\left(\frac{R_p^{(n+2)}}{r^{(n+2)}} - \frac{R_p^n}{r^n}\right)P_n\left(\frac{\mathbf{e}_1\mathbf{r}}{r}\right)\frac{\mathbf{r}}{r} \\ &+ \sum_{n=2}^{\infty} B_n\mathbf{e}_1\left(1 - \frac{\mathbf{rr}}{r^2}\right) \\ &\times\left(\frac{nR_p^{(n+2)}}{2r^{(n+2)}} - \frac{(n-2)R_p^n}{2r^n}\right)\frac{V_n\left(\frac{\mathbf{e}_1\mathbf{r}}{r}\right)}{\sqrt{1-\frac{\mathbf{e}_1\mathbf{r}}{r}}}. \end{aligned} \tag{1.5}$$

This solution take in count also that squirming surface has a finite total energy, given by the constrain $v_s = \frac{2}{3}B_1$ along $\mathbf{e}_1$ where v_s is the velocity in which fluid is moving, measured in the reference system of the squirmer center of mass. With this velocity constrain we ensure that there is not net force acting on the squirmer. We are interested in study a simplified squirmer model, hence we take $B_n = 0$, $n > 2$, keeping only the first two terms in the general expression, eqn. (1.5).

The two non-vanishing terms can model the dynamic effects associated to the squirmers. The polarity is associated with squirmer self - propulsion, through B_1, and the active stresses induced by the apolar term B_2. The active stress is quantified in terms of the squirmer self-propulsion by $\beta = B_2/B_1$ [48], β sign determines squirmer behaviour, if $\beta > 0$ squirmer behaves as puller or as a pusher if $\beta < 0$. Hence, the average fluid flow generated by this simplified model of squirmer can be written as

$$\begin{aligned}\mathbf{u}(\mathbf{r}) = &-\frac{1}{3}\frac{R_p^3}{r^3}B_1\mathbf{e}_1 + B_1\frac{R_p^3}{r^3}\mathbf{e}_1 \cdot \frac{\mathbf{rr}}{r^2} \\ &- \frac{R_p^2}{r^2}B_2P_2\left(\frac{\mathbf{e}_1\mathbf{r}}{r}\right)\frac{\mathbf{r}}{r}.\end{aligned} \tag{1.6}$$

Squirmer model was originally developed to specifically model the swimming of ciliates, but it can also be useful in the study of other types of swimming microorganisms, broadly categorized as “pushers” and “pullers” [50]. Pushers obtain their thrust from the rear part of their body, such as E. coli. In contrast, for pullers the thrust comes from their front part, lile algae genus Chlamydomonas. The squirmer model can represent pushers and pullers by correspondingly changing the surface actuation (squirming profile), rendering it a general model for investigating the locomotion of microorganisms [51].

Chapter 2

Lattice Boltzmann Method

In this chapter, we present the lattice Boltzmann method (LBM) which is a relatively new method in computational fluid dynamics. In the last 20 years, LBM has developed into an alternative and promising numerical scheme for simulating fluid flows [52]. Its strength lies however in the ability to model complex physical phenomena, including single and multiphase flow in complex geometries or chemical interactions between the fluid and the surroundings.

The chapter is divided in sections, where first we make an introduction of different methods for simulate hydrodynamic interactions in soft matter, second the Boltzman equation and its discretization, in section 2.3 the Lattice Boltzmann method itself, next the boundary conditions in LBM, in section 2.5 we explain how is plugged the squirmer model in the LBM scheme, finally we explain the parallelization of our LB code and some features of it and some general conclusions.

2.1 Introduction

Microorganisms and active fluids in general, are systems where the coupling between the fluid and their mesoscopic components (bacteria, active colloids, etc.) affects the dynamics of the system. The mesoscopic elements generate disturbance in the neighboring fluid which changes the fluid flow at long distances, this effect is called hydrodynamic interactions (HI).

Transport equations are used to study these kind of problems where fluid flows are taking in count. On a macroscopic scale, partial differential equations (PDE) like Navier-Stokes equation are used. Since these kind of equations are difficult to solve analytically due to non-linearity, complicated geometry and boundary conditions. A lot of numerical schemes such as finite difference method (FDM), finite volume method (FVM), finite element method (FEM) or spectral element method

(SEM) are used to convert the PDE to a system of algebraic equations. These macroscopic methodology is based on the discretization of the PDE. However, we can lose details of the dynamic of the mesoscopic elements.

Another approach to the problem is to consider a microscopic scale where the motion of all the particles of the system can be simulate (molecular dynamics (MD)). But we deal with the fact of the large disparity between the time-length scales of the solvent (10^{-10} s - 10^{-10} m) and the mesoscopic components (10^{-3} s - $10^{[}-3]$ m). It becomes technically impossible to reach time-length scales of the mesoscopic components and to simulate complex fluids as a consequence.

To close the gap between macro-scale and micro-scale, coarse-grained models have been developed. These methods reduce the degrees of freedom of the solvent but capture the collective modes of the fluid. For example, in Brownian Dynamics (BD), the solvent is represented implicitly by random forces and frictional terms. It is a simplified version of Langevin dynamics where particle inertia is neglected. BD not conserve momentum, so diffusion is present but not hydrodynamics [53]. However, another mesoscopic methods have been created, where the solvent dynamics is explicitly resolved, for example Dissipative Particle Dynamics (DPD) [54, 55] where the fluid is described as N coarsened particles with continuous positions and velocities. The particles interact among them by a soft potentials which leads to large time-steps and reach time scales orders of magnitude larger than the time scales of a MD. DPD was reformulated and slightly modified by P. Español [56] to add a Galilean invariant thermostat, which preserves the hydrodynamics.

As an alternative of these mesoscopic MD-like methods we can find mesoscopic approaches based on kinetic theory. Lattice Boltzmann Method for example, it is based on microscopic models and mesoscopic kinetic equations. The fundamental idea of the LBM is to construct simplified kinetic models that incorporate the essential physics of microscopic processes so that the macroscopic averaged properties obey the desired macroscopic equations [57].

Even though the LBM is based on a particle picture, its principal focus is the averaged macroscopic behaviour. The kinetic equation provides many of the advantages of molecular dynamics, including clear physical pictures, easy implementation of boundary conditions, and fully parallel algorithms. Because of the availability of very fast and massively parallel machines, there is a current trend to use codes that can exploit the intrinsic features of parallelism. The LBM fulfills these requirements in a straightforward manner [57].

From the physical point of view, the lattice Boltzmann method can be interpolated as a microscope for fluid mechanics while a telescope for molecular dynamics [52].

2.2 Lattice Gas Cellular Automata

The fundamental idea behind lattice gas automata is that microscopic interactions of artificial particles living on the microscopic lattice can lead to the corresponding macroscopic equations to describe the same fluid flows.

Historically, the lattice Boltzmann method originates from the lattice gas cellular automata (LGCA) which is a Cellular Automaton (CA)[1] where fluid particles are constrained to move on a regular lattice such that their collisions conserve mass and momentum. It was originally created by Hardy, Pomeau and de Pazzis in 1973 [59] known as HPP model. In this model, the lattice is square, and the particles travel independently at a unit speed to the discrete time. The particles can move to any of the four sites whose cells share a common edge. Particles cannot move diagonally. The HPP model lacked rotational invariance, which made the model highly anisotropic. This means for example, that the vortices produced by the HPP model are square-shaped [52] and it does not reproduce macroscopic hydrodynamics. Ten years after Frisch, Hasslacher and Pomeau [60] discovered that a LGCA with hexagonal symmetry, leads to the Navier-Stokes equation in the macroscopic limit (FHP model).

In general, a lattice gas automaton is a regular lattice with particles residing on the nodes, all particle velocities are also discrete. So we have particles that can move around, but only within lattice nodes. The particle occupation is characterized by the occupation number

$$n_i(\mathbf{x}, t) = \{n_i(\mathbf{x}, t), i = 1...m\}\,, \tag{2.1}$$

n_i is a Boolean array, such that

$$\begin{aligned} n_i(\mathbf{x}, t) &= 0 \qquad \text{site } \mathbf{x} \text{ with no particles at time } t, \\ n_i(\mathbf{x}, t) &= 1 \qquad \text{site } \mathbf{x} \text{ with one particle at time } t, \end{aligned} \tag{2.2}$$

where M is the number of velocities at each node. For example, $M = 4$ for HPP model, while $M = 6$ for FHP model.

This occupation numbers defines a MN-dimensional time dependent Boolean field, where N is the number of lattice sites [52]. The evolution of this field take place in a Boolean phase-space consisting in 2^{MN} discrete states, and evolution equation can be written as:

$$n_i(\mathbf{x} + \mathbf{c}_i, t + 1) = n_i(\mathbf{x}, t) + \Omega_i\left[n(\mathbf{x}, t)\right], \tag{2.3}$$

[1] Cellular automata are regular arrangements of single cells of the same kind, each cell holds a finite number of discrete states that evolves through a number of discrete time steps according to a set of rules based on the states of neighboring cells [58].

where $\mathbf{c}_i$ is the local particle velocity and $\Omega_i\left[n(\mathbf{x},t)\right]$ is the collision operator. Ω_i contain all the possible collisions. Boolean nature is preserved and interactions are completely local. Configuration of particles at each time step evolves in two sequential sub-steps:

- Streaming: every particle moves to the neighbouring node according to its velocity $\mathbf{c}_i$.

- Collision: when there are more than one particle at the same node, they interact by changing their velocity directions according to scattering rules. The collision process is chosen so that the number of particles and the total momentum are conserved. The conservation of energy is not imposed.

Frisch et al. in [60], making use of a probabilistic approach, they considered N_i defined as the average population at a node with velocity i. Since the average is over a macroscopic space-time region, N_i can be written as

$$N_i(\mathbf{x},t) = \langle n_i(\mathbf{x},t)\rangle, \tag{2.4}$$

therefore the mean density as

$$\rho = \sum_i N_i(\mathbf{x},t), \tag{2.5}$$

and the mean velocity

$$\mathbf{u} = \sum_i N_i(\mathbf{x},t)\mathbf{c}_i/\rho. \tag{2.6}$$

With this definitions, they have found a steady state equilibrium solution for the mean population in function of the Fermi-Dirac distribution and then they obtained a set of hydrodynamic equations that goes to imcompressible Navier-Stokes equation in the limit where the Mach number $M = u\sqrt{2} \to 0$ and the hydrodynamic scale $L \to \infty$. However, some problems arise, like the lack of Galilean invariance.

Another drawback is that this method is not efficient to study hydrodynamics because of the statistical noise. In order to solve this problem, the Lattice Boltzmann Method (LBM) was proposed as an independent numerical method for hydrodynamic simulations. McNamara and Zanetti in [61] were the firsts to replace the Boolean field to continuos distributions over the FHP lattice.

2.3 Lattice Boltzmann

The formulation of the Lattice Boltzmann Method (LBM) lies in the replacement of the Boolean occupation numbers, involved in the previous LGCA, with the corresponding ensemble-averaged populations. In this way, the artificial micro-dynamics of LGCA will be more close to the usual kinetic theory [58].

The property of the collection of particles is represented by a distribution function. That means that the Boolean occupation number $n_i(\mathbf{x}, t)$ in LGCA is replaced for a single particle distribution function $f_i(\mathbf{x}, t)$, which is the ensemble average of n_i,

$$f_i(\mathbf{x}, t) = \langle n_i(\mathbf{x}, t) \rangle. \tag{2.7}$$

Occupation number n_i can be 0 or 1 while f_i now is a real functions with a range $0 \leq f_i \leq 1$. Therefore, a discrete kinetic equation for the particle distribution function, which is similar to the kinetic equation in the LGCA (see eq. (2.3)):

$$f_i(\mathbf{x} + \mathbf{c}_i \Delta t, t + \Delta t) = f_i(\mathbf{x}, t) + \Omega_i \left[f(\mathbf{x}, t) \right], \quad (i = 0, 1, ..., M), \tag{2.8}$$

where $\Omega_i = \Omega_i \left[f(\mathbf{x}, t) \right]$ is the collision operator which represents the rate of change of f_i resulting from the collision. Δt is the time increment. Discrete equations like eqs: (2.8) are referred to as lattice Boltzmann equations.

Moreover, it can be shown that eq. (2.8) is a particular discretization of the Boltzmann equation [62]. Since the continuous Boltzmann equation is

$$\frac{\partial f}{\partial t} + \mathbf{v} \nabla f = Q \tag{2.9}$$

where Q is the collision integral. We can expand the function $f_i(\mathbf{x} + \mathbf{c}_i \Delta t, t + \Delta t)$ as

$$f_i(\mathbf{x} + \mathbf{c}_i \Delta t, t + \Delta t) = f_i(\mathbf{x}, t) + \Delta t \frac{\partial f_i}{\partial t} + \mathbf{c}_i \Delta t \nabla f_i + \mathcal{O}\left((\Delta t) \right). \tag{2.10}$$

Replacing in eq. (2.8) and neglecting higher order terms:

$$\frac{\partial f_i}{\partial t} + \mathbf{c}_i \nabla f_i = \frac{\Omega_i \left[f(\mathbf{x}, t) \right]}{\Delta t} \tag{2.11}$$

which is a correspondence to Boltzmann Equation (eq. (2.9)) where $f_i \to f$, $\mathbf{c}_i \to \mathbf{v}$ and $\frac{\Omega_i [f(\mathbf{x},t)]}{\Delta t} \to Q$.

According to Sterling and Chen in [62] LBM makes use of the following definitions and conditions:

- The particle populations f may only move with velocities that are members of the set of discrete velocity vectors $\mathbf{c}_i$. The corresponding populations are denoted f_i.

- A collision operator with a single relaxation time, τ, is used to redistribute populations f_i towards equilibrium values f_i^{eq} . This is also referred to as a BGK collision operator where τ is inversely proportional to density [63]. For constant density flows τ is a constant.

- The equilibrium velocity distribution function is written as a truncated power series in the macroscopic flow velocity.

Therefore, with the BGK approximation, the discrete Boltzmann equation (2.11) becomes

$$\frac{\partial f_i}{\partial t} + \mathbf{c}_i \nabla f_i = -\frac{1}{\tau}\left(f_i - f_i^{eq}\right), \tag{2.12}$$

hence,

$$\Omega_i = -\frac{1}{\tau}\left(f_i - f_i^{eq}\right) \tag{2.13}$$

and the average density, velocity and pressure tensor are given by

$$\rho(\mathbf{x}, t) = \sum_{i=1}^{M} f_i(\mathbf{x}, t), \tag{2.14}$$

$$\rho(\mathbf{x}, t) v_\alpha(\mathbf{x}, t) = \sum_{i=1}^{M} f_i(\mathbf{x}, t) c_{i\alpha}, \tag{2.15}$$

$$p_{\alpha\beta}(\mathbf{x}, t) = \sum_{i=1}^{M} f_i(\mathbf{x}, t) c_{i\alpha} c_{i\beta}, \tag{2.16}$$

where M is the number of directions of the particle velocities at each node. Ω_i is a nonlinear collision operator, thus its evaluation is time consuming. Higuera and Jiménez in [64] have shown that collision operator can be approximated by a linear operator, such as

$$\Omega_i(f) = M_{ij}\left(f_i - f_i^{eq}\right) \tag{2.17}$$

where according to [64]

$$M_{ij} \equiv \frac{\partial \Omega_i(f^{eq})}{\partial f_j}, \tag{2.18}$$

which determines the scattering rate between directions i and j. Since collisions

conserve mass and momentum, M_{ij} satisfy [65]:

$$\sum_{i=1}^{M} M_{ij} = 0 \sum_{i=1}^{M} \Omega_i \mathbf{c}_i = 0. \tag{2.19}$$

Furthermore, due to eq. (2.13),

$$M_{ij} = -\frac{1}{\tau}\delta_{ij} \tag{2.20}$$

Additionally, given the relaxation time τ, the shear and bulk viscosity under LBM framework are

$$\eta = (2\tau - 1)/6\xi = 2\eta/3 \tag{2.21}$$

respectively [66], where we have chosen our units such that $\rho = 1$ for a quiescent fluid, and choose the lattice parameter (LU) as the unit of length, and the time step as the unit of time ($\Delta t = 1$), and the sound speed for the lattice in 3D that we use, $c_s = 1/\sqrt{3}$ in LU.

Different lattice geometries, in which the distribution functions move, can be defined, specified by both the arrangement of nodes and the set of allowed velocities. LB models can be operated on a number of different lattices in two or three dimensions: cubic, triangular, rectangular, hexagonal, etc. A popular way of classifying the different cubic lattices is the D_nQ_m scheme [67]. Here D_n stands for n dimensions while Q_m stands for m speeds.

With this basic algorithm of the LBM by using the single-time relaxation approximation and a particular Maxwell-type distribution for the equilibrium distribution (eq. (8) in [68]), one can recover the Navier-Stokes equations and model single phase fluid with a variety of boundary conditions [52].

2.4 Boundary Conditions

In general, we have a great deal of temporal/spatial flexibility in applying boundary conditions in LBM. In fact, the ability to easily incorporate complex solid boundaries is one of the most exciting aspects of these models. LB is particularly useful in complex fluids such as suspensions of solid colloidal particles [69].

For solid boundaries we separate solids into two types: boundary solids links that lie at the solid-fluid interface and isolated solids links that do not contact fluid. With this division it is possible to eliminate unnecessary computations at inactive nodes [69].

Stationary solid objects were first introduced into lattice-gas simulations by

replacing the normal collision rules at a specified set of boundary nodes by the "bounce-back" collision rule [70]. This collision rule is used to model solid stationary or moving boundary condition, non-slip condition, or flow over obstacles. Name implies that a particle coming towards the solid boundary bounces back into the flow domain. If we want particles to bounce back from a solid, we have to change certain values of distribution functions f_i. For example, velocities f_4, f_7 and f_8 in a fluid node next to solid nodes (called boundary node velocity) will pass the velocity value to the velocities f_2, f_5 and f_6 respectively, this procedure is schematically explained in Fig. 2.1.

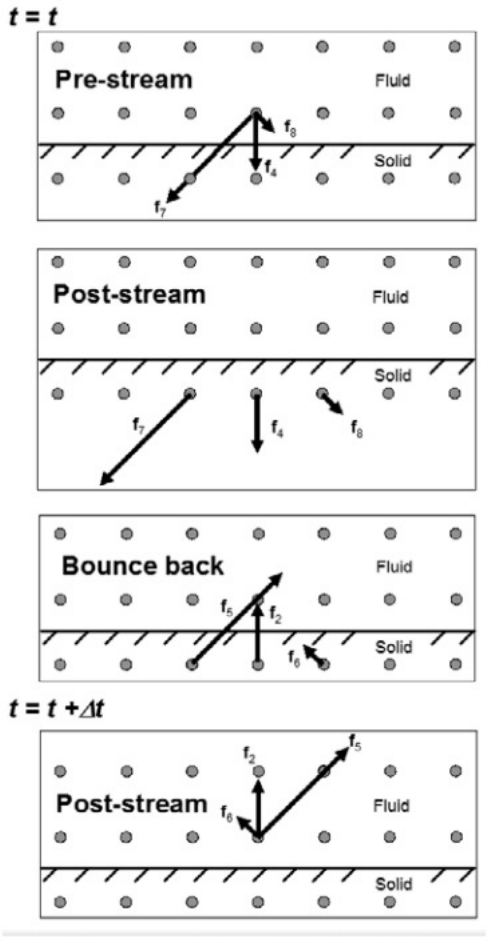

Figure 2.1: Schematic illustration of bounce back rule for interaction with solids. Figure extracted from reference [71], f_i vectors in the figure are the $\mathbf{c}_i$ velocities in the nomenclature we used along this manuscript.

If the solid object is moving with a local boundary velocity $\mathbf{U}$ (like colloidal particle), the bounceback condition has to be modified, and the velocity of the boundary nodes are establish by the solid particle velocity $\mathbf{U}$, its angular velocity

$\mathbf{\Omega}$ and center of mass $\mathbf{R}$, hence, if $\mathbf{u}_b$ is the velocity in a boundary node

$$\mathbf{u}_b = \mathbf{U} + \mathbf{\Omega} \times \left(\mathbf{r} + \frac{1}{2}\mathbf{c}_i - \mathbf{R} \right). \tag{2.22}$$

By exchanging population density between a fluid node and solid node the local momentum density of the fluid can be modified to match the velocity of the solid particle surface at the boundary, without affecting either the mass density or the stress, which depend on the sum of both nodes distributions [72]. In addition to the bounceback, population density is transferred across the boundary node [72], in function of the velocity in a boundary node,

$$\begin{aligned} f_i(\mathbf{x} + \mathbf{c}_i, t+1) &= f_{i'}(\mathbf{x} + \mathbf{c}_i, t^+) + \frac{2\rho \mathbf{u}_b \cdot \mathbf{c}_i}{c_s^2} \\ f_{i'}(\mathbf{x}, t+1) &= f_i(\mathbf{x}, t^+) - \frac{2\rho \mathbf{u}_b \cdot \mathbf{c}_i}{c_s^2}. \end{aligned} \tag{2.23}$$

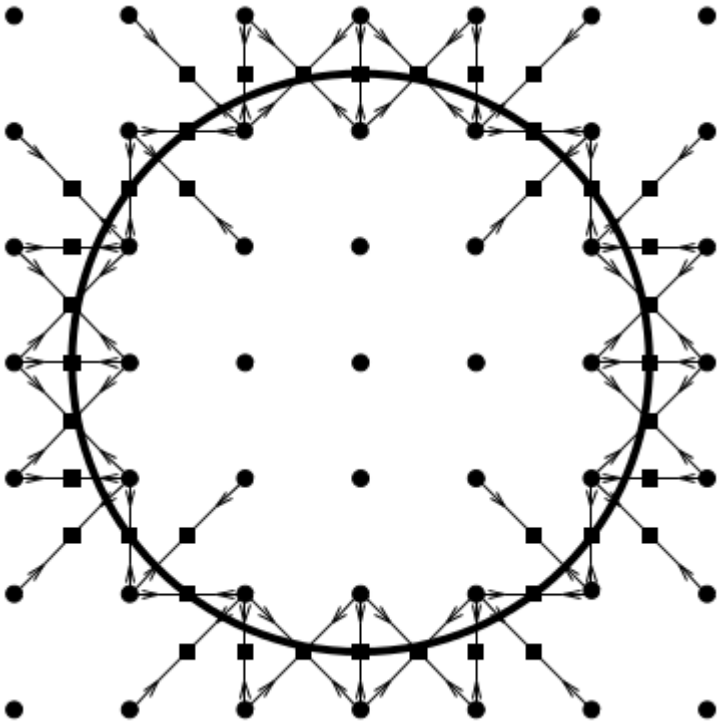

Figure 2.2: Location of the boundary nodes for a circular object of radius 2.5 lattice spacings. The velocities along links cutting the boundary surface are indicated by arrows. The locations of the boundary nodes are shown by solid squares and the lattice nodes by solid circles. Figure extracted from reference [72]

Bounce-back involves changes in the velocity distribution functions which lead to a force and torque acting locally on the fluid. The opposite force and torque are exerted on the particle. Hence, the overall fluid momentum change through bounceback determines the net force and torque acting on the rigid particle, which are used to update the particle linear and angular velocities at each time step. These velocities are then used to update the particle position and direction; the motion of colloidal particles is, hence, determined by the force and torque exerted on it by the fluid, and is resolved by a MD like algorithm [73]. With this method, we ensure a correct description of the dynamic coupling between the collective modes of the solvent and the suspended particles.

The size of the colloid is important, since due to the discretization the colloid is not strictly a sphere (as we show in Fig. 2.2), which could be relevant for the torque calculation. There are "magic" values of the particle radius, including 1.25, 2.3, 3.7, 4.77 which minimise discretisation effects [74]. Most of the results we have shown here are done with simulations with radius of 2.3 lattice units.

Again following [74], mass conservation is enforced, since when particles are near to contact they may not have a full set of boundary links with the fluid, this leads to a potential non-conservation of mass associated with the particle motion.

2.5 Squirmer model coupled to LBM

First two terms of equation (1.6) represent a dipolar field, similar to the one generated by an electric/magnetic dipole. The direction and strength of the fluid flow is specified by the polarity term $B_1\mathbf{e}_1$ in analogy with the electric/magnetic moments. While the B_2 term models a quadrupolar field. B_2 is equivalent to the strength of a quadrupole for a symmetric arrangment of electric/magnetic dipoles, when the dipole moments vanish [75] (without polarity). Then, taking in count that we have only two non-zero terms, the boundary conditions on the surface of the squirmers depicted in equations (1.2) are written as

$$\begin{aligned} u_r|_{r=R_p} &= 0, \\ u_\theta|_{r=R_p} &= B_1 V_1(\cos\theta) + B_2 V_2(\cos\theta). \end{aligned} \tag{2.24}$$

Thus, the velocity in the surface of the squirmer defined as the velocity $\mathbf{u}|_{r=R_p}$

$$\mathbf{u}|_{r=R_p} = [B_1 \sin\theta + B_2 \sin\theta\cos\theta]\,\boldsymbol{\tau}, \tag{2.25}$$

where $\boldsymbol{\tau}$ is a unit vector tangential to the surface of the particle.

In the LB scheme that we use, we added this surface velocity $\mathbf{u}_b$ to $\mathbf{U}$ in

equation (2.22), $\mathbf{u}_b$ is discretized in terms of the velocities of the nodes and is included in the bounceback rules.

2.6 Parallelization

Reason, why LBM is becoming more and more popular in the field of CFD, is the fact that LBM is solved locally. It has high degree of parallelization, hence it is ideal for parallel machines (computational clusters).

We have performed simulations using the *Ludwig* code, which is a LB code for D3Q19 lattice [76]. It is a parallel lattice Boltzmann code which includes moving particles via domain decomposition and message passing using the message passing interface MPI, its parallelization has been tested [77]. A simulation of a fluid in a cubic box with a edge length of $L = 512$ lattice units, needs a RAM memory of almost 20 Gb and it the requirement of memory grows linearly with the grow of the volume, as we see in Figure 2.3.

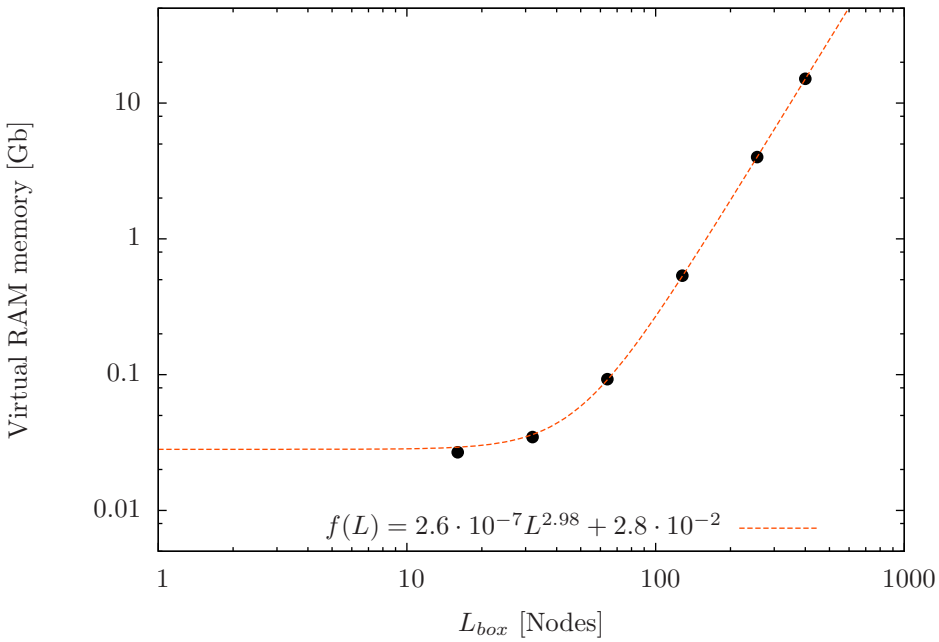

Figure 2.3: RAM memory needed for *Ludwig* as the system size grows. System size is a cubic box of edge length of L_{box} lattice units.

2.7 Conclusions

In this chapter we have described the LBM and the aplications for a squirmer suspension. LBM is a very convenient method for complex system even for systems out of equilibrium, in particular *Ludwig* code has been used for study systems of binary fluids [78], colloidal suspensions [66] , colloidal jamming at interfaces [79], fluid-fluid interfaces [80] and actually for squirmer suspensions [34, 49], like the results showing here. In particular, thanks to the good scalability of the program we were able to studied systems with $\sim 10^6$ particles (see chapter 3 for example).

Chapter 3

Collective motion of a squirmer suspension

3.1 Introduction

We characterize the collective motion that emerge from active particles like spherical active colloids or microorganisms. We have taken in count hydrodynamic interactions explicitly by using Lattice-Boltzmann numerical simulations explained in Chapter 2, and active particles are modelled using a squirmer model where only two parameters are necessary to model how a microorganism swims, as described in chapter 1.

Here we study principally semi-dilute suspensions of squirmers with $\phi = 0.1$, where $\phi = \pi\sigma^3 N/6L^3$, $\sigma = 2.3$ and $L = 120$ both in lattice space units, thus $N = 3400$ for $\phi = 0.1$. To obtain different volume fractions N was changing. We changed β systematically to observe the emergence of collective motion depending on the hydrodynamic signature. We also show a systematic study in terms of the system size, therefore N and L were tuned to observe the effects of finite size. We set $B_1 = 0.01$ and the viscosity $\nu = 0.5$, therefore $u_\infty = 0.007$ and Reynolds number $Re = 0.031$.

We show that semi-dilute microorganism suspensions in 3D can develop collective motion and display polar alignment and giant number fluctuations. We demonstrate that both signatures of collective motion depend on the hydrodynamic properties of the particles. In particular, the emergence of giant number fluctuations is related with the formation of a macroscopic cluster. *This striking phase separation emerges thanks to hydrodynamic interactions that re-orient and align the particles, and not to the reduction of velocity when local density grows. Furthermore, aligned suspensions generate a long-time super-diffusive motion af-*

ter a cross-over from ballistic to diffusive motion generated by the re-orientation of the particles.

3.2 Collective squirmer alignment

We consider a simplified squirmer model with a slip velocity at the squirmer surface of the form

$$\mathbf{u}|_{r=\frac{\sigma}{2}} = [B_1 \sin\theta + B_2 \sin\theta\cos\theta]\,\boldsymbol{\tau}, \tag{3.1}$$

where $\boldsymbol{\tau}$ is a unit vector tangential to the surface of the particle, θ is the angle between the direction of self-propulsion defined by the unit vector $\mathbf{e}$ and the vector perpendicular to τ. B_1 defines the self-propulsion speed of an isolated squirmer, $u_\infty = 2/3B_1$ and B_2 is the apolar term of the velocity and is related with the active stresses generated by the spheres. The active stress is quantified in terms of the squirmer self-propulsion by $\beta = B_2/B_1$, when $\beta < 0$ squirmer it is called pusher and puller with $\beta > 0$, while $\beta = 0$ correspond to a mover or neutral squirmer. We define a characteristic time in terms of the particle size and u_∞ as $t_0 = \sigma/u_\infty$, where σ is the particle diameter.

(To study squirmers, we used the Lattice-Boltzmann method (LBM), this model simulates the hydrodynamics of a liquid and shows excellent scalability on parallel computers [77], it has been successfully used to simulate squirmer suspensions in Ref. [34, 49], where the slip velocity of the squirmer, defined in Eq. (3.1), is plugged in the LBM scheme as boundary conditions (see chapter 2).

In this chapter we will concentrate on the study of semi-dilute suspensions of squirmers with volume fraction of $\phi = 0.1$, where $\phi = \pi\sigma^3 N/6L^3$, the diameter of squirmers $\sigma = 4.6$ and the system size $L = 120$ both in lattice space units, thus $N = 3400$ for $\phi = 0.1$, where N the number of simulated squirmers. We have changed β systematically to observe the emergence of collective motion depending on the hydrodynamic signature. We also show a systematic study in terms of the system size, therefore N and L were tuned to observe the effects of finite size. We set $B_1 = 0.01$ and the viscosity $\nu = 0.5$, therefore $u_\infty = 0.007$ and a characteristic Reynolds number $Re = 0.031$.

Semi-dilute squirmer suspensions can develop alignment between particles, this alignment has been measured [31, 34, 81] by the polar order parameter:

$$P(t) = \frac{1}{N}|\sum_{i=1}^{N} \mathbf{e}_i|, \tag{3.2}$$

where $\mathbf{e}_i$ is the intrinsic orientation of the *i-th* squirmer. At long-times, the suspension reaches a steady state $P(t >> 0) = P_\infty$. If $P_\infty = 1$ the system is completely polarized (all squirmers pointing to the same direction), while $P_\infty \sim 1/\sqrt{N}$ means the system is isotropically oriented. In Fig. 3.1, the black circles show P_∞ as a function of β. Pusher swimmers with $\beta < -1/10$ are isotropically oriented since $P_\infty \sim 1/\sqrt{N}$, for larger values of β P_∞ change abruptly, reaching values close to 1. The suspension becomes strongly polar around $\beta = 0$, where P_∞ reaches the maximum. For pullers, $\beta > 0$, P_∞ decreases with β until $\beta \cong 3$, where P_∞ saturates to $\sim 1/\sqrt{N}$, like pushers with $\beta < -1/10$.

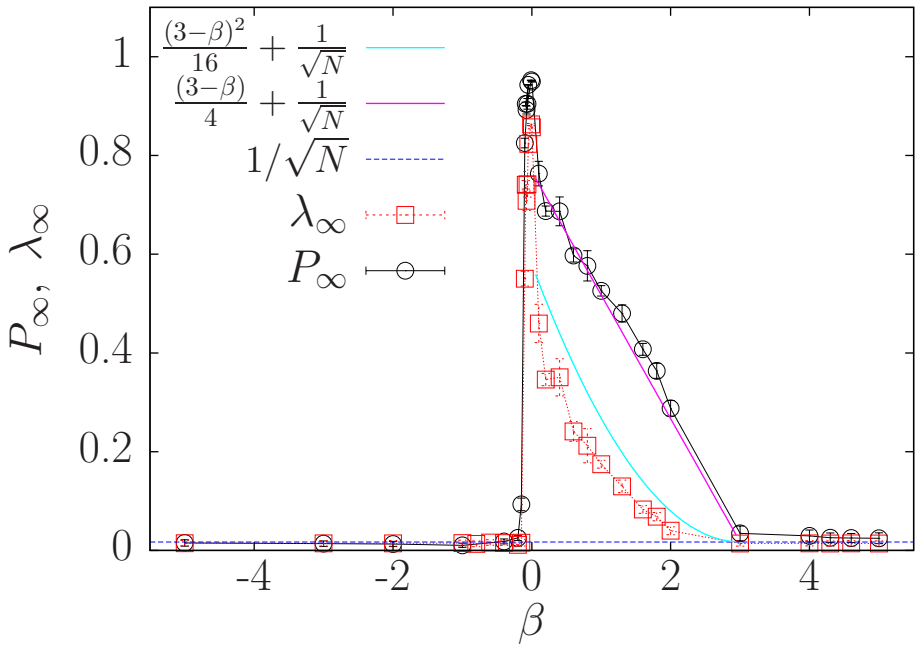

Figure 3.1: Long-time polar, P_∞, and nematic order, λ_∞, parameter for different values of β, ranging from -5 to 5. P_∞ correspond to black circles, while λ_∞ is represented by red squares. Particles with isotropic orientation will have $P_\infty \sim 1/\sqrt{N}$ hence we also show the blue dashed line for $1/\sqrt{N}$. P_∞ has a roughly linear decay in the region $0 \leq \beta \leq 3$, similarly λ_∞ has a quadratic behaviour in the same region of β. Pink curve is the linear fit for P_∞ while cyan curve the parabolic fit for λ_∞.

The value of P_∞ is very sensitive to the system size; this reason explains the difference with respect to the results reported in ref. [34], where $P_\infty > 1/\sqrt{N}$ for some pushers with $\beta < -1/10$ at the same $\phi = 0.1$, but with $N = 2000$ particles. We have verified that for an infinite system P_∞ remains finite (We have done a more detailed study on the finite size effects in section 3.7). The differences in the P_∞ here and the one shown in [34] comes from finite size effects, here the system size is bigger. Here we took $N = 3400$, while in [34] .

Since the system can have nematic order without polar order therefore, additionally to the polar order parameter, we have also computed the nematic order tensor, defined as

$$Q_{hk}(t) = \frac{1}{N}\sum_{i=1}^{N}\left(\frac{3}{2}e_{ih}(t)e_{ik}(t) - \frac{1}{2}\delta_{hk}\right); \tag{3.3}$$

for a $3D$ system [82], where h and k are x, y, z and N the total amount of squirmers. The nematic order parameter $\lambda(t)$ correspond to the largest eigenvalue of Q_{hk}. Similarly to the polar order, nematic order reaches a steady state $\lambda(t >> 0) = \lambda_\infty$ that we also plot in Fig. 3.1. Red squared symbols show us that nematic order is presented for the same β range than polar order and for pullers with λ_∞ decreases quadratically with β until $\beta = 3$. We always find $\lambda_\infty \sim P_\infty^2$, which means that we can consider that in semi-dilute suspensions of squirmers a polar-nematic phase emerges when $-1/10 \leq \beta \leq 3$, and an isotropic oriented phase develops otherwise.

3.3 Number fluctuations

As we pointed previously [34], squirmers can develop emerging flocking and display highly dynamic, mobile flocks or clusters that can form and re-form continuously in time. These structures generate fluctuations in the number of particles. To measure these fluctuations more systematically, we calculate the number fluctuations for different sub-system sizes for a given β, and analyze how fluctuations $\langle \Delta N \rangle$ grow with system size. We expect number fluctuations to grow as a power law of

$$\langle \Delta N \rangle \sim \overline{N}^{\alpha}, \tag{3.4}$$

where $\overline{N}$ is the mean of the number of particles in a given subsystem size. The fluctuations are proportional to $\sqrt{\overline{N}}$ when fluctuations are essentially uncorrelated, as is the case for systems in thermodynamic equilibrium, while active systems either experiments [83] or numerical simulations [84] have shown anomalous density fluctuations with $\alpha \geq 0.75$.

We have seen that α value depends on the β value as we show in Fig. 3.2 where α is plotted for the range $-5 \leq \beta \leq 10$. Pushers with $\beta \leq -1$ have an exponent $\alpha = 0.5$, then α starts to grow slowly as we increase β until $\beta = -0.1$ where $\alpha = 0.56$, then α increases abruptly in the region where pushers are partially aligned ($-0.1 < \beta < -0.01$ see Fig. 3.1) in this region α can reach values up to 0.69 when $\beta = -0.09$. Close to $\beta = 0$ we observe a drop to a rather small value of α, before it develops a maximum for $\beta > 0$. This sudden increase in α as the system changes from pusher to puller indicates the effect that the character of the

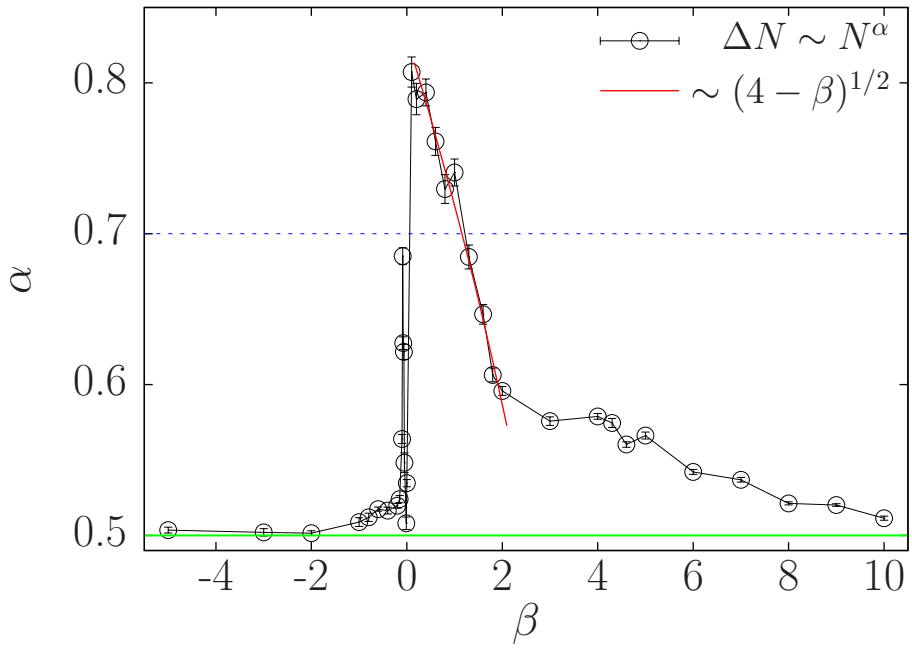

Figure 3.2: Black circles show the exponent α obtained by fitting the number fluctuations as a power law function $\langle \Delta N \rangle \sim \langle N \rangle^{\alpha}$ for different values of β. The green solid line is for $\alpha = 1/2$, which is the case of systems in equilibrium, while the blue dashed line represent $\alpha = 0.7$ which is the threshold we use to define whether the system has giant density fluctuations or just anomalous density fluctuation $(1/2 < \alpha < 0.7)$.

active stresses has on the global organization of the active squirmers. Similarly, for $\beta = 0$ the order parameters are $P_{\infty} = 0.95$ and $\alpha = 0.5$. This abrupt change in α is due to the fact that particles are stronger aligned $P_{\infty}(\beta \in [-0.01, 0]) = 0.95$. Pullers on the contrary, exhibit giant density fluctuations when $0 < \beta \leq 1$ and α decays with β as $\sim (4-\beta)^{1/2}$ up to $\beta = 2$. When $\beta > 2$, we observe a slower decay to $\alpha = 0.5$, we have reached $\beta = 10$ to get an exponent of $\alpha = 0.51$. In general, we can observe in Fig. 3.2 that exponent is not symmetric with respect to β, thus pushers and pullers behave in different ways. Therefore, we observe a strong sensitivity of the number fluctuations with the character of the active stress, while pushers exhibit essentially uncorrelated fluctuations, except in a narrow region close to $\beta = 0$ where a fast increase in α is observed, pullers show a very soft transition from giant to anomalous number fluctuations up to $\beta < 3$, follow by a regime where α slowly decays to $1/2$.

The value of $\alpha = 0.7$ is chosen as the crossover between giant to anomalous number fluctuation because once $\alpha > 0.7$, dynamic clusters are observed. Although the theory states that exponent $\alpha = 1/2 + 1/d$ for cases that exhibit giant density fluctuations [85], where d is the dimension of the system, recent results

have shown that bacterial colonies exhibit anomalous fluctuations with an exponent value $\alpha = 0.75 \pm 0.03$ [83], while simulations of self-propelled particles with either alignment rule [86] or not [12] the scaling exponent is 0.8 for cases associated with a phase separated state.

We have found that fluctuations on the density are not produced by finite size effects, on the contrary, when suspensions exhibit giant fluctuations ($\alpha > 0.7$), α increases as the system size increases as we show in Fig. 3.7 reaching $\alpha \sim 0.91$ for larger systems when $\beta = 0.5$. Therefore, we found a range $0 < \beta \leq 1$ where semi-dilute suspensions of pullers and even pushers with $-0.1 < \beta < -0.01$ can generate giant number fluctuations, there is also a range where alignment is very high such that all particles swim in the same direction uniformly ($\beta = \{-0.01, 0\}$), thus swimmers are not able to form density differences, which give us an exponent $\alpha = 0.5$. As well as pushers with $\beta < -0.1$ where particles are not aligned but the collisions between particles are uniform and the density of particles in the suspension is also uniform. While pullers with $\beta > 1$ generate anomalous number fluctuations and decay very slowly to $\alpha = 1/2$ as β increases. From Figs. 3.1 and Fig. 3.2, it is clear that the alignment produced by hydrodynamic interactions is a key mechanism to have induced fluctuations.

3.4 Emergent clustering in squirmer suspension

In this section we discuss the cluster size distribution. Squirmers exhibit clustering when they reach a steady state, this steady state is characterized by a constant polar order parameter. During this interval of time we calculate the distribution of the cluster sizes.

To identify the clusters we follow the methodology described in Appendix A. Once the clusters are identified, we calculate the fraction of clusters of size s, called $f(s)$. We have followed the criterion elaborated by Chantal, et al. [87]: First, the range of s-values are arbitrarily subdivided into intervals $\Delta s_i = (s_{i,max} - s_{i,min})$ and estimate the total number of clusters within each interval Δs_i, called n_i^t. Secondly, we assign the value of $n_i = n_i^t/\Delta s_i$ to every s within Δs_i. Thus, the total fraction of cluster is $N_c = \sum_i n_i \Delta s_i$ and the fraction of clusters of size s, $f(s) = n_i/N_c$, where s is the closest integer to the central value of $\Delta s_i = (s_{i,max} - s_{i,min})$. The details of the boundaries of the clusters size intervals are explicitly shown in Appendix A. We have found that the cluster size distribution for squirmers behave in general as:

$$f_b(s) = f(1)\ \frac{\exp(-(s-1)/s_0)}{s^{\gamma_0}} + B\ \frac{\exp(-(s-1)/z_0)}{s^{-\gamma_0}}, \tag{3.5}$$

with B, s_0, z_0 and γ_0 constants that depend on β. When $\beta \leq -0.1$, $B = 0$

and distributions are completely unimodal, described by only one power law with an exponential decay given by the fitted parameters s_0 and γ_0. For pushers, the exponent $\gamma_0 = 1.9$ and s_0 does not change significantly as β changes. CSDs for $\beta = -3$ up to -0.2 are plotted with symbols and fitted curves to the data are plotted with lines in the top-left panel of Fig. 3.3. Similarly, $B = 0$ for pullers when $\beta \geq 2$ and for the special case of $\beta = 0$, but $\gamma_0 = 2.15$ for $\beta \geq 2$ and $\gamma_0 = 2$ for $\beta = 0$. In the top-right panel of Fig. 3.3 we show the CSDs for $\beta = 0, 2, 3$. CSDs in these cases are thicker than the CSDs for pushers showed in the top-left panel.

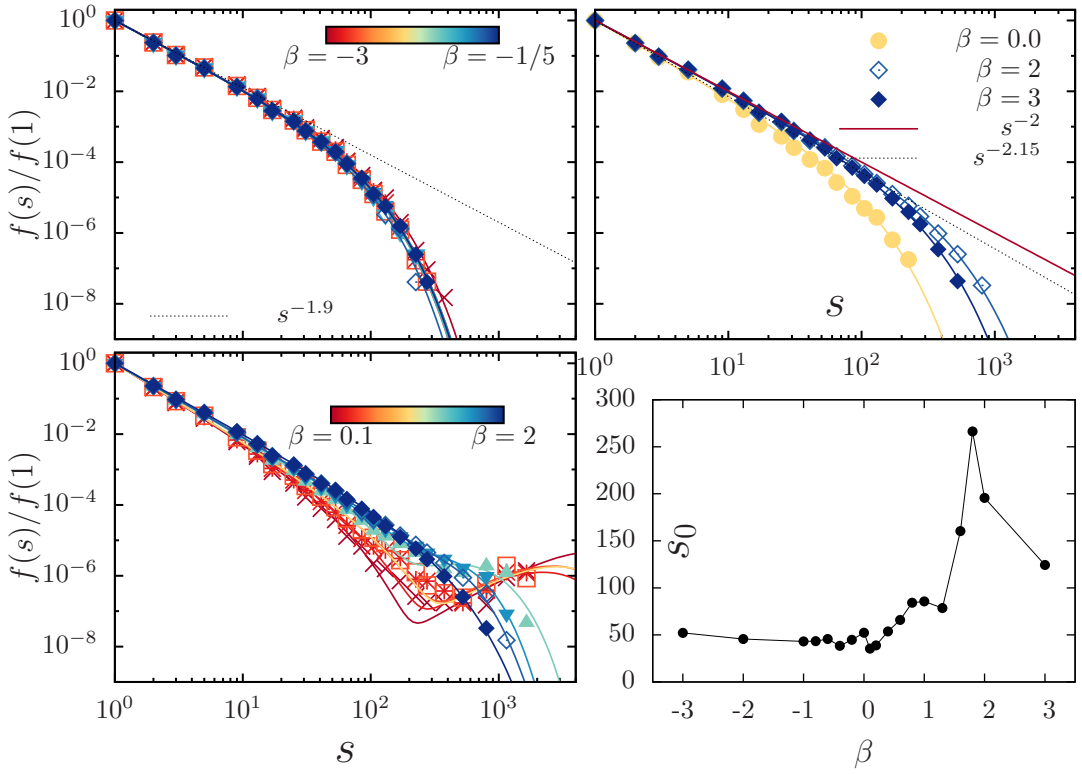

Figure 3.3: CSD of suspensions of squirmers for different β. All CSDs are fitting with an analytical bimodal distribution function of eq. (3.5). Top-left: CSDs for pushers. Top-Right: CSDs for $\beta = 0, 2, 3$. Bottom-left: CSDs for pullers in the range $0 < \beta \leq 2$. Bottom-right: Parameter s_0 as a function of β.

Cluster-size distributions of pullers with $0 < \beta < 2$, exhibit a bimodal behaviour, like the eq. (3.5) with $B \neq 0$, when $0 < \beta \leq 1$ the exponent $\gamma_0 = 2.2$ and prefactor $B \sim 10^{-13}$ with the exponential cutoff $z_0 \sim 1000$ (reddish curves in bottom-left panel of Fig. 3.3) while the range $1 < \beta < 2$ has an exponent $\gamma_0 = 2.075$ and prefactor $B \sim 10^{-10}$ with $z_0 \sim 100$ (blueish curves in bottom-left panel of Fig. 3.3). The exponential cut-off s_0 is plotted in the bottom-right panel of Fig. 3.3 as a function of β, s_0 is approximately constant for pushers with a

value around 50, while for pullers s_0 grows slowly when $\beta < 1$ and then it grows faster, until a maximum of $s_0 = 266$ at $\beta = 1.8$.

The bimodal cluster-size distributions observed for pullers with $\beta \leq 1$ (reddish curves in bottom-left panel of Fig. 3.3) reach cluster-sizes around $s \sim 1600$ particles, which is approximately half of the total amount of particles in the suspension. These clusters can be seen as macroscopic clusters.

3.5 Density-dependent speed

Although the macroscopic clusters, generated by some βs, can be understood as a phase separated state, the nature of this phase differs from the MIPS scenario [16], when macroscopic phase separation emerges as a result of a decrease of particle motility with concentration. In order to identify if hydrodynamic interactions can induce effective decrease in squirmer motility that can, indirectly, lead to the appearance of the macroscopic clusters reported, we have computed the local volume fraction for squirmers with $\beta = -1/2, 0, 1/2$.

The local volume fraction is calculated at the center of every particle in the system. Where we estimate the number of particles around every particle inside of a typical cut-off distance. The cut-off distance we have used is 3σ where σ is the diameter of the particles. Although the choice of the cut-off distance is arbitrary, from a systematic study, we have observed that either the probability distribution of the volume fraction or the density dependent speed does not depend on the cut-off distance, when the distance between 2σ and 4σ.

In Fig. 3.4a we show the probability distribution $PDF(\phi)$ of the local volume fraction for two types of squirmers, pullers with $\beta = 0.5$ (solid symbols) and pushers $\beta = -0.5$ (hollow symbols). Green diamonds correspond to the probability distributions for suspensions with a total volume fraction of $\phi_0 = 0.05$. For pushers the probability distribution ranges from 0 to 0.1, while pullers spread up to $\phi = 0.2$. The increase in the range of local values of ϕ is due to the emergence of large clusters in the system. Similarly, when the average volume fraction is $\phi_0 = 0.1$ (black symbols) pushers have a narrow distribution center in $\phi = 0.1$ while pullers have a wider distribution in which the local volume fraction fluctuates from 0 to 0.35, pullers with $\beta = 0.5$ and $\phi_0 = 0.05$ or 0.1 are suspensions where the macroscopic cluster emerges,

The pdf of the local volume of ϕ does not show a qualitative change when increasing the average volume fraction. The scale of the pdf displaces at large values of ϕ, as expected. However, we never observe that the pdf splits and develops two maxima, as if corresponds in the normal scenario of macroscopic phase separation.

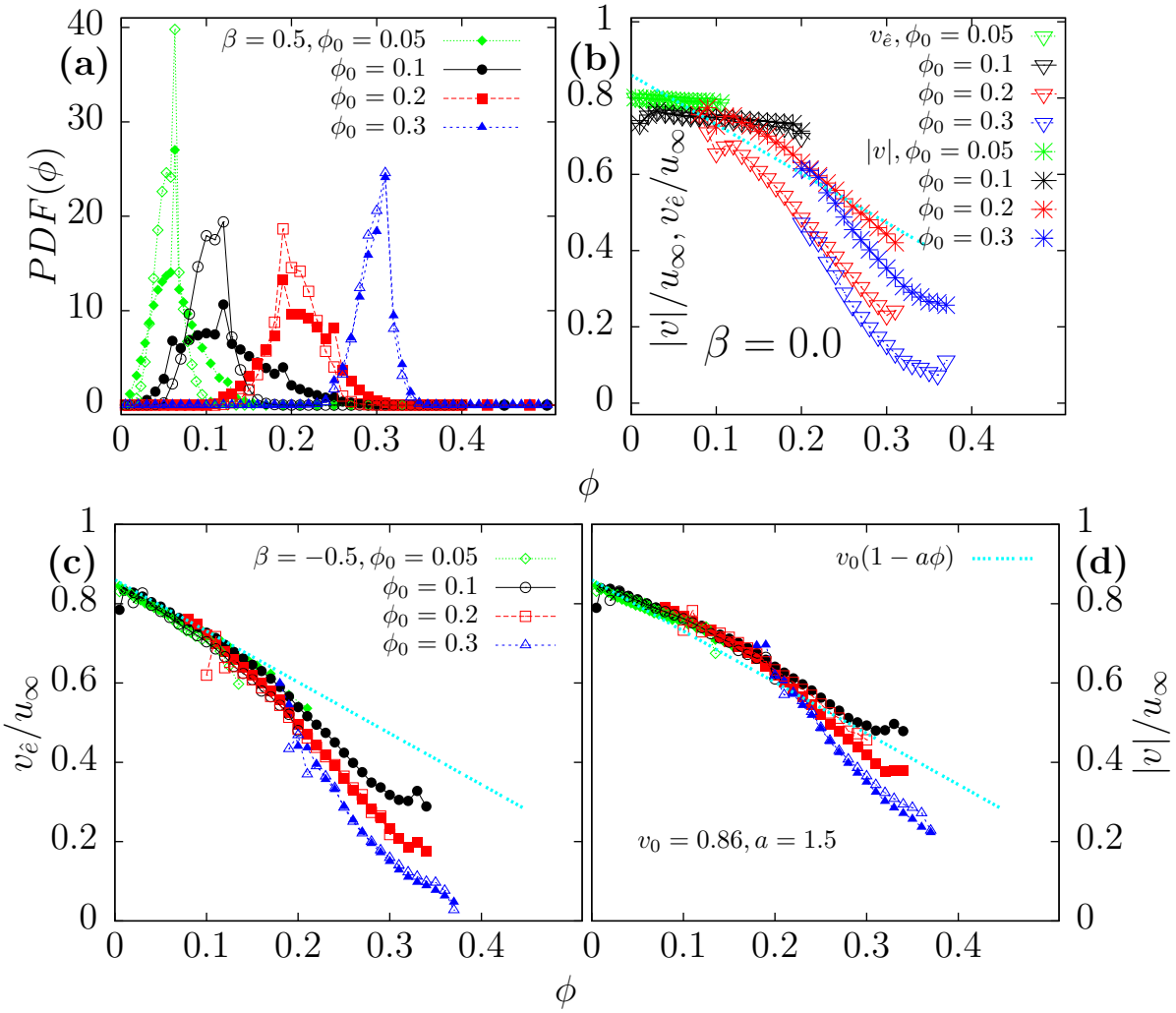

Figure 3.4: (a) Distribution profiles of the local densities for $\beta = \pm 0.5$ with different values of global density. Solid symbols are for pullers with $\beta = 0.5$ while hollow symbols for pushers with $\beta = -0.5$. (b) Density-dependent speed $|v(\phi)|$ and velocity projected to the orientational vector $v_{\hat{e}}(\phi)$ for squirmers with $\beta = 0$. Hollow triangles are $v_{\hat{e}}(\phi)$, stars are $|v(\phi)|$ and each color correspond to different total density ϕ_0. (c) Density-dependent velocity projected to the orientational vector $v_{\hat{e}}(\phi)$ for $\beta = \pm 0.5$. (d) Density-dependent speed $|v(\phi)|$ for $\beta = \pm 0.5$. All velocities are normalized by the asymptotic swim speed of a single squirmer $u_\infty = 2/3B_1$. Color and symbols maps are the same for (a),(c) and (d). Pullers are solid symbols, while pushers are hollow symbols.

Active matter exhibits a range of non-trivial behaviours, like giant density fluctuations [83, 88–90] and unexpected phase separations [8, 91–96] In particular for both ABPs and run-and-tumble bacteria [97, 98], the swim speed depend on the density and decreases with increasing density due to crowding. Hence, these

particles accumulate in regions where they move slowly and it causes further accumulation of particles. This motility-induced phase separation occurs without attractive interactions or orientational order and it has been confirmed in simulations [12, 13, 16], experiments [96] and by a continuum description for the structural evolution [16]. Given this theoretical framework, they have found that velocity dependent linearly with the density. In the cases of squirmers, where hydrodynamic interactions are taking in count, we have found that the system density affects the local particle motility, as we observe in Fig. 3.4b where the density-dependent speed $|v(\phi)|$ and the velocity projected to the orientational vector of squirmers $v_{\hat{e}(\phi)}$ changes as the concentration regime changes for $\beta = 0$.

For semi-dilute cases with $\phi_0 = 0.05$ and 0.1, both velocities do not depend on the local density, since all the suspension is aligned, although all particles move in the propulsion direction $|v(\phi)| = v_{\hat{e}(\phi)}$ this speed is less than $u_\infty = 2/3B_1$, due to the hydrodynamic field generated by neighbour particles. For a more concentrate case where $\phi_0 = 0.2$ or 0.3, speed and projected velocity depend on the local density and motility is reduced as local density increases. For $\phi_0 = 0.2$ $|v(\phi)|$ and $v_{\hat{e}(\phi)}$ follow a linear behaviour in their range of local densities where values are more relevant statistically. While $\phi_0 = 0.3$ case follows an asymptotic decay to a non-zero value. Which tell us that particles always move even for concentrated regimes where local density can reach values up to $\phi = 0.35$. Another important remark is the difference between the value of the speed and the projected velocity. Speed is always greater than projected velocity for a given density. This contrast correspond to the hydrodynamic flow around the particle that contributes to the total speed of the particle.

For squirmers with $\beta = \pm 0.5$, the velocity along the self propelled direction decays as a function of the local density as we observe in Fig. 3.4c, regardless of the average volume fraction. For $\phi_0 = 0.05$ (green diamonds), for both pushers and pullers $v_{\hat{e}(\phi)}$ decays linearly until $\phi = 0.15$ according to the cyan curve in Fig. 3.4c, then both cases decay faster, where pushers decay even faster than pullers due to the partial alignment of pullers. The same behaviour is found at higher volume fraction $\phi_0 = 0.1$ (black circles). On the contrary, for denser systems with total volume fraction of $\phi = 0.2$ projected velocity for either pushers or pullers decays almost in the same way, a tendency even more clearly seen at $\phi = 0.3$.

$|v(\phi)|$ for $\beta = \pm 0.5$ plotted in Fig. 3.4d, follows the same pattern than projected velocity. But as in $\beta = 0.0$, the speed taking in count the velocity induced to the particle by hydrodynamic flows around the particles. Thus, speed is greater than projected velocity for a given local density.

Phase separation is observed for active particles like ABPs or Run-Tumble bacteria even without attractive interaction or orientational order, and the distribution profile of the local densities in the phase separation region show a two

well defined coexistence densities [16], while the $PDF(\phi)$ for squirmers has a unimodal shape, where the thickness of the distribution depend on the hydrodynamic signature. When macroscopic clusters appears, the $PDF(\phi)$ is wider than other cases, this cluster is very dynamic and form and re-form very fast, therefore this loose cluster can not form a binodal state, like MIPS for active brownian particles in [16].

On the other hand, swim speed is affected by hydrodynamic interactions, since density-dependent speed changes as β changes. When squirmers are highly aligned with $\beta = 0$ and $\phi \leq 0.1$ both velocities do not change as local density change, otherwise velocities decay as density increases. This behaviour is due to the collisions as in ABPs, however squirmers do not follow a linear behaviour. We have also found that pullers with macroscopic clusters generate non-zero velocities, decaying very slow to zero at high density due to the orientational order, whereas the velocities of pushers and squirmers with higher average density decay faster to zero.

3.6 Mean Square Displacement

We want to analyse the squirmer dynamics as a function of their activity. In particular, we want to understand the impact that the global polarization observed for pullers has on squirmer motion. To this end, we concentrate first in the Mean Square Displacement (MSD) defined as

$$\left\langle \Delta r^2(t) \right\rangle = \frac{1}{N} \sum_{i=1}^{N} \left[\vec{r}_i(t) - \vec{r}_i(0) \right]^2 , \tag{3.6}$$

Where N is the total amount of squirmers in the suspension. In Fig. 3.5a we show the MSD for squirmers such as orientational order is absent, MSDs evolve from a initial ballistic regime to a linear one. Thus, we are able to determine the diffusion coefficient, by calculating the slope of the MSD at long-times, since according to the Eistein relation:

$$\frac{\langle \Delta r^2(t) \rangle}{\sigma^2} = 6D \frac{t}{t_0}, \tag{3.7}$$

where σ is the diameter of the squirmer, t_0 the time that a squirmer needs to travel one diameter at velocity $u_0 = 2/3B_1$ and D the diffusion coefficient. We observe that diffusivity decreases as $|\beta|$ increases, as we can see in the inset of Fig. 3.5a, consistent with other previews observations with a small system ($N = 64$) of squirmers at the same concentration [28]. When a finite fraction of the squirmers show orientational order, we see that the MSD behaves super-diffusively at long

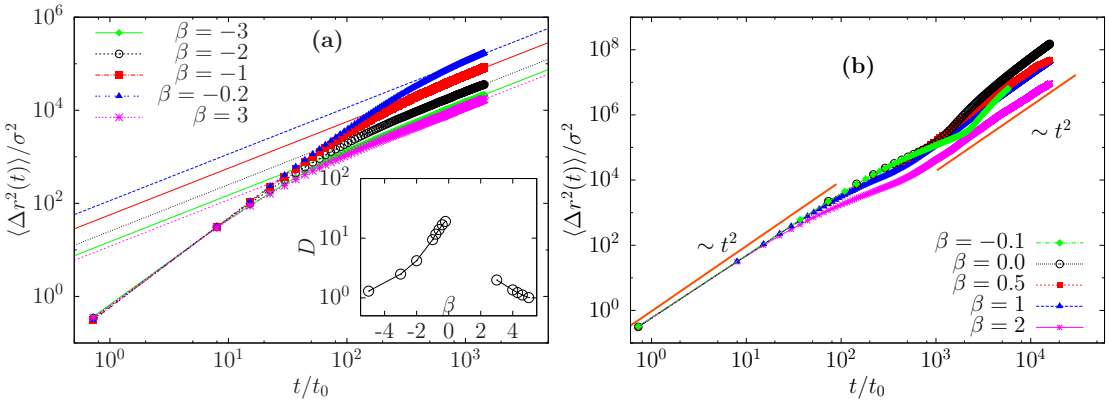

Figure 3.5: (a) Mean-squared displacement for squirmers without alignment, lines correspond to a linear fitting at long t when diffusive regime ($\Delta r^2(t) \sim t$) is present. Inset: Diffusion coefficient as a function of β. D is only defined when suspension has a diffusive behaviour. (b) Mean-squared displacement for aligned squirmers for β between $-0.1 \leq \beta \leq 2$. Orange solid line describe the ballistic regime.

times (Fig. 3.5b), the evolution of the MSD to a super-diffusive regime is a consequence of the hydrodynamic field generated by the squirmers.

In Fig. 3.5a MSDs evolve to a diffusive regime at $t > 10^2 t_0$ and remain in this regime, whereas in Fig. 3.5b MSDs evolve to a transient diffusive regime follow by a crossover to a steady super-diffusive regime.

The precise time where the crossover to diffusive regime occurs will depend on β. The greater the value of $|\beta|$ the shorter the time to diffusive regime. Similarly, the time of crossover to super-diffusive regime also vary with β. The time that squirmers spend in the transient diffusive regime coincides with the time that polar order needs to reach the steady state where $P(t) = P_\infty$.

3.7 System size analysis

Given the proven accuracy of the Ludwig code [77] we are able to reach 3D periodic systems with edge length up to 1280 node-node distance, thus we have studied semi-dilute squirmer suspensions with a total number of particle up to $\sim 4 \times 10^6$. We show in this section how the polar order, exponent of the number fluctuations, CSD and MSD depend on the system size. We found that orientational order, giant number fluctuations, the emergence of a macroscopic cluster and the super-diffusive regime at long-times are all intrinsic to the hydrodynamic signature and not to the system size.

3.7.1 Polar Order

We show that polar order decrease with the system size, but it reaches an asymptotic value at large N. When $\beta = 0.5$ (purple circles in Fig. 3.6) P_∞ goes from 0.77 at $N = 514$ to an asymptotic value of 0.16 when $N \approx 10^6$. Analogously, at $\beta = 1.6$ P_∞ drop from 0.47 to 0.17 when $N = 263500$, in this case we can not conclude whether the polar order goes to zero or to a constant value as $\beta = 0.5$ (yellow squares in Fig. 3.6). But, for cases where $P_\infty \approx 1/\sqrt{N}$ at $N = 3400$ like pushers with $\beta = -0.5$, or pullers with $\beta = 3$ they still have the $1/\sqrt{N}$ dependency as the system grows, as we show in (blue circles and green squares in Fig. 3.6). The general drop in the long-time polar order that we observe for the different values of β as the system size grows, explain why Ishikawa et al. in [30] and Evans et al in [31] have reported higher values of the polar order for different values of β, since they have used systems with $N = 64$ particles, whereas us in [34], we have used $N = 2000$ in which there is a higher value of P_∞ in comparison with Fig. 3.1 where we have used $N = 3400$. Additionally, Delmotte

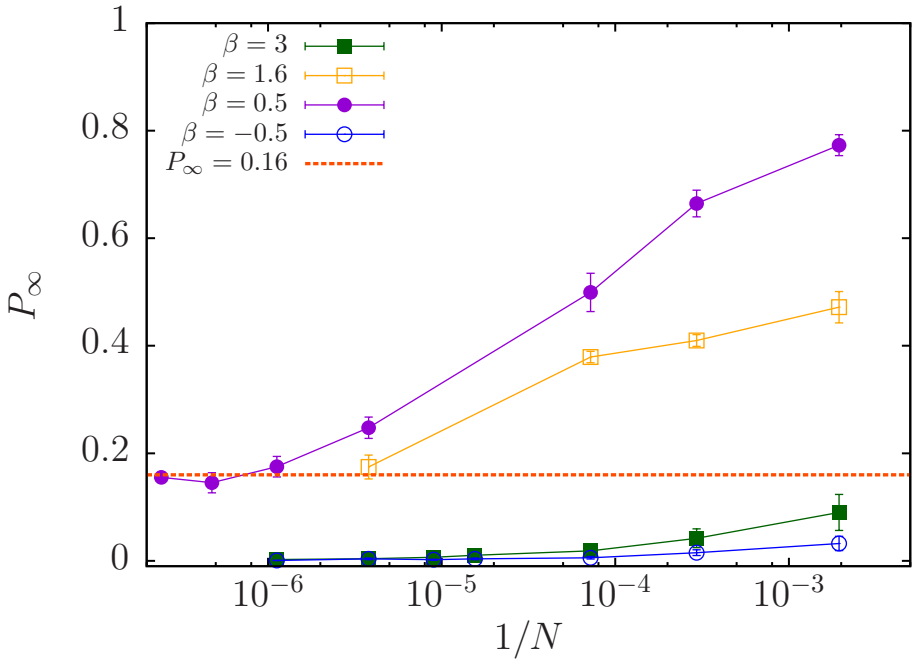

Figure 3.6: Long time polar order as a function of the system size for different βs.

et al. in [81] have examined how the system size affects to the polar order of a semi-dilute suspension of pullers with $\beta = 1$, they were able to reach system sizes of $N = 37690$ squirmers with $L/a = 116$, where a is the particle radius and L the edge length of the simulation box, they found that long time polar order reaches an asymptotic value of $P_\infty = 0.452$. In particular, when $N = 11158$, $L/a = 77$

the value of $P_\infty \approx 0.46$ while in our case, we have found that $P_\infty = 0.50 \pm 0.03$ for $\beta = 0.5$ and $P_\infty = 0.38 \pm 0.01$ for $\beta = 1.6$ at approximately, the same system size of $N = 13890$, $L/a = 83$. Therefore both methodologies are in agreement for the same system size.

However, since we are able to reach sizes of $N \approx 4 \times 10^6$, $L/a = 556$ we observe that long-time polar order drops even further, and it reaches a constant value of $P_\infty = 0.16$ for $\beta = 0.5$, thus one can expect that pullers with $\beta = 1$ should has a value of $P_\infty < 0.16$.

3.7.2 Number fluctuations

In the same way we calculate the number fluctuations for different values of β in section 3.3, here we calculate the number fluctuations for different system sizes. Since $\Delta N \sim N^\alpha$, we have found that the exponent α grows slowly with the system size, reaching or approximately reaching a plateau, the value of α in the plateau depend on β. For pullers with $\beta = 0.5$ we found that α grows from 0.78 for $N = 2000$ to 0.92 ± 0.01 for $N = 2 \times 10^6$ (purple circles in Fig. 3.7), which means that giant fluctuations are enhanced when the system grows. When $\beta = 1.6$ (yellow squares in Fig. 3.7) we also see that anomalous fluctuations observed for $N = 3400$, where $\alpha = 0.657 \pm 0.006$ are enhanced, reaching $\alpha = 0.81 \pm 0.01$ for $N = 263500$, the number fluctuations however are clearly smaller than for $\beta = 0.5$. When $\beta = 3$ (green squares in Fig. 3.7), exponent α reaches a plateau very quickly at $\alpha = 0.59$ once $N \geq 13890$, in the same way for pushers with $\beta = -0.5$ (blue circles in Fig. 3.7), where α remains around 0.5 for all the system sizes.

The fluctuations in the density are not a finite size effect at all for squirmer suspensions. In fact, anomalous and giant fluctuations are enhanced by the increment on the size of the system, as we observe in Fig. 3.7 for $\beta = 0.5$ and 1.6. This effect tell us that giant number fluctuations are generated by correlations between the squirmers at really long distance and these correlations emerge due to the hydrodynamic signature, since only with two of four values of β are observed.

3.7.3 Clustering

As we show in section 3.4, when $\beta \leq 1$ the CSDs have a local maximum for clusters-sizes around $s \approx N/2$ (reddish curves in bottom-left panel of Fig. 3.3). The development of large clusters is very sensitive to the system size therefore, we have had to carry a systematic analysis of the dependency of the CSD on the system size to identify the intrinsic tendency of squirmer suspensions to form clusters. In order to measure the size of the clusters, we have calculated the CSD,

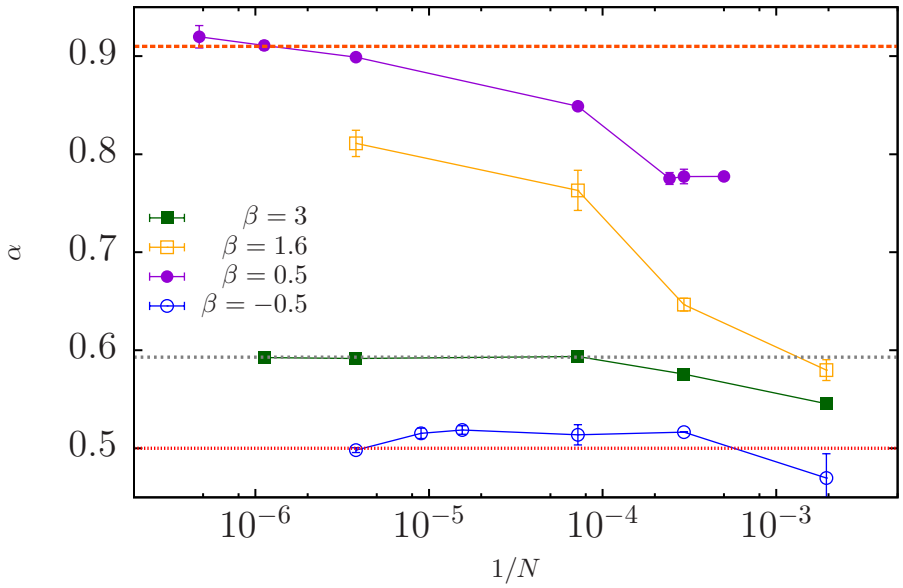

Figure 3.7: Exponent α as a function of the system size for different βs.

in in Fig. 3.8 we show the CSDs for various system sizes at a fixed volume fraction of $\phi = 0.1$, and fixed puller strength $\beta = 0.5$.

The CSD is the average fraction of clusters $f(s)$ composed by s particles. When the system has a number of particles $N \sim 10^3$ (green diamonds in Fig. 3.8) the maximum cluster size is 1600, the CSD follows a continuum function and it can be approximated by the bi-modal function defined in Eq. (3.5) where $\gamma_0 = 2.5$, s_0 and z_0 controls the exponential cut-off of the first and second peak of the bimodal distribution respectively [6, 7].

If we increase the system size to $N = 13890$ (black hollow circles on Fig. 3.8) the maximum cluster size also increases to 6000 particles. Moreover, although CSD keeps the same bimodal shape it breaks in two sections, since cluster sizes of 1500 to 3000 are not observed.

When the total number of particles grows one order of magnitude, with $N = 263500$ (red squares on Fig. 3.8), we observe that CSD has the same behaviour of eq. (3.5) for cluster sizes up to 5000 and a range of big cluster sizes that emerge around 10^5 but with a lack of clusters of sizes between 5000 and 3×10^4. If system grows even further to $N \sim 8 \times 10^5$ (blue triangles on Fig. 3.8) CSD behaves like the previous smaller system with a larger lack of cluster-sizes from 5000 to 4×10^5 and for even larger system of $N \sim 2.1 \times 10^6$ the CSD remains with the same behaviour as eq. (3.5) but the lack of cluster-sizes goes now from 6000 to 10^6.

This striking effect tell us that squirmer suspensions with $\beta = 0.5$ can generate a phase with two coexistence states, one state made of microscopic clusters of sizes

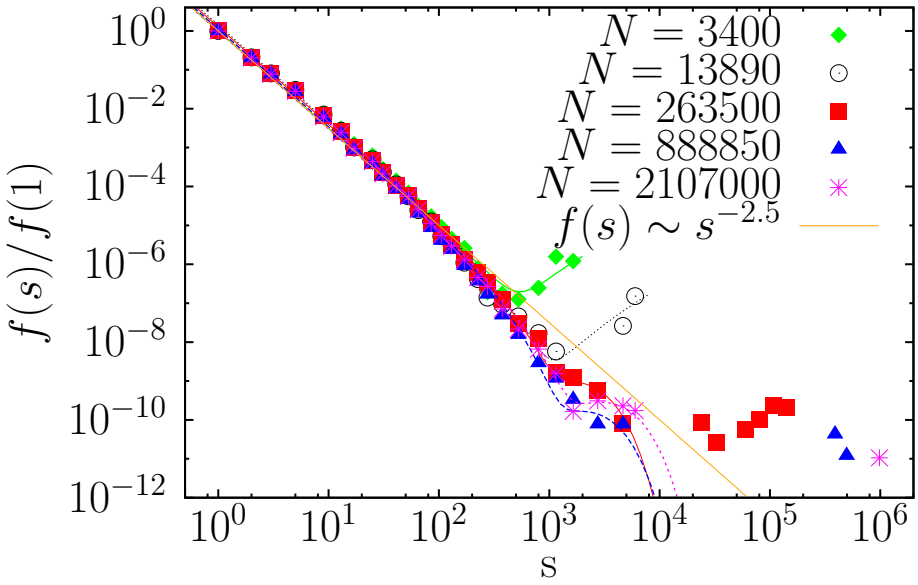

Figure 3.8: Normalized CSD of suspensions of squirmers with $\beta = 0.5$ for different system sizes. For large enough systems, a macroscopic cluster of size comparable to the system size emerges. All CSDs are fitted with an analytical bimodal distribution function, Eq. (3.5). In all the CSDs, the values of the parameters used to fit the bimodal distribution show a weak dependence on system size. The fitted parameters are very similar, $s_0 \approx 10^2$, $10^{-18} \leq B \leq 10^{-14}$, $z_0 \approx 10^3$ and $\gamma_0 = 2.5$. Yellow solid line is the power law function $f_b(s) = 1/s^{2.5}$ depicted here as a reference.

up to 6000 in which the size distribution does not change with the system size and a macroscopic cluster made of $N/2$ particles.

The formation of this macroscopic cluster is driven by the competition between the hydrodynamic signature and the global density. In other words, it is due to the re-orientation of the particles given by the hydrodynamic field around them and the number of collision between particles given by the amount of particles in the suspension.

3.7.4 Mean Square Displacement

At $\beta = 0.5$ we observe giant number fluctuations and orientational order, therefore mean-squared displacement performs multi-crossover. But the striking effect comes when we enlarge the system from $N = 3400$ to $N = 2107000$. As we show in Fig. 3.9, the second crossover, from diffusive to super-diffusive motion depend on the system system size. When the system is not so big $N = 3400$ diffusive time is very short and and second crossover is around $t/t_0 = 500$, this time increases

with the system size, the black circles represents $\Delta r^2(t)$ with $N = 13890$ where the second crossover is at $t/t_0 = 600$, the red squares where diffusive time is even longer for $N = 263500$ and it last until $t/t_0 \sim 1000$, while $N = 888850$ last until $t/t_0 \sim 2500$. For larger systems we are not able to see the second crossover.

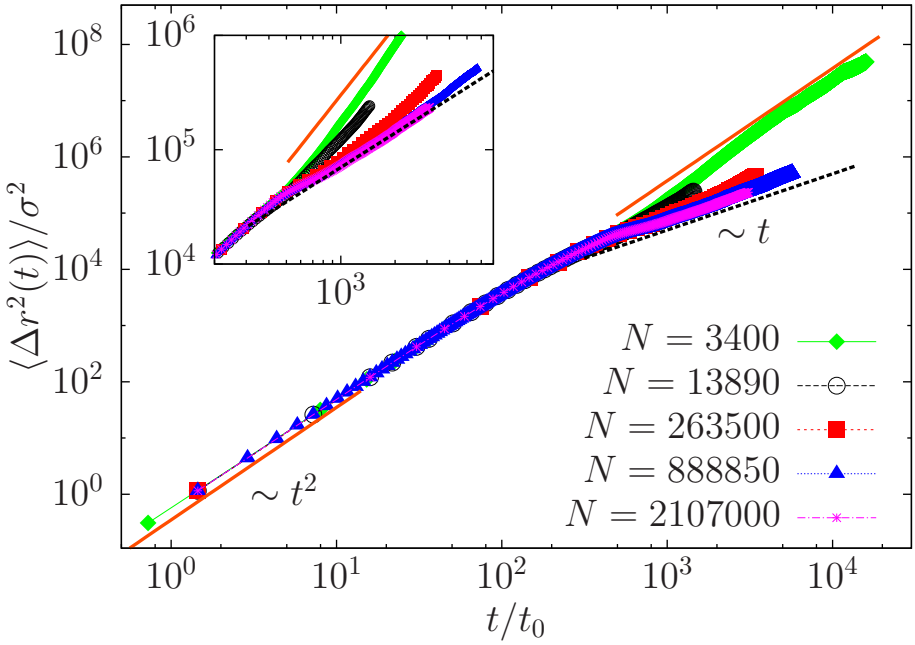

Figure 3.9: Mean-squared displacement for $\beta = 0.5$ and volume fraction $\phi = 0.1$, for different system sizes. Inset: Zoom-in of the MSD at long times, to observe the cross-over of the MSD from ballistic to diffusive regime and ballistic again. Orange solid line describe the ballistic regime, while gray dashed line the diffusive regime.

Since first crossover from ballistic to diffusive motion occurs at the same time for every size, we can say that this effect is driven mainly by the collisions among the particles that only depend on the volume fraction, while the second crossover is driven mainly by the long range hydrodynamic flows generated by the same particles. Although the diffusive time vary with the system size, the emergence of alignment and the macroscopic cluster in the suspension is generated independently on the size.

3.8 Conclusions

In summary, we have used Lattice-Boltzmann methodology to carry out simulations of semi-dilute squirmer suspensions, where hydrodynamic interactions are

taking in count explicitly. A systematic study in terms of the hydrodynamic signature was developed, we found that polar order and number fluctuations depend on β. Suspensions with Giant Number Fluctuations generate dynamic clusters that it can consider as a macroscopic cluster after a systematic study in terms of the system size, the mechanisms which driven to this phase separated phase are totally different than the mechanisms for other active systems without hydrodynamic interactions [15, 16].

Furthermore in general, aligned suspensions develop a multi-crossover Mean Square Displacement, where suspensions reach a super-diffusive motion at long-times. Ishikawa and Pedley [29] also found anomalous diffusion for small $|\beta|$, they studied the spreading of squirmers in non-uniform suspensions and they said that this ordering phenomenon may be interpreted as a taxis towards lower cell concentration. Therefore, dynamic clusters could be related with the taxis towards lower concentration of particles.

Chapter 4

Swimming and interacting in a plane.

4.1 Introduction

In this chapter we present a systematic study of the phase behaviour of attractive particles swimming in 2D, but taking in count hydrodynamic interactions in 3D and we compare our results with active Brownian particles in 2D simulated including both translational and rotational diffusion.

We have used various analysis tools, either static measures for morphological studies like cluster-size distribution and radius of gyration or more dynamic parameters as the translational and rotational velocity of the clusters.

There have been several recent studies in 2D evaluating the phase behaviour such as Ref. [24] where the authors simulate 2D swimmers and found that phase separation is suppressed by hydrodynamic interactions, or in Ref. [25] where the authors simulate swimmers strongly confined by walls in a quasi-2D geometry and observe a phase separation at high concentration. On the other side, the authors of Ref. [26] show that squirmers swimming on a plane without walls can indeed form aggregates with an orientational order, in accordance with a previous result obtained by Llopis and Pagonabarraga [27].

Inspired by experiments with particles [9] and bacteria [99] which exhibit an attractive interaction, numerical studies have been carried out using Brownian dynamics simulations in three dimensions [100, 101] and two dimensions [95]: more recently Matas-Navarro and Fielding studied the influence of hydrodynamic interactions among self-propelled attractive disks, both on clustering and phase behaviour. In their work, they also compared with the phase behaviour of active Brownian particles without translational diffusion coefficient [102].

Even though the authors of Ref. [102] performed a systematic study of Attractive Brownian particles and squirmers in 2D for several densities, here we focus in the low densities regime, where it has been shown in Ref. [103] that the nature of the instability is different for pushers and pullers and in Ref. [100] that a dilute suspension of attractive Brownian particles form clusters when attraction competes with activity.

According to the squirmer model, explained in chapter 2, the velocity on the surface of the squirmer defined as the flow velocity in the particle surface $\mathbf{u}|_{r=R_p}$

$$\mathbf{u}|_{r=R_p} = [B_1 \sin\theta + B_2 \sin\theta\cos\theta]\,\boldsymbol{\tau}, \tag{4.1}$$

where $\boldsymbol{\tau}$ is a unit vector tangential to the surface of the particle.

To start with, we study a semi-dilute two-dimensional system of self-propelled Lennard-Jones particles taking into account hydrodynamics interactions (with Lattice Boltzmann). Next, we compare our results to numerical simulations of Brownian self-propelled disk particles.

In a suspension of Lennard-Jones active colloids, each colloid experiences two antagonist forces, i.e. attraction (F_{LJ}, due to the Lennard-Jones interaction) and self-propulsion (F_d):

$$\xi = \frac{F_d}{F_{LJ}}, \tag{4.2}$$

where $F_d = 6\pi\eta R_p v_s$, being η the system's viscosity, R_p the radius of the colloid, $v_s = \frac{2}{3}B_1$, v_s is the asymptotic velocity reached for one single particle as we explain above. Whereas F_{LJ} is the attractive force due to the Lennard-Jones interaction, at distance where attraction is maximum. Thus

$$F_{LJ} = -\nabla V(r_{ij})|_{\frac{d\nabla V(r_{ij})}{dr_{ij}}=0} \tag{4.3}$$

and

$$V(r_{ij}) \quad = \quad 4\epsilon\left[\left(\frac{\sigma}{r_{ij}}\right)^{12} - \left(\frac{\sigma}{r_{ij}}\right)^{6}\right]; \tag{4.4}$$

where σ is the particle's diameter.

For every value of ξ, the active suspension was simulated for 10^6 LB time steps, where the time unit is the time needed for an active particle to move a distance of one diameter that corresponds to $10^6/t_0$, being $t_0 = \frac{\sigma}{v_s}$ where σ is the particle diameter and $v_s = \frac{2}{3}B_1$ the asymptotic active particle's velocity. Hence, the total simulation time is 1450 (up to 3000 in few runs), to estimate the cluster size distribution we used a time window between 1000 and 1400 (or between 2600 and 3000) depending on how fast the steady state is reached. Whereas for the

Brownian case, we simulated the system from $\xi = 0.7$ up to $\xi = 4$. Active particle suspensions are systems out of equilibrium where big correlations in size emerge, therefore in numerical simulations, it is of paramount importance to model big systems. With Lattice-Boltzmann method we are able to simulate systems that are big enough that we can avoid finite size effects, we have used a Lattice Boltzmann code which includes moving particles via domain decomposition and parallelization (using MPI) [76]. Thanks to the efficiency that it has to run on high performance hardware and the advantage at the level of the modelling approach.

In this paper the system consists of a quasi two-dimensional diluted suspension of N= 10 000 self-propelled particles interacting via a truncated and shifted Lennard-Jones, like eq. (4.4), where the potential is shifted so that $V(r_{ij}) = 0$ at $r_{cut} = 2.5\sigma$. We have set the particle diameter σ to 4.6 lattice node-to-node distance [74].

The concentration is set to $\phi = 0.10$ (where $\phi = \pi/4\rho\sigma^2$, $\rho = N/L^2$ and L the simulation box edge). In order to simulate a quasi two-dimensional system, we prepare a $L \times L \times k\sigma$ box and impose to each particles that its contributions to the translational velocity $v_z = 0$ and to the rotational velocity $\omega_x = \omega_y = 0$. In the simulations with hydrodynamics, the slab is thicker than a particle diameter ($k = 5$). The main reason being the use of a cell list to compute the colloid-colloid interactions [1]. Whereas in the simulations without hydrodynamics, we model 2D active Brownian particles where $k = 0$. In either case, we did not take into account the presence of confining walls like in Ref. [25]. The setting of $k = 5$ will influence in the hydrodynamic effects over the suspensions, thus we avoid a strong confinement which would screen hydrodynamics interactions. This slab system is also different than the 2D case of attractive squirmers of Ref. [102]. Where squirmer model is purely 2D.

To simulate the squirmers, we did not use any kind of thermal fluctuations: velocity fluctuations were simply induced by the particles' activity (with $B2$), even in out of equilibrium, and acted as an effective temperature when competing with conservative forces [102, 104].

To avoid finite size effects, we have used a box size L about 35 times r_{cut}. (As a double check, we have also run simulations for larger systems where we observed the same behaviour).

For the Brownian dynamics simulations, the active disks are represented by

[1] When using **Ludwig** [77] to simulate hydrodynamically interacting particles, we should stress that the program uses a cell list to compute particle-particle interactions (that scales as $O(N)$). For efficiency purposes, one should set the size of the cell list as small as possible, always making sure to capture all possible interactions. Since the maximum interaction distance is the LJ cutoff (2.5σ), and the cell list size should be larger than the cutoff distance, we consider at least two cells per processor domain, which corresponds to a slab's thickness larger than 5σ.

their positions and self-propulsion directions $\{\mathbf{r}_i, \theta_i\}$ for $i = 1$ up to N. These positions and directions satisfy the coupled overdamped Langevin equations,

$$\dot{\mathbf{r}}_i = D\beta \left[\boldsymbol{F}_{LJ}\left(\{\mathbf{r}_i\}\right) + F_p\hat{\boldsymbol{\nu}}_i\right] + \sqrt{2D}\boldsymbol{\eta}_i^T, \tag{4.5}$$

$$\dot{\theta}_i = \sqrt{2D_r}\eta_i^R. \tag{4.6}$$

Where $\boldsymbol{F}_{LJ}$ is the force given by the Lennard-Jones potential in eq. (4.4). F_p is the magnitude of the self-propulsion force which, in the absence of interactions, will move a particle with speed $v_p = D\beta F_p$, $\hat{\boldsymbol{\nu}}_i = (\cos\theta_i, \sin\theta_i)$ and $\beta = \frac{1}{K_B T}$. D and D_r are translational and rotational diffusion constants, which in the low-Reynolds-number regime are related by $D_r = 3D/\sigma^2$. The η_i^R are Gaussian white noise variables with $\langle\eta_i(t)\rangle = 0$ and $\langle\eta_i(t)\eta_j(t')\rangle = \delta_{ij}\delta(t - t')$.

One can represent a β-ξ state-diagram (being $\beta = \frac{B_2}{B_1}$ the active stress parameter defined above) showing that the suspension's collective behaviour dramatically changes depending on the chosen value of ξ for a given β. For large values of ξ either isotropic or aligned suspension can be found depending on the hydrodynamic signature of the squirmers. When $0 < \beta < 1$ an aligned state is more stable whereas an isotropic state is stable otherwise. As a matter of fact, aligned state tends to promote flocking in the semi-dilute suspension as we have commented in previous chapter. When ξ is small enough so attraction and propulsion compete, as observed in Ref. [100], particles can form a steady-state cluster distribution. If the interaction strength is too strong, hence ξ is very small and the squirmers coarsen into a macroscopic cluster.

Therefore we have basically three general scenarios, one when flocking emerges due to the hydrodynamic interactions and attractive interactions are almost negligible, a second one when clustering emerges due to the competition between activity and attractive interactions and finally a last scenario when attraction between particles dominates and coarsening emerges. The last two scenarios are observed in either micro-swimmer and self-propelled Brownian particles.

We prepare the system with ξ ranging from the purely hydrodynamic case ($\xi = \infty$) to the cases where attraction dominates more and more (i.e. $\xi = 6.03$, $\xi = 1.8$ and $\xi = 0.6$). Since ξ is directly proportional to B_1 and inversely to ϵ, changing the value of ξ corresponds to setting the value of B_1 ($B_1 = 0.01$) while changing the depth of the attraction. The choice of $B_1 = 0.01$ is motivated from the need to have the same Reynolds number (Re) in all simulations, (since Re is proportional to B_1). Our choice of B_1 is a compromise between considering a low Re while reducing the computational time needed to reach "steady state".

For every value of ξ we select different values of β ranging from -3 to 3. This

chosen interval allows us to observe in the suspension different behaviours: one where the long range polar order is practically zero, i.e. the system is isotropic, and another (when $0 < \beta < 1$) where the long range polar order of the system is different from zero, i.e. the system is aligned [34].

In what follows, we will perform a cluster analysis, where we compare results computed for $1 < \xi \leq 6$ and $\xi = \infty$ analysed in the same time interval. To improve the statistics, we group same-size clusters (identified over the entire time-window) in bins (see Appendix A.1), as in Ref. [87] and compute the average values within each bin of the following quantities: the cluster-size distribution, the clusters' radius of gyration, the polar order within a cluster and particles' orientation with respect to their translation velocity within a cluster.

4.2 Mean Cluster size

Given that neither the mean cluster size nor the global polar order should change when the system reaches a steady state, we could make use of them to know whether the system is in a steady state or not. Mean cluster size and the global polar order [34] should not change with time once the system reaches a steady state. Having identified all clusters in the system (for every time step) by means of the procedure described in the Appendix A, we start with calculating the mean cluster size in each time frame.

We observe three possible scenarios. In the first one, identified when $\xi < 1$, the suspension shows a coarsening behaviour (as shown in the Figure 4.1 top, representing the mean cluster size for $\xi = 0.6$ and different values of β). Despite of the hydrodynamic signature, we always identify coarsening, as shown by the fact that the mean cluster size for $\xi = 0.6$ is monotonically increasing up to $t/t_0 = 10$:

this implies that the competition between activity and attractive interaction dominates coarsening leading to a dependence as $t^{1/2}$ independently of β. For longer times, the stress originated by the squirmers, competes with attractive interactions, thus affecting coarsening, since a suspension with $\beta = 3$ coarsens faster than a suspension with pushers with $\beta = -3$ (whereas for smaller values of β the difference between pushers and pullers is negligible). It is important to stress that B_2 is the one responsible for the velocity of coarsening but not for the coarsening mechanism.

This behavior is more evident when $\xi = 0.7$ (Fig. 4.1, bottom) where pullers coarsen whereas pushers evolve towards a steady state.

It has been already shown [102] that coarsening for 2D squirmers with $\beta = 0$ follows $t^{2/3}$, which corresponds to diffusive aggregation, whereas we have just

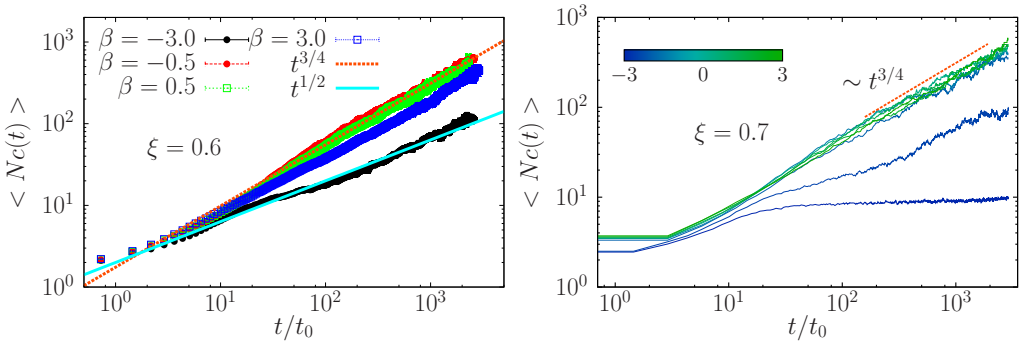

Figure 4.1: (Top) Mean cluster size as a function of time for $\xi = 0.6$. Dashed orange and solid cyan curves represent $\sim t^{3/4}$ and $t^{2/3}$ respectively. (Bottom) Mean cluster size for $\xi = 0.7$, with β between -3 and 3, the bluer the curve the smaller the value of β. When squirmers coarsen (all cases except $\beta = -3$) $\langle N_c(t) \rangle \sim t^{3/4}$ as in $\xi = 0.6$.

demonstrated that spherical squirmers on a plane show a crossovers at different time scales.

The other two scenarios can be identified when activity dominates (for $\xi > 1$). In this case suspensions either reach very quickly a steady state or the mean cluster size has an oscillatory behavior, depending on the hydrodynamic signature.

In Figure 4.2 we represent the evolution in function of the time of the mean cluster-size for different cases of squirmers with $\xi = 1$ and β from -3 to 3. On the top side, we have the cases of Brownian particles at different interaction strength, where coarsening is not presented. We can observe that mean cluster size evolve to a steady value that range from 7 for $\xi = 4$ to a mean cluster size of 60 to $\xi = 1.6$.

Next, we represent the mean cluster size for $\xi = 1$ when hydrodynamics interactions are considered for several values of β (bottom panel in Figure 4.2). We observe that pullers and $\beta = 0$ suspensions coarsen while pushers suspensions reach a steady state. Within the chosen parameter space, we could not find mean cluster sizes larger than 10 particles. This is in contrast to what happens in the Brownian cases, where the mean cluster sizes are larger than 10 particles (when attractive interaction strength competes with the activity).

We now focus on the suspension with hydrodynamics interactions and increasing value of ξ. When $\xi = 1.8$ (top-left panel in Figure 4.3) coarsening disappear even for pullers, and a steady state cluster sizes distribution is reached for all squirmers. The stress activity dictates the magnitude of the average cluster size, since pullers form larger clusters than pushers. If we now increase ξ even further (top-right panel of Figure 4.3), once more we observe all systems reaching a

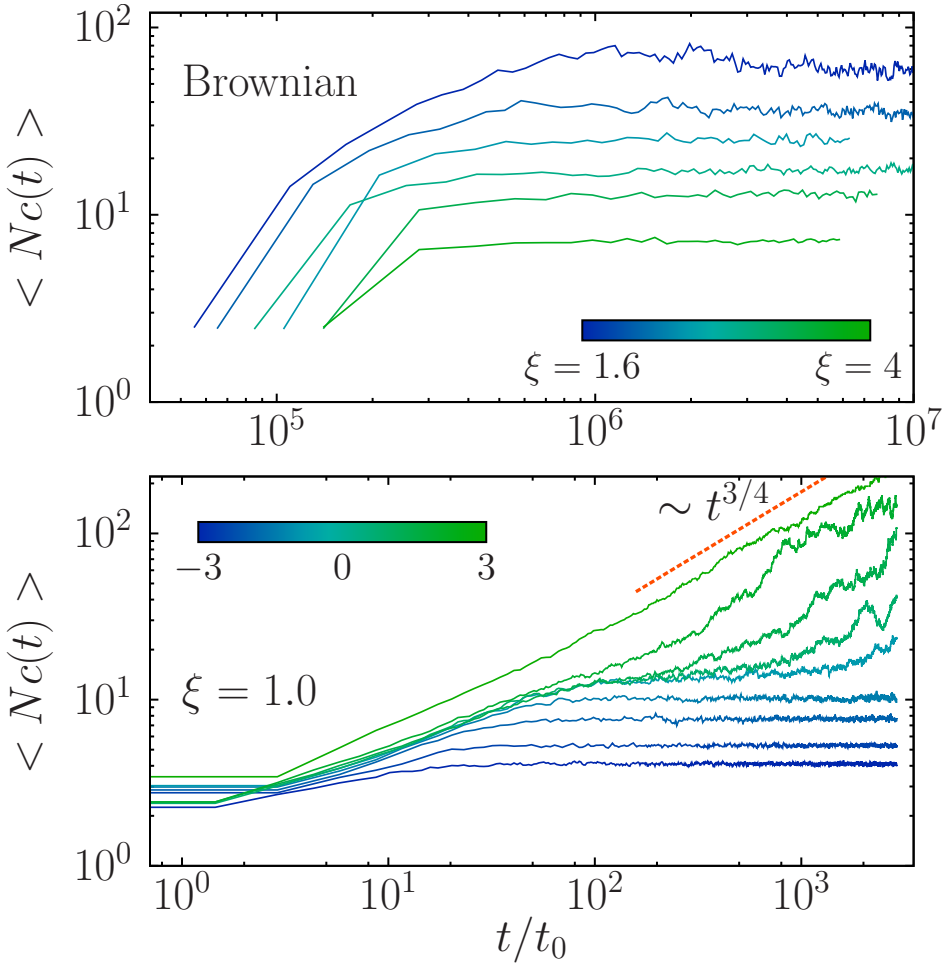

Figure 4.2: Mean cluster size as a function of time for different cases. (Top) Brownian particles at different values of interaction strength where coarsening is not presented, from $\xi = 1.6$ to 4. (Bottom) Squirmers with $\xi = 1$ for various values of β from -3 to 3. Pullers correspond to green curves while pushers correspond to blue curves

steady state cluster size distribution independently on the value of β. The average clusters size is now smaller than in the $\xi = 1.8$ case, and for $\beta = 0.5$ the system passes through a metastable cluster-size before reaching the stable one.

To conclude, we also analyze the case when $\xi = \infty$ (bottom-left panel in Figure 4.3). Once more, systems reach a steady-state clusters size distribution for all values of β. However, when $\beta = 0.5$ and ξ is 6.03 or ∞, after a meta-stable state $< N_c(t) >$ oscillates at long time scales (having run these simuations much longer than the others), the only difference between the two runs being how quickly the steady state is reached (faster in the $\xi = \infty$ case than in the $\xi = 6.03$ one).

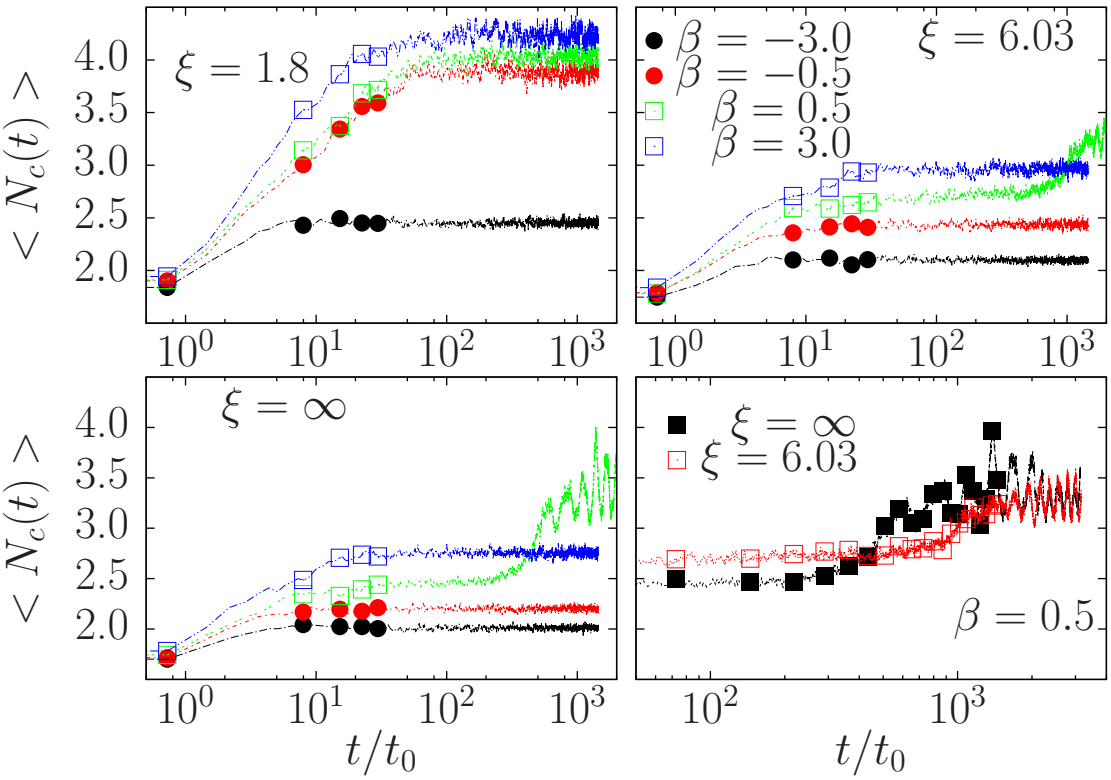

Figure 4.3: Mean cluster size as a function of time for different cases. (Top-Left) Squirmers with $\xi = 1.8$. Circles correspond to $\beta < 0$ whereas squares to $\beta > 0$. (Bottom-Left) Squirmers with $\xi = \infty$. (Top-Right) $\xi = 6.03$ and (Bottom-Right) It represents the mean cluster size for $\beta = 0.5$ and $\xi = 6.03$ and $\xi = \infty$ but time interval extended up to $t/t_0 = 3000$.

This difference in the relaxation time is a consequence of the attractive potential being the same the specific active stress ($\beta = 0.5$), (which is the parameter that produces these oscillations) being the only present when there are no attractive interactions at all ($\xi = \infty$): The stress generated by the squirmers induces both alignment and clustering between them, resulting in oscillations of the mean cluster size as shown in the bottom-right panel of Figure 4.3.

Figure 4.2 and 4.3 summarize all our results obtained both for the Brownian system and for the squirmers one: on the former, cluster formation is due to the competition between attraction and self-propulsion; in the latter, cluster formation is due to the competition between attraction and active stress, and can result in different behaviours depending on whether the squirmers behave like pushers or pullers (when $\xi = 1$, pullers coarsen whereas pushers evolve towards a steady state cluster size distribution).

When self-propel activity is greater than attractive interactions as in $\xi = 6.03$

a clustering regime is also found. However, stress activity starts to compete with attractive interactions, as can be observed in the long time behaviour of $\beta = 0.5$, due to the fact that particles try to align when they swim thus forming bigger clusters. In the purely hydrodynamic case when $\xi = \infty$ clustering regime with a small mean cluster size is stable for all cases.

In Figure 4.2 snapshots for attractive brownian particles with $\xi = 1$ (Fig. 4.2-a) and $\xi = 4$ (Fig. 4.2-b) as well as several regimes of interactive squirmer suspensions with $|\beta = 0.5|$ are shown (Figures 4.2 c to h). For $\xi = 1$ ABPs' coarsen, whereas for $\xi = 4$ a steady state clustering is observed. For squirmers a more complex phenomenon occurs, since for $\xi = 1$ we observe either coarsening if $\beta = 0.5$ (Fig. 4.2-c) or clustering if $\beta = -0.5$ (Fig. 4.2-d).

Increasing the value of ξ coarsening will disappear both for squirmers and for ABP. But clusters will have smaller sizes, in mean, than their Brownian counterpart. However, even though the value of $\xi = 4$ for ABP is similar to that of xi=5 for squirmers, distribution of the particles is clearly different among them (as one could already guess from Figures 4.2-b versus 4.2-e and f).

Comparing figure 4.2-e and 4.2-g, one can observe how pullers form clusters of particles moving in the same direction (figure 4.2-e) , that percolate when the collective behaviour only depends on the stress activity. On the contrary, for pushers the suspension is completely homogeneous, as we observe in Fig. 4.2-h).

4.3 Number fluctuations

In [84], Fily, et al. show the three different phases in their system by a color map of the exponent of the density fluctuations (number fluctuations) in the area fraction-activity plane, in a similar way we show here how the collective behaviour of a suspension of active particles changes in a β-ξ state-diagram in terms of the exponent of the density fluctuations. To calculate this exponent one has to measure in each subsystem the fluctuations of the number of particles $\langle \Delta N \rangle$ as a function of the mean value of particles in the same subsystem. This curve will have a power law behaviour $\langle \Delta N \rangle \sim N^{\alpha}$, where a value of $\alpha < 0.7$ corresponds to the presence of Giant Density Fluctuations (GDF) in the suspension, which is a typical signature of systems of phase separation in suspensions of active particles. On the contrary, an exponent of $\alpha = 0.5$ corresponds to an homogeneously distributed suspension. To calculate this exponent one has to make sure to have reached the steady state, given that spurious giant density fluctuations for very strong attractions due to an initial coarsening.

To quantify the large fluctuations found for large values of ξ, we compute the mean number of particles $\overline{N}_s$ and the standard deviation ΔN in subsystems

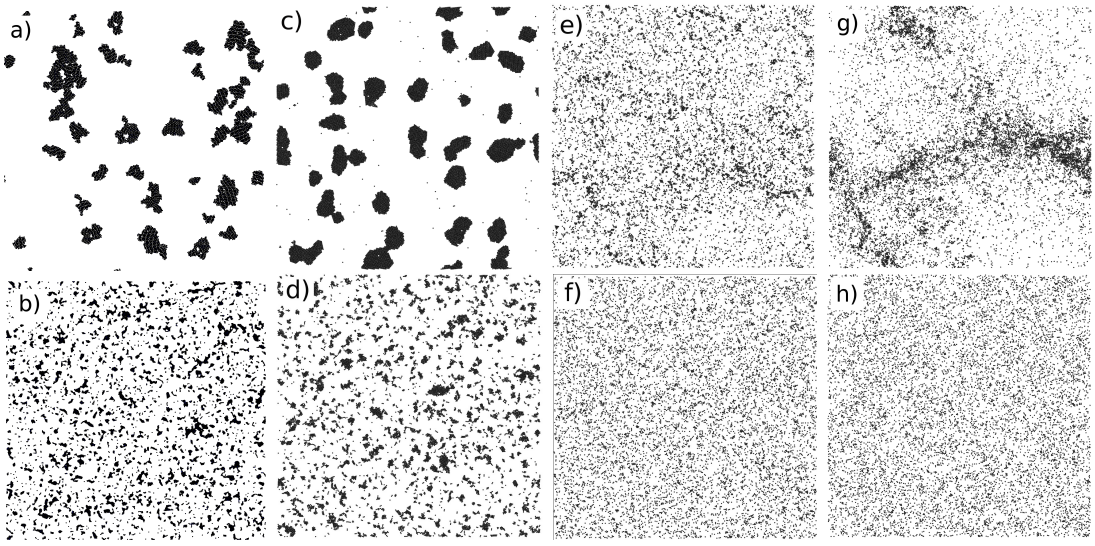

Figure 4.4: Snapshots for different values of interaction strength for ABP's and squirmers supensions. The first column represent Brownian particles, whereas all other columns are squirmers. a) Brownian particles with $\xi = 1$, b) Brownian particles with $\xi = 4$, c) squirmers with $\xi = 1$ and $\beta = 0.5$, d) squirmers with $\xi = 1$ and $\beta = -0.5$, e) squirmers with $\xi = 5$ and $\beta = 0.5$, f) squirmers with $\xi = 5$ and $\beta = -0.5$, g) squirmers with $\xi = \infty$ and $\beta = 0.5$ and h) squirmers with $\xi = \infty$ and $\beta = -0.5$. All snapshots for squirmers were taken at $t/t_0 = 1450$.

of different sizes. For homogeneous suspensions $\Delta N \sim N_s^{1/2}$, while suspensions with large density fluctuations follow $\Delta N \sim N_s^{4/5}$, also known as giant density fluctuations [86, 88]. The scaling exponent of 4/5 has been observed either in experiments with bacteria colonies [83] or in numerical simulations of self-propelled polar particles [86]. Here we found a wide range of values for the scaling exponent. The way the number of squirmers fluctuate in the suspension will depend both on the interaction strength and on the hydrodynamic signature, Figure 4.5 shows the color map of the scaling exponent α in terms of (ξ^{-1}, β). The scaling exponent values are between $(0.47, 0.85)$ and we can identify three regimes: one with scaling exponent of ~ 0.5 for homogeneous suspensions (in blue), another one with intermediate values between 0.6 and 0.7 (yellow-orange). Suspensions in this regime have an amount of large and loosely packed dynamic clusters, Giant Density Fluctuations (GDF) is reached when $\alpha > 0.7$, as in the case of squirmers with $\xi > 5.0$ and $0 < \beta < 1$ (red-orange).

On the one side pusher suspensions ($\beta < 0$) have a scaling exponent of around 0.5 that grows very slow as attraction strength increases ($\xi^{-1} \to 1$), reaching values of $\alpha = 0.64$ for $\beta = -0.5$ and $\xi = 1$. and no GDF are present.

On the other side, pullers with $\beta > 1$ have an exponent around 0.6, despite of

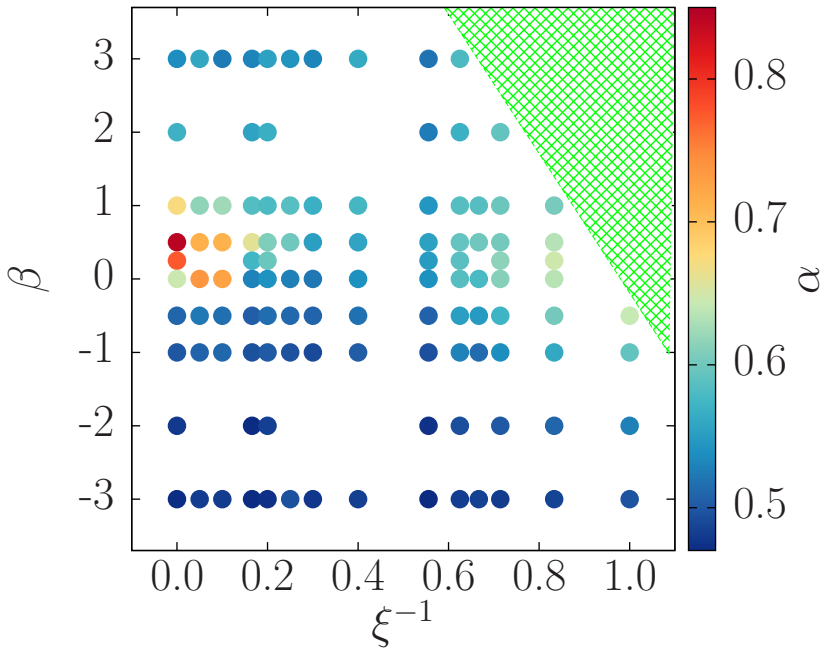

Figure 4.5: Color map of the scaling exponent α for values of ξ and β where coarsening is absent. Red corresponds to GDF, yellow-orange to the anomalous exponent, where partially large fluctuations are found and blue is for homogeneous suspensions. The green area represents the values where coarsening is found.

the value of the interaction strength. When $0 \leq \beta \leq 1$ stress activity makes that anomalous number fluctuations emerge, from a maximum value of α at $\xi = \infty$ to a value typical for homogeneous suspensions ($\alpha \to 0.5$) as $\xi \to 1$.

In Fig. 4.5 shows two remarkable phase separations, one purely caused by hydrodynamics when pushers form dynamic clusters that percolates and the second one caused by interaction strength (coarsening), but modulated by the hydrodynamic interactions (green area). For example, when $\xi^{-1} = 1$ only pullers coarsening, while pushers evolve to a steady state cluster distribution.

4.4 Cluster-size distribution

In Figure 4.6 we represent the cluster-size distribution (CSD) for different values of ξ and several values of β between -3 and 3, calculated as the average fraction of clusters $f(s)$ of a given number of particles s. The top-left panel shows CSD for $\xi = 1.8$: the CSD are wider as β increases without reaching the purely algebraic function (orange dashed line), Brownian CSD at the same value of ξ correspond to larger cluster sizes compared to the squirmers. For $\xi = 6.03$ (top right panel) CSD with $\beta < 0$ have approximately the same shape. Then the distributions are

wider for increasing values of β till $\beta = 0.5$ where distribution almost reaches an algebraic shape. When β becomes larger than 0.5 the distribution width decreases again. In the Brownian case, the CSD resembles that for pushers. If $\xi = \infty$ (bottom right panel) the CSD for pushers are the same as those for pushers when $\xi = 6.03$ up to the value of $\beta = 0.5$ where the CSD has a purely algebraic shape. If $\beta > 0.5$ then distribution width decreases again, as in $\xi = 6.03$.

Cluster size distribution can be expressed by

$$f(s) \sim \ s^{-\gamma_0} \ \exp(-s/s_0) \tag{4.7}$$

where $\gamma_0 = 1.972$ and s_0 controls the exponential cut-off of the distribution [105]. s_0 has been related with the clusters shape and velocity [6, 7]; more recently it has been found that the divergence of the cluster size cut-off is related to the location of the phase separation of a suspension of Brownian self-propelled repulsive disks [84, 105]. In the case under study, i.e. a dilute suspension of interacting spherical squirmers, the value of s_0 should depend on the hydrodynamic signature tuned by β and on the interaction strength modulate by ξ.

Fitting the CSD data to equation (4.7), we observe that s_0 increases with β when attractive interactions compete with activity ($\xi = 1.8$) (bottom-right side of Figure 4.6). Whereas, when either self-propel activity is larger than attractions ($\xi = 6.03$) or there is only activity ($\xi = \infty$), s_0 increases with β till reaches a maximum at $\beta = 0.5$. Distributions with large cluster size cut-off s_0 behave like a power law

$$f(s) \sim s^{-\gamma_0} \tag{4.8}$$

with $\gamma_0 = 1.972$. This value comes from hydrodynamic issues only, and it is completely different on the one side from the percolation exponent [106] of equilibrium systems (being far from equilibrium), on the other side from exponent obtained for other active systems without hydrodynamic interactions [84, 105]. Where $\gamma_0 = \{1.7, 1.0\}$.

Typically, suspensions of thermal particles in thermodynamic equilibrium have a cluster size distribution as

$$f(s) \sim \exp(-s/s_0) \tag{4.9}$$

The difference between this expression and our results could be seen as a signature of how far from equilibrium the active suspensions are.

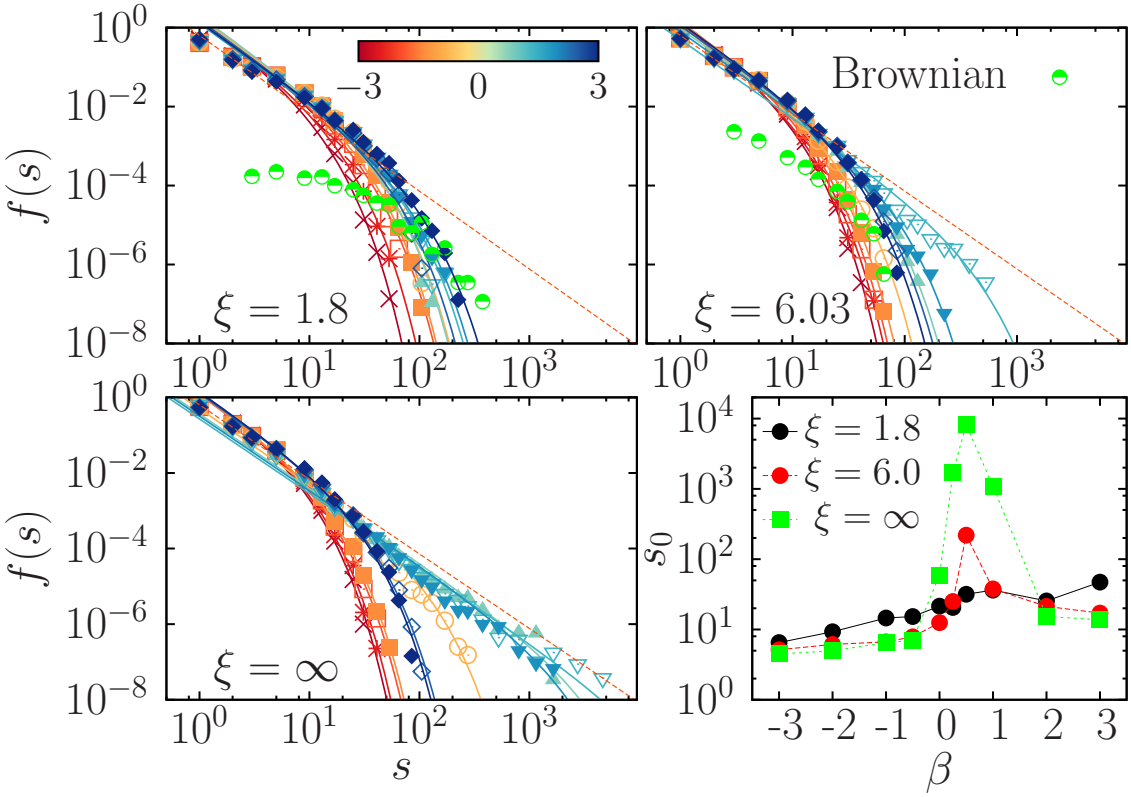

Figure 4.6: Cluster-size distribution $f(s)$ for different values of ξ and β. Blue symbols correspond to pushers $\beta < 0$ and green ones to pullers $\beta > 0$. Solid lines correspond to $f(s) \sim \exp(s/s_0)/s^{1.97}$ and the orange dashed line to $f(s) \sim s^{-1.97}$. Top-left: $\xi = 1.8$. Top-right: $\xi = 6.03$. Bottom-left: $\xi = \infty$. Bottom-right: Cluster size cut-off s_0 as a function of β for three different values of ξ. s_0 was obtained by fitting $f(s)$ to equation (4.7). $f(s)$ for $\beta = 0.5$ and $\xi = \infty$ has been fitted with an algebraic function of the form of equation (4.8).

4.5 Morphology of squirmer clusters

In order to study the properties of finite-size clusters, we first of all need to detect them. We identify clusters in the system in the following way: two particles belong to the same cluster whenever their distance is smaller than a given cutoff, $r_{ij} < r_{cl} = 1.8\sigma$ (see Appendix A). The number of particles belonging to the same cluster will be indicated as s (where s is the cluster size).

We first evaluate the fraction of clusters of size s, $f(s)$ as a measure of the cluster-size distribution. To calculate $f(s)$ we apply the same criterion as in Ref. [87]: (i) We arbitrarily subdivide the range of s-values into intervals $\Delta s_i = (s_{i,max} - s_{i,min})$, where we define the total number of clusters within each interval Δs as n_i^t; (ii) then we assign the value $n_i = n_i^t/\Delta s_i$ to every s within Δs_i, therefore

the fraction of clusters of size s can be written as $f(s) = n_i/N_c$ where N_c is the total number of clusters, computed as $N_c = \sum_i n_i \Delta s_i$.

Next, we determine the radius of gyration for every cluster (averaging over same-size clusters)

$$R_g = \sqrt{\sum_{i,j=1}^{s} \frac{(\vec{r_i} - \vec{r_j})^2}{2s}} \tag{4.10}$$

where we divide by 2 to avoid double counting. To measure polar order within a cluster, we estimate

$$P = \left| \frac{\sum_{i=1}^{s} \vec{e_i}}{s} \right| \tag{4.11}$$

where $\vec{e_i}$ is the orientation of each individual particle. The particles' orientation with respect to the cluster's translation ($\vec{v}_{CM}$) is estimated as

$$\Omega = \sum_{i=1}^{s} \frac{\vec{v}_{CM} \cdot \vec{e_i}}{s} \tag{4.12}$$

where $\vec{v}_{CM}$ is the center of mass' velocity of the cluster.

4.5.1 Radius of gyration

In order to find structural differences among clusters, we start with analysing the radius of gyration $Rg(s)$ of clusters containing s particles. $Rg(s)$ is calculated using eq. (4.10). In FIG. 4.7 we represent the mean radius of gyration normalized by the particle's radius for different values of ξ and β. In the regime where attraction competes with activity ($\xi = 1.8$ top-left side of FIG. 4.7), we can see that $Rg \sim s^{\gamma}$ with $\gamma < 2/3$ approximately, for all values of $\beta > -3$. Changes in γ are very small however $Rg(s)$ mildly decreases as β increases. When $\xi = 6.03$ (top-right in fig. 4.7), $Rg(s)$ follows an exponent greater than 2/3 for pushers, whereas blue curves are all above the reference orange curve. This means that clusters of pushers with $\xi = 6.03$ are less compact in comparison with the ones of pushers with $\xi = 1.8$. Another interesting feature is that the $Rg(s)$ slope decreases with β up to $\beta = 0.5$ where the minimum value for γ is reached, then γ increases as β increases.

The morphology of the clusters with $\xi = \infty$ behaves in the same fashion as squirmers with $\xi = 6.03$, with pusher clusters less compact than with $\xi = 1.8$ and a minimum slope for $\beta = 0.5$ followed by a re-expansion of the clusters for $\beta > 0.5$.

In terms of the exponent values we can see that clusters with $\xi = 1.8$ are more compact as β increases, since γ decreases, therefore clusters of pushers are less

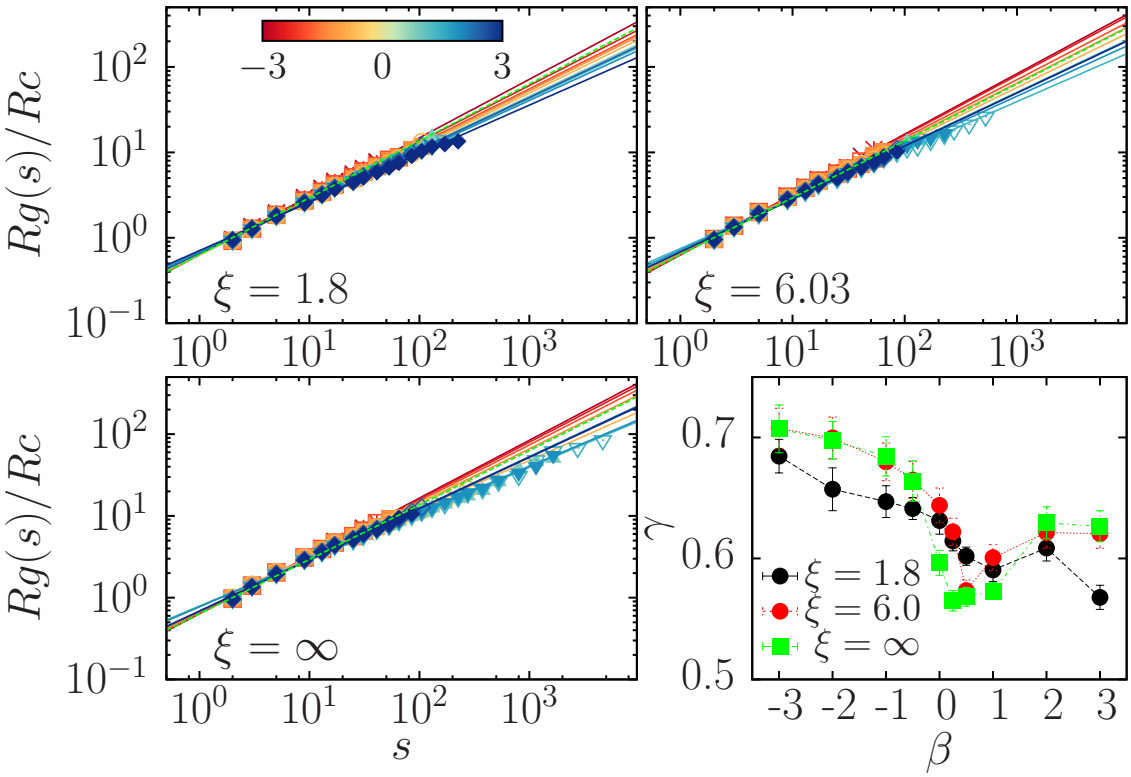

Figure 4.7: Radius of gyration $R_g(s)$ (normalized by the particle's radius) as a function of the cluster-sizes for values of ξ ranging from 1.8 up to ∞ and β between 3 and -3. Blue symbols correspond to pushers $\beta < 0$ and green ones to pullers $\beta > 0$. Solid lines represent $Rg(s) \sim s^{\gamma}$ and the orange dashed line $Rg(s) \sim s^{2/3}$. Top-left $\xi = 1.8$, Top-right: $\xi = 6.03$, Bottom-left: $\xi = \infty$ and Bottom-right: γ exponent as a function of β and ξ.

compact than clusters of pullers. On the contrary, when activity dominates as in $\xi = 6.03$ or $\xi = \infty$ a phenomenon of clusters re-expansion occurs given by the hydrodynamic signature.

In both cases as β goes to 0.5, clusters will be more compacted since γ value decreases. For $\beta = 0.5$ clusters reach their more compact shape and after that they start swelling again.

4.5.2 Polar order

In [34] we computed the global polar order of the squirmer suspensions, to evaluate the degree of alignment of the suspension. Polar order close to one corresponds to an aligned state while polar order close to $1/\sqrt{s}$ to an isotropic. Following equation (4.11) we calculate the polar order for each cluster averaged over all

clusters of the same size. In the top panel of Fig. 4.8 we observe that polar order decreases with the cluster size: pushers (in red) have a faster decay than pullers (in blue) with respect to the reference orange dashed curve ($\sim s^{1/2}$). However, both pushers and pullers present clusters without any alignment. When $\xi = 6.03$ (middle panel) pushers show a decay below the reference curve, whereas pullers with $\beta < 1$ drastically change their behaviour compared to pullers at $\xi = 1.8$ showing big clusters with high polar order. When there is no attraction at all

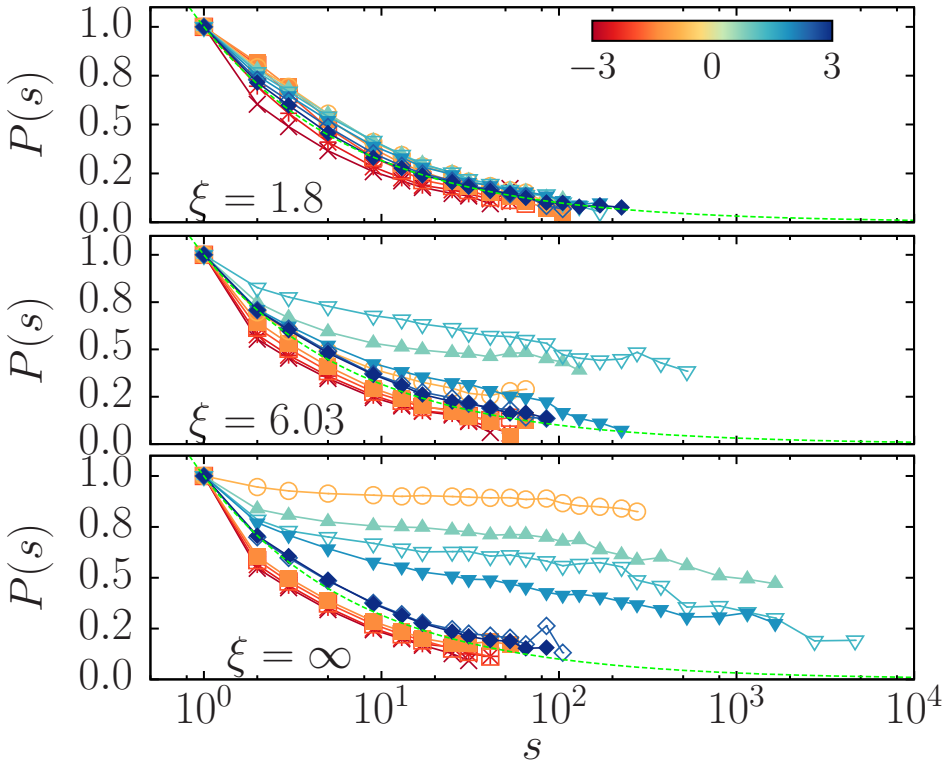

Figure 4.8: Polar order parameter P as a function of the cluster-size for values of ξ ranging from 1.8 up to ∞ and β between -3 and 3. The orange dashed line corresponds to $P(s) \sim s^{-1/2}$.

(bottom panel) pushers behave in the same way as in $\xi = 6.03$, polar order decays fast to zero but pullers decays slower: as the smaller the value of β the slower the decay of polar order parameter.

To see whether the clusters move in the same direction as their particles, we compute the orientation of the particles within a cluster with respect to the cluster's center-of-mass velocity using equation (4.12). In FIG. 4.9 we show the mean value of Ω as a function of the cluster size. The top-left panel shows $\Omega(s)$ for $\xi = 1.8$, indicating that the orientation decays very fast for all β values. However, when attraction is reduced (top-right panel FIG. 4.9) pullers with $\beta < 1$ have a slow decay given that it is possible to find a partial orientation for big clusters

(as shown in figure 4.8). For $\xi = 6.03$ pullers with $\beta > 1$ decay in the same way as pullers with $\xi = 1.8$ however, pushers decays faster. The same holds for pushers without attraction, where particles orientation decay very fast (bottom-left panel FIG. 4.9). When $\beta = 0$ the clusters orientation decay is very slow, almost independent of cluster size, given that in this case the global aligned state is stable. Therefore, as the β value increases the decay velocity in the orientation increases. If we fit $\Omega(s)$ with a power law $s^{-\omega}$ what we have are all the fitted curves depicted in FIG. 4.9 (bottom-right panel). This fitted exponent ω help us to describe the behaviour of the orientation in clusters as a function of ξ and β. A high ω value means fast decay in the orientation, while a low value means high orientation in the clusters. When attractive interactions competes with activity at $\xi = 1.8$, exponent values are between 1.06 and 0.71 which means that orientation decays very fast and big clusters are not oriented at all.

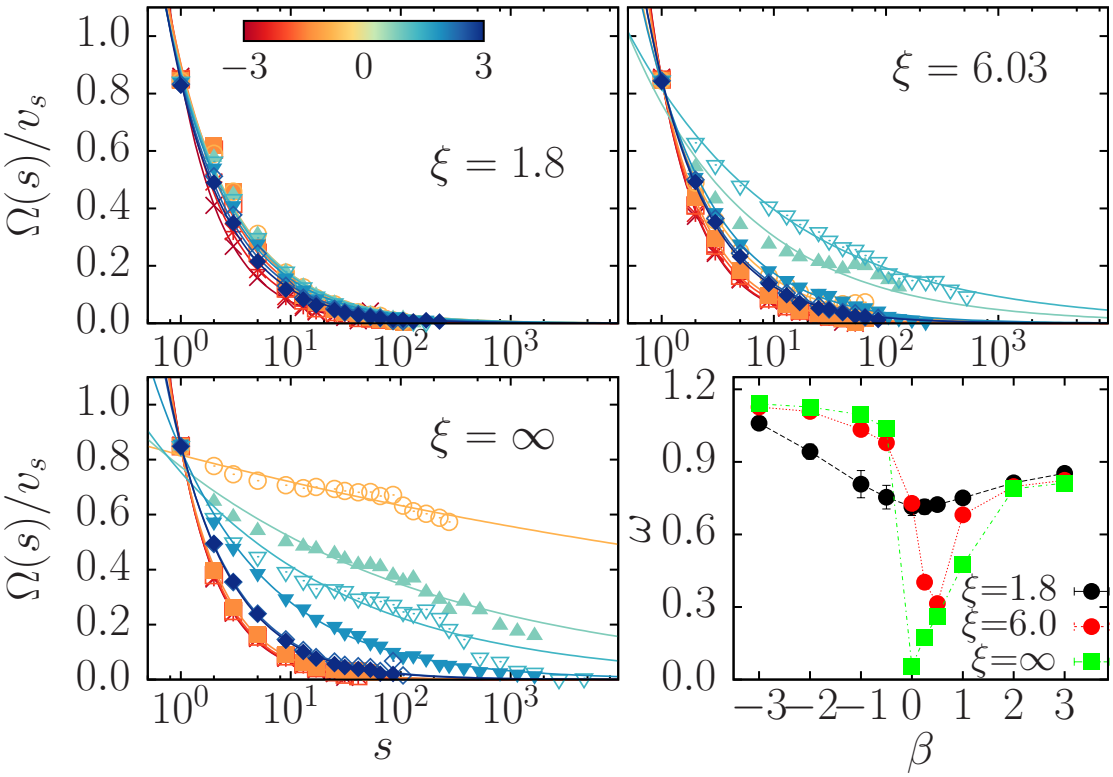

Figure 4.9: Ω as a function of the cluster-size for values of ξ ranging from 1.8 up to ∞ and β between -3 and 3. Solid lines correspond to $\Omega(s) \sim s^{-\omega}$ Top-left: $\xi = 1.8$, Top-right: $\xi = 6.03$, Bottom-left: $\xi = \infty$. Bottom-right: ω exponent value fitted as a function of β and ξ. $\Omega(s)$ is normalized by the overdamped velocity reached by one squirmer ($v_s = 2/3B_1$).

However, despite the strong attractive interaction, active stress is also playing a roll since clusters of pushers are less oriented than pullers. When $\xi = 6.03$

pushers have a faster decay, since ω is higher than in $\xi = 1.8$ until $\beta = 0$, once $0 < \beta < 1$ the exponent goes to 0.3. For $\beta < 1$ ω increases again to values around 0.8. A very similar behaviour in ω is found with $\xi = \infty$, where pushers and pullers with $\beta > 1$ have the same exponent in comparison with the systems with the same β for $\xi = 6.03$, the difference appears in the GDF range ($0 \leqslant \beta \leqslant 1$) where ω almost reaches 0.06. These small values on ω are due to the alignment that squirmers show for this range of β.

4.6 Dynamics of squirmer clusters

In order to evaluate the rotational and translational velocities of finite-size clusters, we first of all need to detect them. To identify cluster we used the methodology described in A. Here we focus the motility of these clusters. To detect translational motion of the cluster, we compute the velocity of its center-of-mass as $\vec{v}_{CM} = \sum_{i=1}^{s} \vec{v}_i/s$, whereas to detect the angular velocity we compute for every cluster size and average over same size clusters the following quantity: $\mathbf{L}_G = \mathbf{I}_G \cdot \boldsymbol{\omega}$ (being $\mathbf{L}_G$ is the angular momentum and $\mathbf{I}_G$ is the inertia tensor of a rigid body relative to the center of mass).

4.6.1 Translational velocity

In order to determine how clusters move, we first compute the mean translational velocity with respect to their centre of mass of clusters of size s.

$$\mathbf{v}_{cm}(s) = \sum_{i=1}^{s} \mathbf{v}_i/s, \tag{4.13}$$

In top-left side of FIG. 4.10 we observe the translational velocity for interactive squirmers with an interaction strength of $\xi = 1.8$ all β cases has the same power law shape, when clusters are small there is no difference among all the β cases, for bigger cluster sizes ($s > 50$) we can see that velocity for pusher clusters (the bluest data) is slightly below of velocity for puller clusters (the greenest data), however due to the small difference we can say that squirmer clusters velocity decreases in the same fashion independently of the value of β. The exponent is around $-1/2$. When interaction is softer ($\xi = 6.03$) cluster velocities will change for some cases of squirmers, in comparison with the later cases. In the top-right side of FIG. 4.10 we show the clusters' velocity for several values of β and $\xi = 6.03$. Pusher clusters velocity (the bluest data) remains with the same behaviour, $\mathbf{v}_{cm}$ $s^{-1/2}$. However, when $\beta \leq 0$ velocity will decay slower and the precise value will depend on the hydrodynamic signature. Clusters with $\beta = 0.25, 0.5$ and 1 are faster than the

rest of pullers since velocity decays very slow for small sizes ($s < 20$) however it is important to notice that big clusters ($s > 20$) with $\beta = 0.5$ and 1 does not follow the same power law decay than small clusters, this is because the emergency of this big clusters is different. Big clusters at this stage swim coherently and they collide with the small clusters that reduce the velocity of the big clusters. Naturally, as bigger the cluster more chances to collide with other clusters will have. Then a higher reduction on its velocity. Pullers in other range of β, will decay faster than aligned case till they reach the general decay of pushers again.

When $\xi = \infty$ the velocity of clusters with $\beta < 0$ decays like power law $v_{CM}(s) \sim$

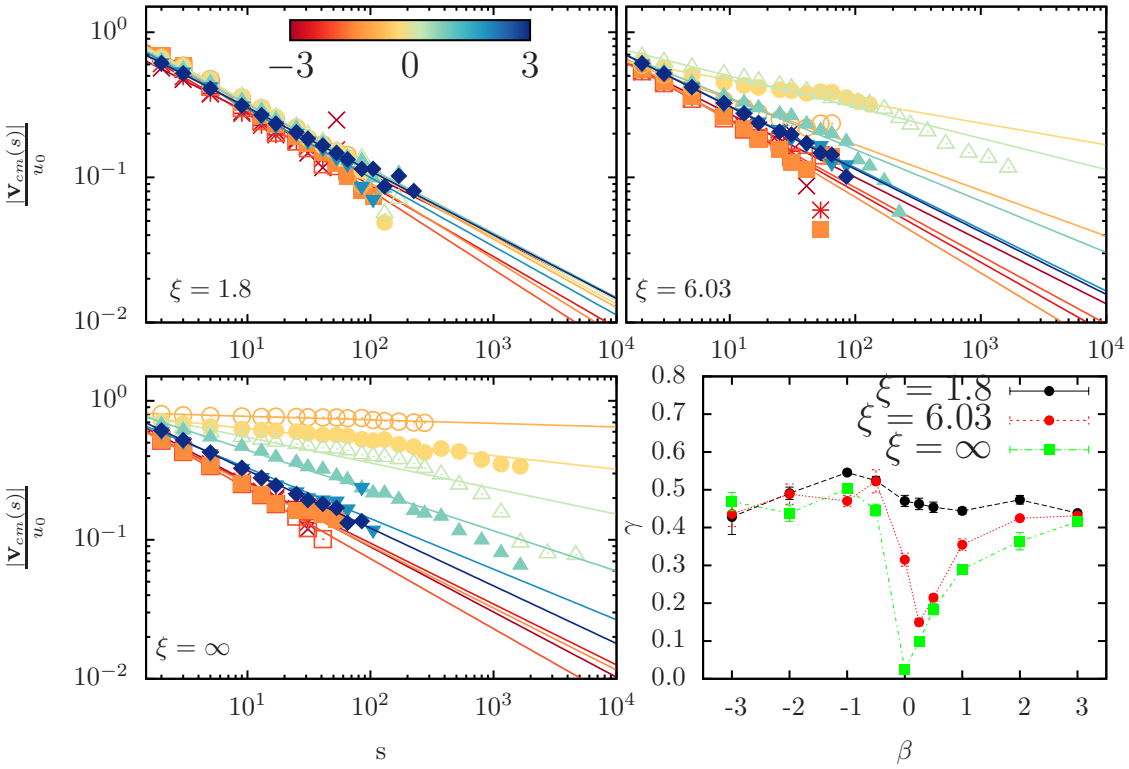

Figure 4.10: Translational velocity $v_{CM}(s)$ normalized by $u_0 = 2/3B_1$ as a function of the cluster-size s for values of ξ ranging from 1.8 up to ∞. With β between -3 and 3. The values of β are indicated in the legend. Solid lines are fitted curves of $v_{CM}(s) \sim s^{-\gamma}$. Top-left: $v_{CM}(s)$ for interactive squirmers with $\xi = 1.8$. Top-right: $v_{CM}(s)$ for interactive squirmers with $\xi = 6.03$. Bottom-left: $v_{CM}(s)$ for pure hydrodynamic squirmers with $\xi = \infty$. Bottom-right: Exponent value fitted from $v_{CM}(s)$ in function of β. Black circles correspond to fitted exponent for $\xi = 1.8$, red-circles to $\xi = 6.03$ and green squares to $\xi = \infty$.

$s^{-\gamma}$ with $\gamma \sim 1/2$ as the same way as pushers with $\xi = 1.8$ or 6.03. Therefore we can say that velocity of pusher clusters is not affected by the attractive forces. On the other hand, when $\beta = 0$ the velocity of clusters will be very similar between

them no matter the size of the cluster due to the high alignment that exist and then less collision between clusters in comparison with $\beta = 0.25, 0.5$ and 1 where it is clear that big clusters have different behaviour than the power law that small clusters follow. As well as in $\xi = 6.03$ due to the collisions of this big cluster that emerges in this range of parameters. Therefore, if we plot the fitted exponent in terms of β for each ξ value, what we have is the curves plotted in the bottom-right side of FIG. 4.10. Black circles that correspond to $\xi = 1.8$ which basically follows a horizontal line around $1/2$, then for $\xi = 6.03$ we have the red circles that tell us that pusher follows the same horizontal line at around $1/2$ then $\beta = 0$ due to the emergency of alignment at this point, increases the velocity of big clusters and then a reduction in γ. When $\beta = 0.25$ we have more alignment suspension and clusters swim faster then a value of $\gamma = 0.15$ if we increase β γ starts increase again to $\gamma = 1/2$ when β reaches 3. Green curve correspond to $\xi = \infty$, pushers have an exponent of around $1/2$ but once β is not negative suspension align. Hence, when $\beta = 0$ velocity of clusters is almost the same for all sizes since all particles are swimming in the same direction therefore $\gamma \sim 0$ for $\beta > 0$ clusters velocity is reduced gradually as β increases hence γ value increase gradually till reach the value of $1/2$ again.

4.6.2 Angular velocity

We now estimate the angular velocity as a function of cluster size, we compute the angular momentum $\mathbf{I}_G$ and the inertia tensor $\mathbf{I}_G$, at each cluster knowing that

$$\mathbf{L}_G = \mathbf{I}_G \cdot \boldsymbol{\omega} \tag{4.14}$$

from this equation we obtain the angular velocity $\boldsymbol{\omega}$ (see Appendix B). We can see on top-left side of FIG. 4.11 angular velocity of clusters of size s for suspensions of interactive squirmers with interaction strength of $\xi = 1.8$ with $\beta \, \epsilon \, [-3, 3]$. Angular velocity decays for all the β values as a power law, $|\omega(s)|$ decays faster to clusters of pushers with $\beta = -3$ and -2 then for $\beta = 0$ angular velocity decays slower than the other cases, after this value $|\omega(s)|$ decays gradually faster with β. When activity is grater than attractive interactions as in $\xi = 6.03$, angular velocity for pusher clusters will decay faster than pullers, as we see in top-right side of FIG. 4.11, where bluest data are below of the greenest data. Another interesting observation is that big clusters of pullers with $\beta = \{0.25, 0.5, 1\}$ follows a different functional form than a power law and as well as the translational velocity this is due to the emergency of aligned clusters. Same behaviour it is found when $\xi = \infty$ and β in the region where alignment emerges. In the bottom-left side of FIG. 4.11 we can see how data for big clusters of pullers with $\beta \leq 1$ have a huge deviation from the power law. While $\beta = 0$ due to the maximum alignment, it follows

completely the power law $|\omega(s)| \sim s$. Angular velocity for pusher clusters decay even faster than the aligned suspensions. If we fit the angular velocity data to a

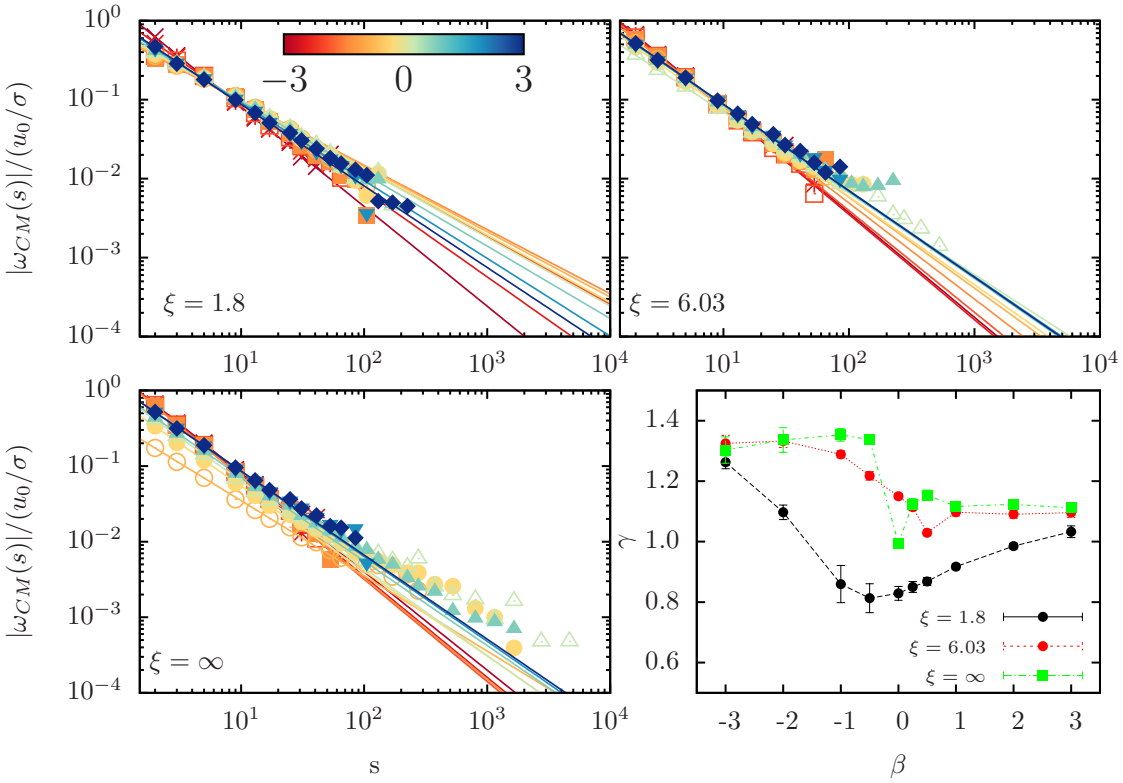

Figure 4.11: Angular velocity $\omega_{CM}(s)$ normalized by u_0/σ, where $u_0 = 2/3B_1$ and σ the diameter of squirmers, as a function of the cluster-size s for values of ξ ranging from 1.8 up to ∞. With β between -3 and 3. The values of β are indicated in the legend. Solid lines are fitted curves of $\omega_{CM}(s) \sim s^{-\gamma}$. Top-left: $|\omega_{CM}(s)|$ for interactive squirmers with $\xi = 1.8$. Top-right: $|\omega_{CM}(s)|$ for interactive squirmers with $\xi = 6.03$. Bottom-left: $|\omega_{CM}(s)|$ for pure hydrodynamic squirmers with $\xi = \infty$. Bottom-right: Exponent value fitted from $|\omega_{CM}(s)|$ in function of β. Black circles correspond to fitted exponent for $\xi = 1.8$, red-circles to $\xi = 6.03$ and green squares to $\xi = \infty$.

power law function we can put the value of the exponent in terms of the β value and interaction strength ξ. As we can see in the bottom-right side of FIG. 4.11, where black circles correspond to the exponent value for $\xi = 1.8$ in function of the hydrodynamic signature. Exponent for this case is between 1.25 and 0.8. It decays with β from 1.25 in $\beta = -3$ till $\beta = 0$ where exponent reaches 0.8 once $\beta > 0$ exponent start to increase to 1 at $\beta = 3$. When hydrodynamics dominates against direct interactions like in $\xi = 6.03$ or in $\xi = \infty$ we can recognize a transition from a exponent value of 1.3 for pushers to a exponent value of 1.1 for pullers. In the case of $\xi = 6.03$ this transition is softer than in the purely hydrodynamic case.

Here we have characterized the dynamic behaviour of interactive squirmer suspensions in terms of the cluster distribution, calculating the translational velocity and the angular velocity in function of the cluster size. Clusters in cases where interaction competes with the activity ($\xi = 1.8$) have the same scaling exponent for the translational velocity which means that the dynamic of the clusters is the same no matter the value of β, however scaling exponent for angular velocity depends on the value of β which means that clusters for different β are not rotating in the same way, therefore stress activity works as a tune parameter to the way how the clusters rotates. In the cases where activity dominates, like in $\xi = 6.03$ and $\xi = \infty$ the clusters velocity behaviour is in function of the alignment of the suspension, since clusters of suspensions where isotropic state is stable have the same scaling exponent of $\sim 1/2$ whereas clusters of suspensions where aligned state is stable, the scaling exponent will decrease from $1/2$ to 0 in the case of totally aligned state as in $\beta = 0$ and $\xi = \infty$. Another interesting feature of the clusters velocity is that big clusters that generate the giant density fluctuations do not follow the power law function, since these clusters collide with smaller clusters.

Angular velocity for cases where activity dominates, like in $\xi = 6.03$ and $\xi = \infty$ we can distinguish two general scaling exponent values, one for pushers that is around 1.3 while pullers have a scaling exponent of 1.1. However, big clusters in the transition area do not follow the power law function which tell us that the nature of this big clusters is not the same as the small ones.

4.7 Conclusions

We showed here a systematic study of semi-dilute suspensions of interactive squirmers restricted to swim in a slab. Squirmers can see as active particles that self propel and stress the fluid in function of the β parameter. In our case squirmers can also interact isotropically among them by a Lennard-Jones force. The competition between this isotropic force and self-propulsion measured by the parameter of interaction strength ξ and the active stress defined by β gives a huge variety of cooperative or collective behaviours of interactive swimmers. From the systematic study of the (ξ, β) parameters that we developed, we can divide interactive swimmers in three big regimes. One regime where squirmers aggregate in a one single cluster called coarsening regime, another one with a constant mean cluster size at the steady state and a regime where temporal mean cluster size have small oscillations at the steady state. The last two regimes are more important in this study, since we are more interested in the competition between interaction and activity and coarsening regime is found only when $\xi < 1$, which means a clear domination of attractive interactions to the activity. In this chapter we present

a systematic study of semi-dilute suspensions of interactive squirmers restricted to swim in a slab. Squirmers simulate active particles that self propel and stress the fluid in function of the β parameter. Moreover, in our case squirmers also interact isotropically via a short-range Lennard-Jones attraction. The competition between this isotropic force and the self-propulsion (measured by the parameter ξ) and the active stress β gives a huge variety of behaviours of the interactive swimmers. From the systematic study in the (ξ, β) plane, we can divide interactive swimmers in three regimes. One regime where squirmers aggregate in a one single cluster (coarsening regime), another with a steady-state mean cluster size and a regime where mean cluster size have small oscillations with time. In our study we will be focusing on the the last two regimes (obtained for $\xi > 1$), since we are more interested in the competition between interaction and activity whereas the coarsening regime is only found when $\xi < 1$, corresponding to a clear domination of attractive interactions over activity. Analyzing the density fluctuations exponents we could detect transitions from coarsening to clustering, when the cluster distribution was showing a diverging cut-off.

To study the clusters' morphology, we evaluated the radius of gyration : When attractive interactions competes with activity we found that clusters shrink as β grows, while in the case when activity dominates a contraction-expansion effect occurs in function of the hydrodynamic signature. Another interesting feature we found is that not only the morphology changes with ξ and β parameters, but clusters alignment. Reason why clusters appear for different reasons. In one case clusters are formed due to collisions between particles while when GDF appear big clusters emerge because of the alignment enhanced for the stress activity of squirmers.

Here we have characterized the dynamic behaviour of interactive squirmer suspensions in terms of the cluster distribution, calculating the translational velocity and the angular velocity in function of the cluster size. Clusters in cases where interaction competes with the activity ($\xi = 1.8$) have the same scaling exponent for the translational velocity which means that the dynamic of the clusters is the same no matter the value of β, however scaling exponent for angular velocity depends on the value of β which means that clusters for different β are not rotating in the same way, therefore stress activity works as a tune parameter to the way how the clusters rotates. In the cases where activity dominates, like in $\xi = 6.03$ and $\xi = \infty$ the clusters velocity behaviour is in function of the alignment of the suspension, since clusters of suspensions where isotropic state is stable have the same scaling exponent of $\sim 1/2$ whereas clusters of suspensions where aligned state is stable, the scaling exponent will decrease from 1/2 to 0 in the case of totally aligned state as in $\beta = 0$ and $\xi = \infty$. Another interesting feature of the clusters velocity is that big clusters that generate the giant density fluctuations

[107] do not follow the power law function, since these clusters collide with smaller clusters.

Angular velocity for cases where activity dominates, like in $\xi = 6.03$ and $\xi = \infty$ we can distinguish two general scaling exponent values, one for pushers that is around 1.3 while pullers have a scaling exponent of 1.1. However, big clusters in the transition area do not follow the power law function which tell us that the nature of this big clusters is not the same as the small ones.

Chapter 5

Dynamics of a squirmer suspension at a liquid interface

5.1 Introduction

Following A. Dominguez idea [108, 109], we have carried out LB simulations of a system of squirmers under partial confinement, the motion of squirmers are restricted to move on a plane but their dynamics is influenced by hydrodynamic interactions mediated by the unconfined, three-dimensional flow of the embedding fluid. We have studied the geometric effect on the macroscopic behaviour of the squirmer suspension, for different values of β and various densities.

Furthermore, since in [34], we have shown that semi-dilute squirmer suspensions in 3D can develop collective motions like alignment and fluctuations on the density, and both, clearly non-equilibrium phenomena are generated by two basic mechanisms: the re-orientation of particles given by the hydrodynamics among particles and the collision between particles due to the self-propulsion of them. Hence, we have analysed numerically the effect of the re-orientation and the collision between squirmers due to the self-propulsion, to the global alignment and to the clustering by cancelling either the self-propulsion or the re-orientation, respectively. When squirmers only are able to re-orient and they are fixed in the plane, we found that polar order disappears for all cases of squirmers, but alignment is still present parallel to the swim plane for pullers, while pusher suspensions are more isotropically stable. This alignment that emerges due to the confinement of fixed particles is studied more systematically by doing simulations of different sizes, we found that this alignment emerges completely due to the confinement restriction and the hydrodynamic interactions among particles and it is not a finite size effect. Due to this geometrical constriction, we also show the eigenvector associated to the nematic order, to analyse if particles re-orient normal or parallel

to the confinement plane. Given rise to the fact that pullers with fixed position align parallel to the plane. A systematic study of the cluster size distribution is also showed for this system and contrasted with the case where particles can not re-orient. We found that partial confinement plays a key role in the cluster sizes as well as the hydrodynamic signature.

We investigate squirmer suspensions, where particles are confined to move in a plane but solvent is everywhere in 3D. Both cases consist of a three-dimensional fluid with particles embedded in it, these particles interact only hydrodynamically by the squirmer model explained in chapter 1.

The particles can move only in a plane (2 dimensions), but particles can rotate in all directions. Areal concentration was set to $\phi_A = 0.10$, where $\phi_A = \pi\sigma^2 N/(2L)^2$. In this case $L \sim 102\ \sigma$ and $N = 1336$. Both systems are modelled under the numerical frame described in 2 Lattice-Boltzmann.

Additionally, we carried out simulations with various concentrations, concentration was defined through the global areal concentration $\phi_0 = \{0.10, 0.2, 0.4\}$, where $\phi_0 = \pi/4\rho_A\sigma^2$, being σ the particle's diameter and $\rho_A = N/L^2$. Where L is the side of the box in the three directions. $L \sim 102\ \sigma$ and for the three values of ϕ_0 the number of particles was $N = \{1336, 2672, 5344\}$ correspondingly.

The squirmers are pointing out in random 3D directions initially as well as their position in the plane.

5.2 Orientational parameters

We calculate the global polar order parameter in order to study the stability of the either aligned or homogeneous-isotropic state. Here we show how this order parameter evolve in the time, also we show the temporal polar order normal to the surface where particles move and its standard deviation, Probability Distribution Function of the Z component of the orientation vector of the squirmers is also presented here to show when squirmers move parallel to the plane where they are confined and when they point out in direction normal to the surface. Initially, squirmers are isotropically oriented in the three directions. We calculated all these parameters to three different concentrations and activity stress β range from -3 to 3. In this section we show results for squirmer suspensions where initially squirmers are isotropically oriented in 3D.

5.2.1 Global polar order of a squirmer suspension at an interface

Global polar order is defined in terms of the fixed unitary orientation vector of the squirmers as in equation (3.2)

In FIG. 5.1 we show the global polar order as a function of time for three different concentrations. Time is normalized by a Stoke's time, which is defined as the time that a squirmer needs to move one diameter

$$\tau \equiv \frac{\sigma}{\frac{2}{3}B_1} \tag{5.1}$$

For dilute regime ($\phi = 0.1$) top-left plot in FIG. 5.1, polar order follows same behaviour than squirmer suspensions swimming in 3D without any restriction [34]. Squirmer suspension with $\beta = 0$ evolve to a totally aligned state (yellow curve), when $-1.5 < \beta < 2$ and $\beta \neq 0$ a partial aligned state is stable. Other value of β out of this range will have an isotropic state. If we double the concentration of squirmers top-right plot in FIG. 5.1, we found that aligned states are stable for the same values of β than semi-dilute regime. However, if we increase concentration even further to $\phi = 0.4$ global polar order will be affected, and the alignment will be reduced for all β. From Fig. 5.1 we see that polar order $P(t) \to 1$ for $\beta = 0$ (yellow curves) for all the concentration regimes. Therefore alignment state for $\beta = 0$ does not depend strongly on the density of squirmers. However when the system is partially aligned at semi-dilute regime ($\phi = 0.1$) polar order is reduced by 0.2 in the concentrated regime ($\phi = 0.4$).

5.2.2 Normal polar order

In order to calculate how many squirmers are pointing out perpendicular to the plane where they are confined, we calculate the normal polar order which is defined in terms of the Z component of the fixed unitary orientation vector of the squirmers, since Z direction is normal to the surface where squirmers can move. Similarly to global polar order, one can write normal polar order as

$$P_z(t) = \frac{1}{N}\sum_{i=1}^{N} \vec{e}_i(t) \cdot \hat{k} \tag{5.2}$$

which is the mean of the projection of the orientation vector in the direction of $\hat{k}$ vector over all the squirmers in the suspension. $P(t) \to 1$ means that most of the squirmers are pointing out to the positive side of the plane while $P(t) \to -1$ means that most of the squirmers are pointing out to the negative side of plane.

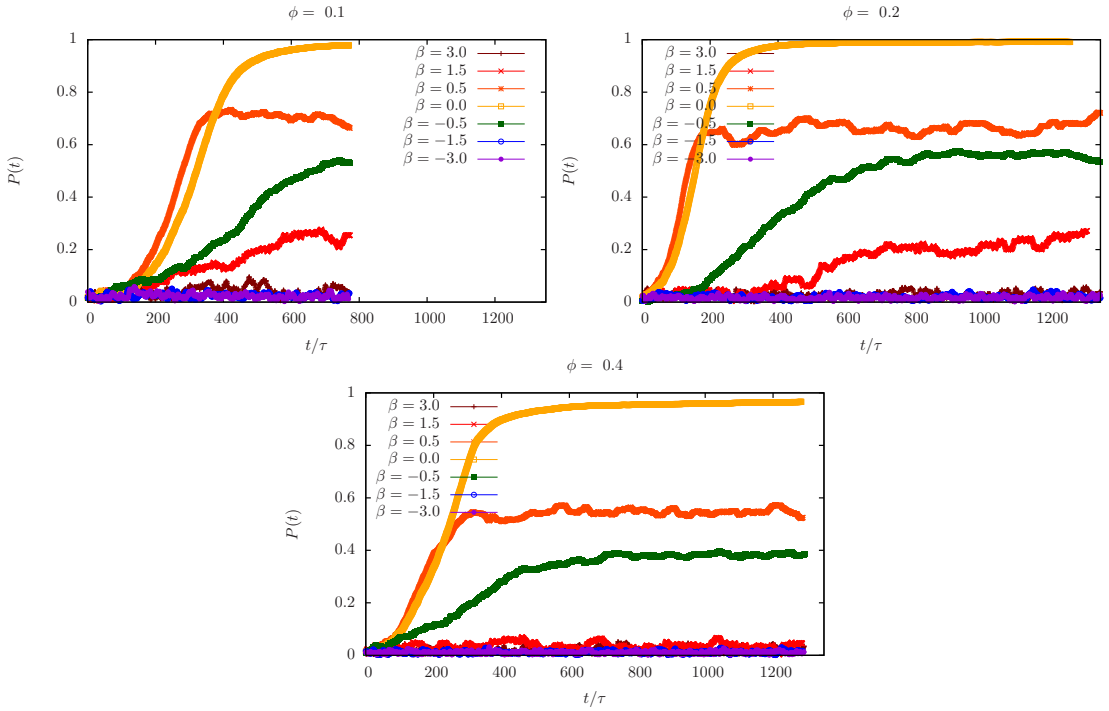

Figure 5.1: Polar Order parameter $P(t)$ as a function of time, for three different densities, and β between -3 and 3. Time is normalized by a Stoke time, defined in Eq. (5.1).

$P(t) \to 0$ implies that either half of the total amount of squirmers are pointing out to the positive side of the surface and half to the negative side or all squirmers are pointing parallel to the swim plane. On FIG. 5.2.2 we show the normal polar order parameter as a function of time for three different concentrations and different values of β. Time is normalized by a Stoke's time defined in equation (5.1). For $\phi = 0.1$ (top-left plot) normal polar order parameter is 0 for all $\beta \neq 0.5$, for $\beta = 0.5$ we have a partial alignment and most of them are pointing out to the negative side of the surface. If we double the concentration of squirmers to $\phi = 0.2$ (top-right plot), we observe same results in β, but now for $\beta = 0.5$ most of them point out to the positive side of the surface. Similarly, for $\phi = 0.4$ (bottom plot) we observe a normal order parameter $P(t)$ around zero, but $\beta = 0.5$ have a small positive normal order parameter $\neq 0$. We can see that all cases with $\beta = 0.5$ normal polar order parameter evolve from the initial condition where all particles are isotropically aligned which gives a normal order parameter equals to zero, to a normal polar order value different to zero, the non-zero value emerges approximately at the same time, independently of the squirmer concentration $\sim 200\tau$.

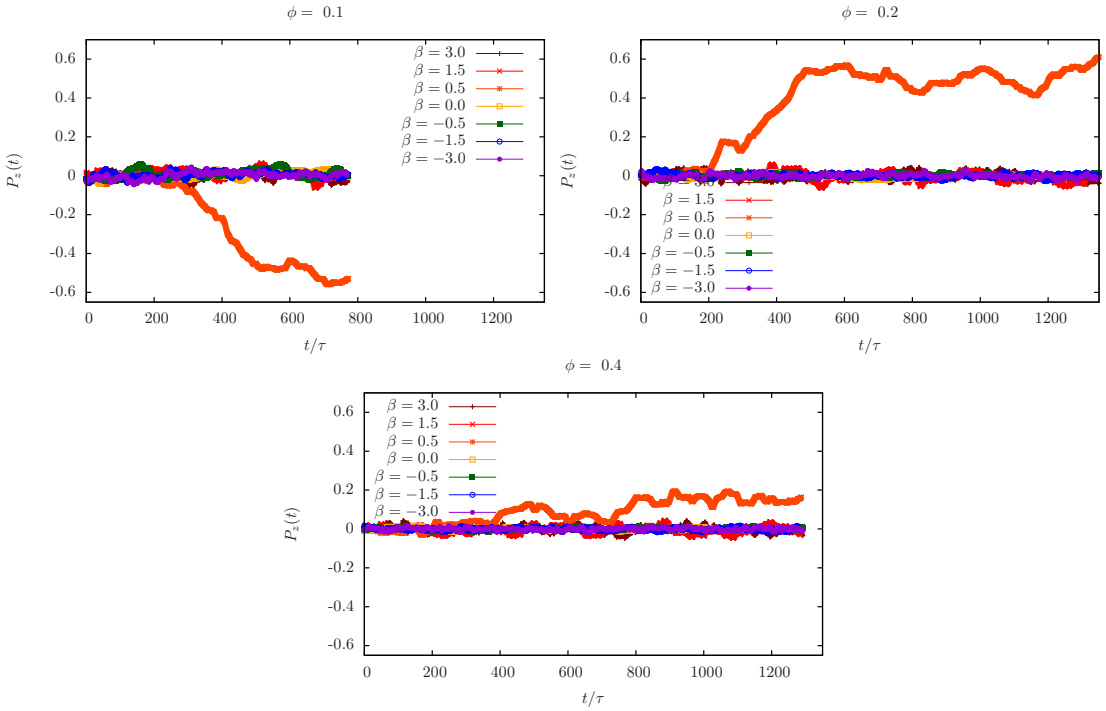

Figure 5.2: Normal Polar Order parameter $P_z(t)$ as a function of time, for three different densities and β between -3 and 3.

5.2.3 Standard deviation of normal polar order

Since normal polar order could be zero for two different states, one it is when particles point out normal to the surface either to the positive or negative side of the plane with the same probability or the secon option is when particles swim parallel to the surface. To differentiate both cases, we calculate the standard deviation of de normal polar order, defined in terms of the second moment of the normal polar order

$$\sigma\left(P_z(t)\right) = \frac{1}{N}\sqrt{\sum_{i=1}^{N}\left(\vec{e}_i(t)\cdot\hat{k} - Pz(t)\right)^2} \tag{5.3}$$

given this σ parameter and the normal order parameter, we have that if $P_z(t) \to 0$ and $\sigma \to 1$ then particles point out normal to the surface either to the right or to the left with the same probability, whereas if $P_z(t) \to 0$ and $\sigma \to 0$ then it means that squirmers like to swim parallel to the squirmers' plane. When $\phi = 0.1$ pushers (violet, blue and green curves in top-left plot of FIG. 5.3) have a $\sigma \sim 0.7$, since $P_z(t) \sim 0$ to these cases, therefore pushers are swimming pointing out either in direction to z or $-z$ with the same probability. For pullers with $\beta > 0.5$ $P_z(t) \sim 0$

also, but σ is 0.5 this means that squirmer have the same behaviour than pushers but closer to the swim plane. When $\beta = 0.5$ σ decrease since particles start to align partially in direction of $-z$. In the same way, when $\beta = 0$ σ decrease almost to zero. In this case normal polar order is zero hence, particles are aligned parallel to the plane XY. When concentration grows to $\phi = 0.2$ we found the same behaviour for σ (top-right plot) with a little increase in σ for puller cases. When ϕ is even higher $\phi = 0.4$, the difference in σ among pullers and pushers disappear (bottom plot). However, when $\beta = 0$ standard deviation does not depend on the concentration, therefore squirmers keep pointing parallel to the plane.

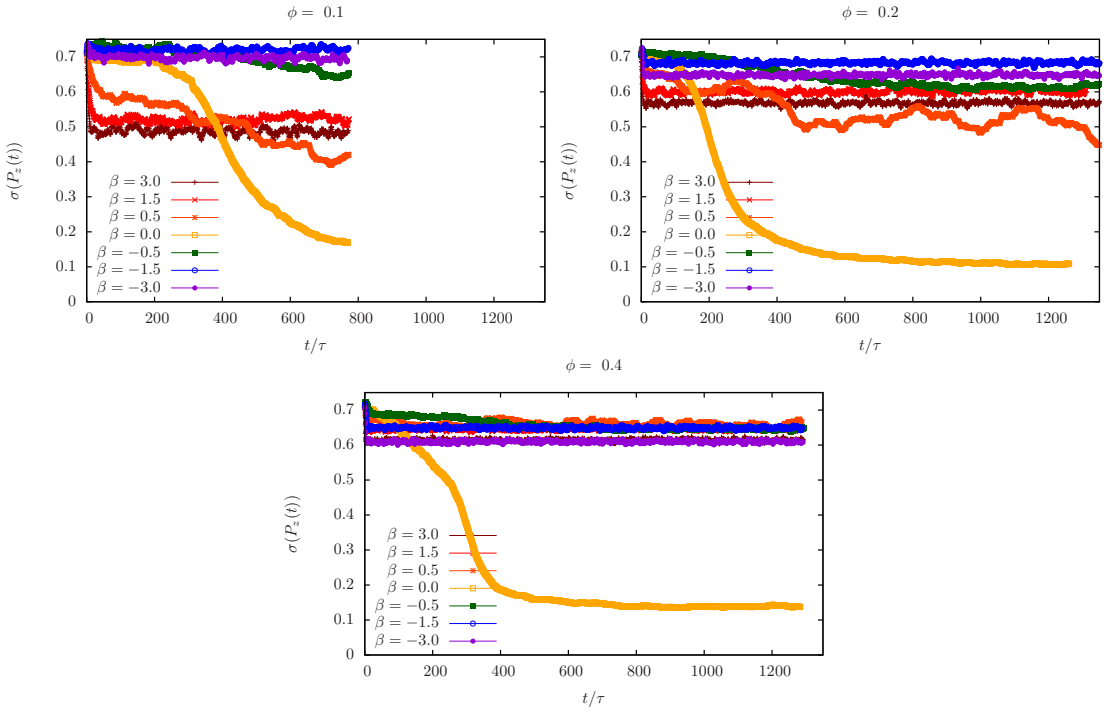

Figure 5.3: Standard deviation of Normal Polar Order parameter $\sigma(P_z)$ as a function of time, for three different densities and β between -3 and 3.

5.2.4 Probability Distribution Functions

Here we show distribution function of the orientation vector projected in the Z direction $PDF(\vec{e}_i(t) \cdot \hat{k} - Pz(t))$. Distribution functions are calculated at long-time states from $t_0 \sim 467\tau$ till $t_f \sim 500\tau$. This PDF complements the results given by the normal polar order parameter and its standard deviation. For semi-dilute regime with $\phi = 0.1$ (top-left plot of FIG. 5.4) we show that pushers' PDFs ($\beta < 0$) have a bimodal distribution with two maxima equally high in ± 1 which means that squirmers are pointing either $-z$ or z with the same probability,

pushers with $\beta > 0.5$ on the contrary point out less to the direction normal to the surface. As we can see in the red and brown PDFs where maximum is in $\vec{e}_i(t) \cdot \hat{k} = 0$, however some squirmers still point out in the direction outside of the surface, since tails of the PDF are non-zero (red and brown curves). When $\beta = 0.5$ squirmers are partially aligned as we saw on FIG. 5.1, with FIG. 5.2.2 we showed that this partial alignment is in the $-z$ direction and in FIG. 5.4 (orange curve) we can see that squirmers are indeed pointing out in $-z$ direction. For $\beta = 0$ (yellow curve) PDF is center at zero, with a narrow peak, and without tails when $-0.5 > \vec{e}_i(t) \cdot \hat{k} > 0.5$ this tell us that squirmers are aligned with the plane where they swim and there are no squirmers pointing normal to the surface where they swim. If we increase the concentration of squirmers to $\phi = 0.2$ (top-right plot FIG. 5.4) we found that PDF's for pushers still have the bimodal distribution we found for more dilute regime, as well as pullers with $\beta < 0.5$ where distributions are center at zero, but in this case distributions are thicker in comparison with more dilute cases. Distributions of squirmers with $\beta = 0.5$ and $\beta = 0$ show that squirmer are aligned, PDF for $\beta = 0.5$ is center in 1 therefore squirmers are pointing normal to the surface, while PDF for $\beta = 0$ is center in zero, these two last distributions are narrower than similar cases with $\phi = 0.1$.

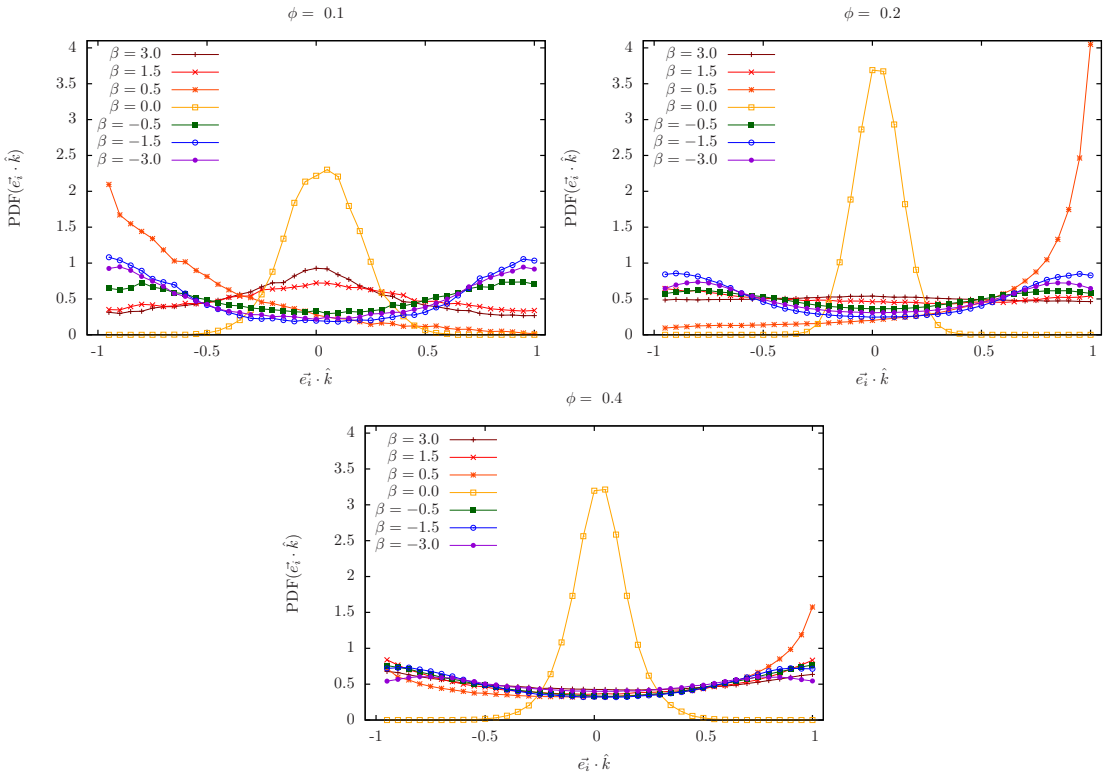

Figure 5.4: PDF of the projection on Z direction of the orientation vector of the squirmers, for three different densities.

If we increase concentration even further to $\phi = 0.4$ distributions for pushers lost their bimodality and we found that squirmers alignment is more isotropically distributed, as well as in the puller cases with $\beta > 0.5$ where distributions center at zero disappear for a more constant distribution like distributions for pushers. PDF for $\beta = 0.5$ is also more like a constant distribution with a little maximum at 1. It seems that concentrate regimes reduce alignment in the suspension when $\beta \neq 0$ since PDF for $\beta = 0$ still has a big maximum center at zero and it is as narrow as the distribution for $\phi = 0.2$ with the same β.

All these results of the PDFs are in agreement with the results of the normal polar order parameter and its standard deviation analysed in previous sections.

5.3 Orientational parameters. Competition between active stresses and self-propulsion

We show how polar and nematic order parameters will depend on the active stress with and without the competition with the collisions due to the self-propel activity. We also present the component normal to the plane of the eigenvector related to the nematic order, which it is the largest positive eigenvalue.

5.3.1 Long-time polar order for trapped squirmers

In FIG. 5.5 we show the long time polar order parameter for two systems, one where particles can move freely in the plane of confinement and another where particles are set in fixed random positions but both systems can re-orient freely in all directions. We calculated the polar order as in eqn. 3.2 and then took the long-time period to calculate P_∞. We can see that P_∞ for free squirmers confined in a plane has a similar behaviour than P_∞ for free squirmers in bulk. With a maximum polar order at $\beta = 0$ and an asymmetry between pushers ($\beta < 0$) and pullers ($\beta > 0$) where pullers with $\beta < 3$ are more aligned than pushers counterpart. Whereas fixed squirmers have not any polar order for all value of β. The constrain that they have of not moving according to the self propulsion give rise to an stability of the isotropic state for all cases of β.

5.3.2 Nematic order parameter

In FIG. 5.6 we show the long time nematic order parameter for the same two systems described above. The black circles represent the nematic order for free squirmers confined in a plane, as well as the polar order, nematic order has a

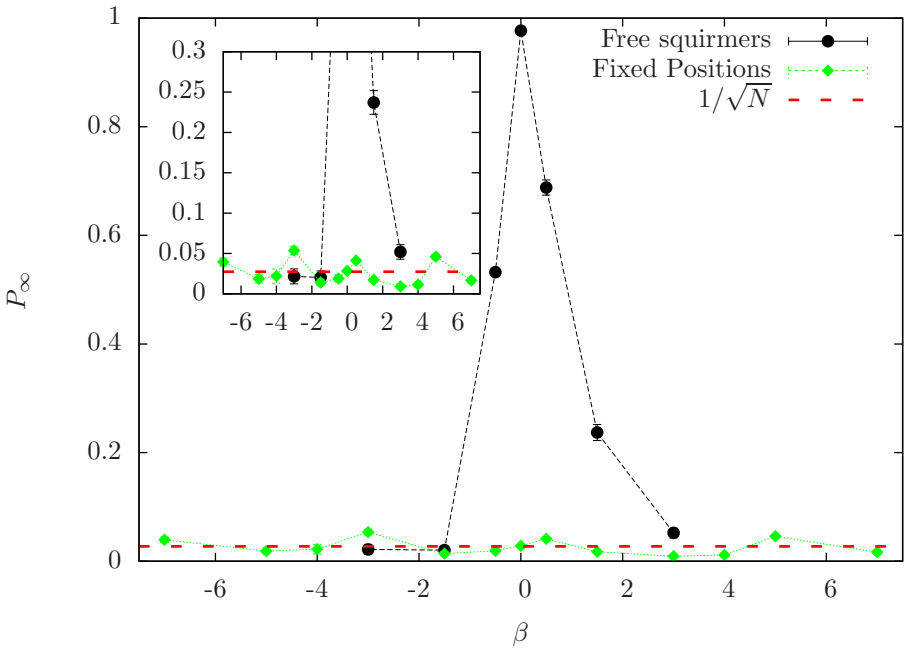

Figure 5.5: The long time polar order P_∞ as a function of β for free squirmers (black circles, β between -3 and 3) and for fixed squirmers (green diamonds, β is taken from -7 to 7 in this case). Red dashed line is the value of $1/\sqrt{N} = 0.027$. Inset shows a zoom in of same data to see P_∞ for squirmers with fixed positions in a more detailed way.

maximum on $\beta = 0$ and an asymmetry between pushers and pullers. However in this case we have a non-zero nematic order order for $\beta < 0.1$ in contrast with the free squirmers in bulk where nematic order is $\sim 1/\sqrt{N}$. Green diamonds in FIG. 5.6 represent the nematic order for fixed particles confined in a plane. We found that nematic order is $\sim 1/\sqrt{N}$ when $\beta < -1.5$ which means that squirmers are not aligned at all and the stable state of these suspensions are the isotropic state where all particles are pointing out in all directions, once $\beta = -1.5$ nematic order increase as β increase till nematic order reaches a value around $\lambda_\infty \sim 1/5$, when $\beta = 0$ the nematic order does not change and keeps the value around $1/5$. This partial alignment of $1/5$ for pullers emerges exclusively by the hydrodynamic signature of the squirmers and the hydrodynamic interaction between them, since particles do not move in the space and also for the geometrical constraint that particles are confined in a plane, which generates a particular flow around the particles that give rise to this collective motion of partial alignment. The full alignment found it for free squirmers confined with $\beta = 0$, or even the semi-aligned system with $\beta = 0.5$ are not recovered with fixed squirmers, which tell us that such aligned states depend also in the collisions due to the intrinsic self-propulsion of the particles. As well as the non-zero nematicity for $\beta < -0.5$.

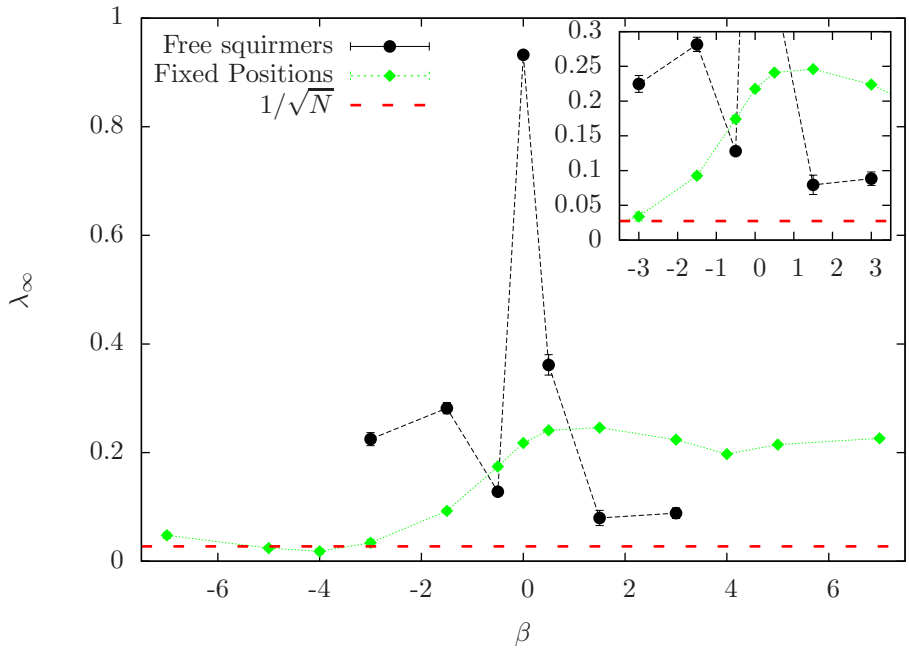

Figure 5.6: The long time nematic order λ_∞ as a function of β for free squirmers (black circles, β between -3 and 3) and for fixed squirmers (green diamonds, β is taken from -7 to 7). Red dashed line is the value of $1/\sqrt{N} = 0.027$.Inset shows a zoom in of same data to see λ_∞ for squirmers with fixed positions in a more detailed way.

Given the unexpected results for fixed particles confined in a plane of zero polar order but non-zero nematic order. We developed some systematic simulations of confined particles and fixed random positions for $\beta = \{-3, 0, 3\}$ where we gradually change the system size, in order to see if this behaviour is finite size effect [110]. In FIG. 5.7 we show the long-time nematic order parameter for four different system sizes. We keep the same area fraction of particles of 0.1 for all cases, hence number of particles and simulation box change at each system size, $L/\sigma = \{25.6, 51.2, 102.4, 204.8\}$, $N = \{84, 336, 1336, 5376\}$ respectively.

As we see in FIG. 5.7, the functional shape of the curves does not change as we change the system size, when $\beta = -3$ nematic order is $\sim 1/\sqrt{N}$ then increase to $\lambda_\infty \sim 1/5$ at $\beta = 0$ and it keeps at around this value when $\beta = 3$. Moreover, if we focus on the inset of FIG. 5.7 we can see that change in the magnitude of the long-time nematic order parameter is minimal as we increase the system size. Therefore, the nematicity that emerge for pullers confined at fixed positions is intrinsic to hydrodynamic effects and the geometrical constraint of confinement and it is not a finite size effect.

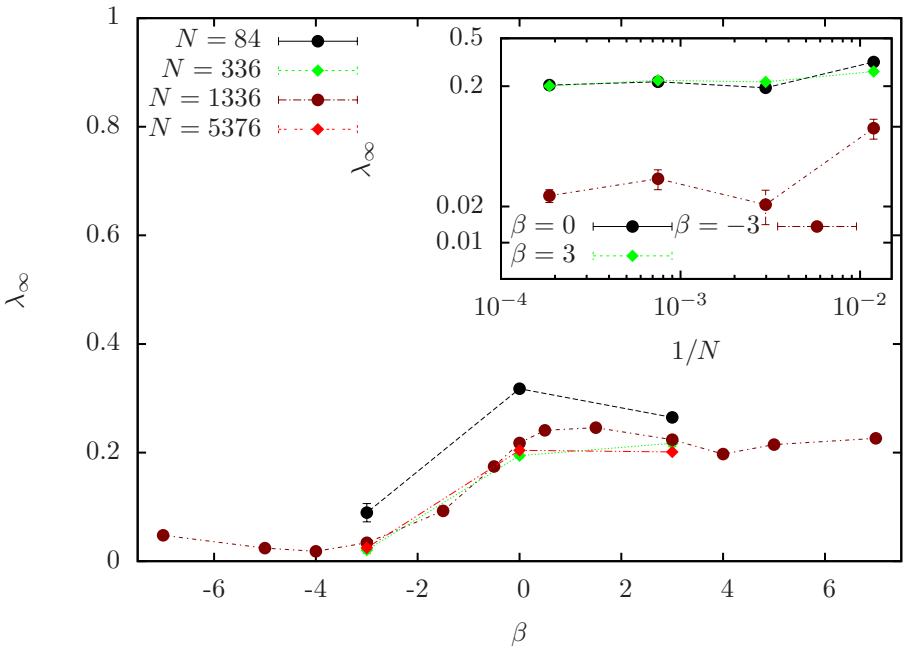

Figure 5.7: The long time nematic order λ_∞ as a function of β for particles in fixed positions, each curve represent one system size. Inset: Long-time nematic order as a function of the system size for three different values of β. $\beta = -3$ (red circles), $\beta = 0$ (black circles) and $\beta = 3$ (green diamonds).

5.3.3 Eigenvectors squirmer orientation at an interface

As we said in previous sections, the nematic order parameter is related to the largest positive eigenvalue of $\mathbf{Q}(t)$ tensor. This eigenvalue $\lambda_+(t)$ fulfils the eigenvalue equation

$$\mathbf{Q} \cdot \mathbf{v}_+ = \lambda_+ \mathbf{v}_+ \tag{5.4}$$

where $\mathbf{v}_+$ is the eigenvector associated to the eigenvalue $\lambda_+(t)$. In order to quantify whether particles are pointing out in the plane where they swimming or they are swimming pointing out outside of the plane, we calculate the z-component of the eigenvector defined in eqn. (5.4). Since z-direction is the normal direction of the plane where particles are confined. Therefore, if the z-component ($v_{\lambda_+ z}(t)$) is zero means that all particles are swimming pointing out parallel to the plane of confinement. Conversely, if this value is non-zero it means that most of the particles are pointing outside of the plane. In FIG. 5.8 we show $v_{\lambda_+ z}$ as a function of time for different values of β, particles are initially pointing out in 3D random directions then depending on their hydrodynamic signature will evolve to different states. When $\beta < 0$ $v_{\lambda_+ z}(t) \sim 1$ which means that most of the particles are partially aligned in a plane normal to the confinement plane, alignment is partial since the eigenvalues associated to these eigenvectors are not 1 but around 0.2 as

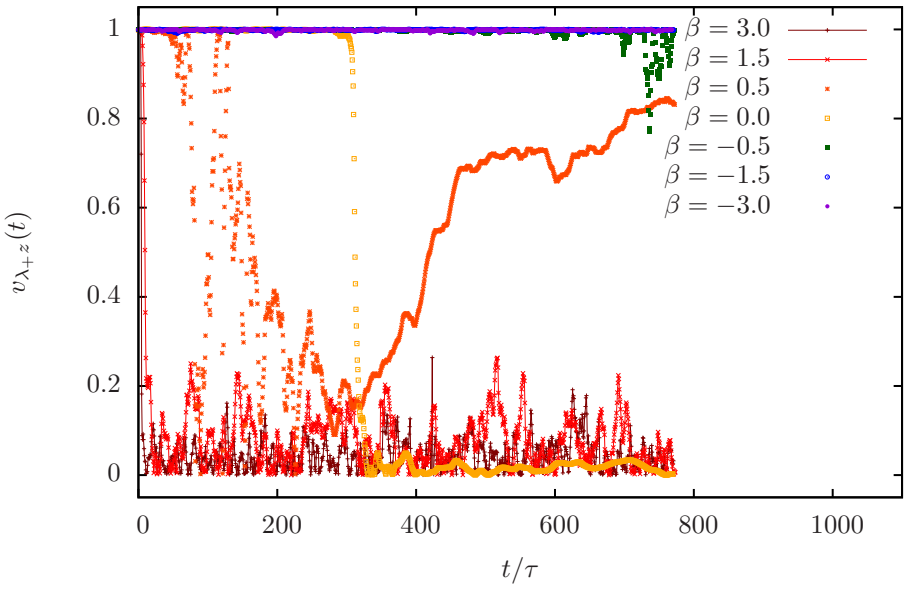

Figure 5.8: The z-component of the eigenvector $v_{\lambda_+ z}(t)$ of free squirmers confined in a plane. Different curves represent different value of β.

it can be seen in FIG. 5.6. On the contrary, when $\beta = 0$ particles are completely aligned since nematic order is almost 1 but alignment is on the plane of confinement, since $v_{\lambda_+ z}(t) \sim 0$ as we can see on the yellow curve of FIG. 5.8. We can observe a very fast transition from the initial isotropic state to completely aligned state around $t \sim 300\ \tau$. At $\beta = 0.5$ the z-component of the eigenvector evolve to a state aligned perpendicular to the confinement plane (orange stars on FIG. 5.8), but first particles evolve to a state where particles are not aligned with z-axis at short times ($t < 300\ \tau$) once $t > 300\ \tau$, $v_{\lambda_+ z}(t)$ start to grow relatively fast to a aligned state parallel to z-axis. Moreover, most of the particles that are aligned are also pointing in the same direction, since polar order is also ~ 0.7 as it can be observed in FIG. 5.5, where $P_\infty = 0.7$ for $\beta = 0.5$. In the same way as $\beta = 0$, where $P_\infty \sim 1$. For pullers with $\beta > 0.5$ $v_{\lambda_+ z}(t)$ is around zero at all time, with fluctuations from 0 to 0.2. If particles are fixed in random positions and they are only allowed to re-orient we found that $v_{\lambda_+ z}(t)$ goes to zero dramatically fast as a function of β when $\beta > -3$. As we show in the left side of FIG. 5.9, where we observe how the z-component of the eigenvector associated to the nematic order goes to zero for all β ranged from -3 to 3, although all cases goes zero, the relaxation time from initial isotropic state to the steady state it depends on the β value, in the inset of left plot of FIG. 5.9 we show a zoom in of the z-component at short times and it is possible to see the dependency in β of the relaxation time: the greater the value of β the shorter the relaxation time. Another important remark is when $\beta = -3$ $v_{\lambda_+ z}(t)$ has much more fluctuations in time than any other case

with $\beta > -3$, this effect is due to the fact the eigenvalue for $\beta = -3$ is almost zero, as we saw in FIG. 5.6, hence the equation for get the eigenvectors (eqn. 5.4) has more numerical fluctuations. This effect is observed for all cases where eigenvalue is close to zero, as we present in the right plot of FIG. 5.9 where the same z-component of the eigenvector $v_{\lambda_+ z}(t)$ is showed for cases with $\beta < -3$, pushers in these cases have a eigenvalue close to zero and that is the reason why $v_{\lambda_+ z}(t)$ fluctuates a lot, specially when $\beta = -4$ (green data). Special remark when $\beta = -7$ and -5, since fluctuations in both cases are very small despite that eigenvalues are close to zero. It seems that this small nematicity ($\lambda_+ \sim 0.048 \pm 0.006$ and 0.024 ± 0.004) correspond to a partial alignment in the z-direction. Similar to the aligmnement normal to the confinement plane that we observed for pushers when particles can move freely (FIG. 5.8). Additionally in this plot, we show $v_{\lambda_+ z}(t)$

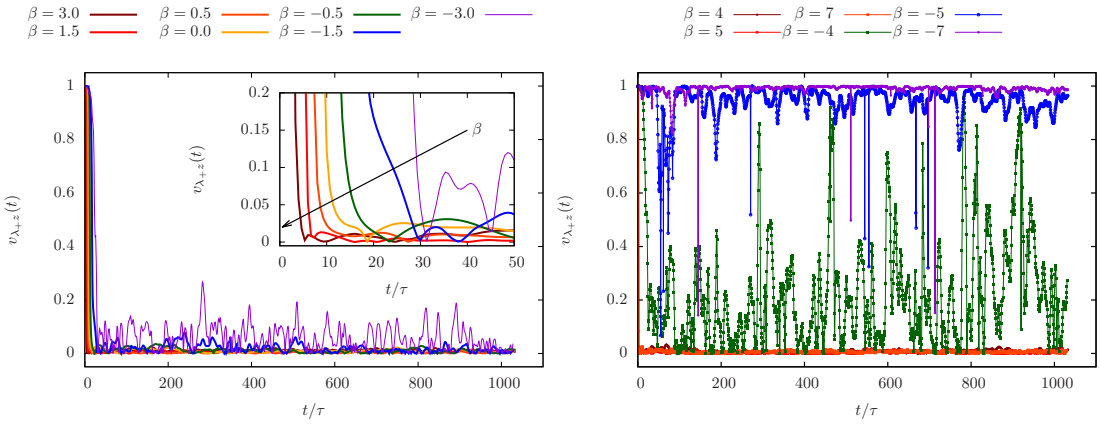

Figure 5.9: The z-component of the eigenvector $v_{\lambda_+ z}(t)$ of fixed squirmers. Left plot correspond to β values from -3 to 3. Inset: Zoom in of same plot, black arrow represent the direction of growth of β, the greater the value of β the shorter the relaxation time. Right plot correspond to greater values in magnitude of $\beta = \{\pm 4, \pm 5, \pm 7\}$.

for $\beta > 3$ and we observe that particles remain aligned to the confinement plane like the other cases of pullers with $\beta < 4$, since z-component of the eigenvector is zero and the eigenvalue associated to all cases of pullers is ~ 0.2 as we showed in FIG. 5.6.

5.4 Conclusions

We have analysed spherical squirmer suspensions with squirmers restricted to move in one plane. Our analysis was focused on the global orientation of the suspension measured by the global and normal order parameters and the probability

distribution functions of the orientations. We found that at long times, suspensions reach a steady state of alignment where depending on the hydrodynamic signature (β) and concentration (ϕ) we can have either an aligned state or an isotropic one. We were able to characterize all the cases in five general scenarios. One with $\beta = 0$ where squirmers are aligned parallel to the plane where they move. Squirmers are aligned and move in the same direction. This case depend very weak on the concentration. Another one for pushers which alignment is normal to the plane where they can move, however they are not moving in the same direction. If concentration increase pushers lose their alignment and suspension becomes isotropic which can be seen as a third case. A fourth case for pullers with $\beta > 0.5$ in the semi-dilute regime ($\phi = 0.1$) where they are partially aligned with the plane in which they can move but do not move in the same direction. If concentration increase, suspension becomes isotropic like the third case described before. Last case, when $\beta = 0.5$ suspension is aligned partially in the direction normal to the plane and squirmers move in the same direction. The alignment and polarity is not so much affected when concentration increases.

Striking results were found for the long-time polar order, since this parameter behaves in the same way as the bulk system with a maximum in $\beta = 0$ and polarity is vanish if particles are fixed. But Nematic order will depend on the β value, despite that particles can not self-propel. We have a not negligible value of nematic order when particles are pullers and it turns out that particles align parallel to the plane of confinement.

Chapter 6

Conclusions and perspectives

Summary of results

As we mentioned in 1, active systems nowadays has become a hot topic in science, specially active systems where hydrodynamic interactions are present. Several interesting questions have been arise, from both sides. From the theoretical point of view, questions like whether exist a equation of state for these systems or why active matter exhibit giant density fluctuations, breaking the familiar $\sqrt{N}$ equilibrium scaling of number fluctuations in subregions with N particles on average [4]. From a more technological point of view, we have that many systems like micro-organisms play a vital role in many biological, medical and engineering phenomena [37]. Therefore, to apply simulations to these kind of systems is of paramount importance, since many of the analytical work turns to be very hard, specially if hydrodynamic interactions are taking in count and shed some light to understand systems that can bring us many benefits.

With all that as a motivation, during these years of research for this thesis, we have carried out systematic LB simulations of micro-swimmers. We have used a very well tested code [76] which follow the theoretical framework explained through all the chapter 2. *Ludwig* is a coded that has been tested for use in parallel environments, thus it can reach large enough systems in reasonable time.

Following the idea of Evans et al. in [31], we have done a first systematic study using LB with squirmer suspensions in order to reproduce the previous results of the polar ordering as a function of the active stress, we have found approximately, the same functional shape of the long time polar order, but the aligned region in their case was wider in β. Another interesting difference was the findings of significant aggregates for pullers in 3D, which Evans et al. [31] did not mention, probably because their system is very small ($N = 64$ particles) while our system reached 2000 particles. With the results of the temporal correlation function of

the density fluctuations and the pair correlation functions for the positions and the orientations of the particles in [34], we were able to conclude that the flocking observed for pullers with $0 < \beta < 1$ leads to large elongated structures, like Vicsek bands [111].

This striking macroscopic effect found in squirmers swimming in a semi-dilute suspension, was deeply studied by us. The main results are depicted in chapter 3, where have shown a complete characterization of the collective motion of squirmers swimming freely with no constrains. We have found that not only the degree of polar order but the value of the exponent of the number fluctuations depend on the hydrodynamic signature of squirmers In particular we found GDF (giant number fluctuations) for certain range where flocking is observed, which can be related with a phase transition. To compare this transition with the very well known transition for self-propels particles the MIPS [15] we calculate the density dependence speed and the PDF of the local density and we show that behavior is totally different, therefore the transition observed for squirmers is generated by other parameters besides the density and the velocity of self-propulsion [16]. Mean square displacement was also calculated, and the cluster size distribution (CSD), where we found anomalous diffusions for some cases. We also found a way to characterize the macroscopic cluster generated by squirmers, via CSD. Finally a complete finite size effect study is presented, where we have verified that the emergent macroscopic cluster is completely generated by high correlations between swimmers.

Another interesting system is whether the particles attracts each other, and a competition between attractive interactions and activity strength is present. Inspired in some real experiment [8, 99] we add an attractive force to the squirmers and confined to move and rotate in a plane, where the fluid is also confined in a slab with periodic boundary conditions. The goal here is to observe wether the hydrodynamic interaction play a key roll in the generation of clusters and their morphology in comparison with active particles simulated with Brownian Dynamics, besides of the experiments. A complete study on the morphology and the dynamic of the clusters formed by attractive squirmers is shown in chapter 4.

Finally, from both theoretical and experimental work, it has observed that colloids partially confined in an interface, where their dynamics are influenced by hydrodynamic interactions mediated by the unconfined fluid. Hence for the same problem but with active particles instead of colloids, turns to be a very interesting problem, A. Dominguez has investigated the linear stability of these kind of systems, while us have been carried out a set of simulations at long times, where we can observe the influence of the unconfined fluid in the formation of coherent structures on the particles. We have shown in chapter 5 how both polar and nematic order change depending on the 3D velocity fluid generated by the

particles themself. For example, one striking result is that the long-time polar order behaves in the same way as the bulk system with a maximum in $\beta = 0$ and polarity is vanish if particles are fixed. But Nematic order will depend on the β value, despite that particles can not self-propel. We have a not negligible value of nematic order when particles are pullers and it turns out that particles align parallel to the plane of confinement. Very important to remark that simulations and in particular our computational scheme allow us to do such kind of exercise, where we can cancel one of the parameters of the systems, therefore we are able to have a more general understanding of the influence of the different parameters of a real complex system.

Perspectives

Several lines and ideas have been generated along the realization of this project:

- The results presented in chapter 3 open the door to more questions, like whether the macroscopic cluster observed independtly of the system size is in fact a band under the vicsek model scheme or is a completelly different new phase produce only by hydrodynamic interactions.
- From the interactive squirmers swiming in 2D we have a couple of ideas. i) To change the potential between the particles an put a explicit Janus potential, where a more direct comparison with both experiments and theory could be reached. ii) We already calculate the morphology and the dynamics of the clusters generated by experiments of photoactive colloids [112]. Now we are going to compare with squirmer suspensions, in order to try to find a correlation between the morphology and the dynamics of the clusters.
- We have identified singular coherent structures for squirmers under partial confinement like the squirmers in chapter 5. To understand this system in a more rigours way by the study of linear stability of a theoretical mean field theory like in [109] would be very interesting.

Capítulo 7

Resúmen en castellano

Los sistemas activos, se definen como materiales fuera del equilibrio termodinámico compuestos por muchas unidades interactuantes que individualmente consumen energía y colectivamente generan movimiento o estreses mecánicos. Ejemplos se pueden encontrar en un enorme rango de escalas de longitud, desde el mundo biológico hasta artificial, incluyendo organismos unicelulares, tejidos y organismos pluricelulares, grupos de animales, coloides auto-propulsados y nano-nadadores artificiales. Actualmente se están desarrollando experimentos en este campo a un ritmo muy veloz, en consecuencia son necesarias nuevas ideas teóricas para traer unidad al campo de estudio e identificar comportamientos "universales" en estos sistemas propulsados internamente.

El objetivo de esta tesis es el estudiar mediante simulaciones númericas, el comportamiento colectivo de un modelo de micro-nadadores. En particular, el modelo de squirmers, donde el movimiento del fluido es axi-simétrico. Existen estructuras coherentes que emergen de estos sistemas así que, el entender si las estructuras coherentes son generadas por la firma hidrodinámica intrínseca de los squirmers individuales o por un efecto de tamaño finito se vuelve algo de primordial importancia. Nosotros también estudiamos la influencia que tiene la geometría en la aparición de estruturas coherentes, la interaction directa entre las partículas, la concentración, etc.

Esta tesis reporta nuevas fases de suspensiones de squirmers que se caracterizan por forma una distribución de tamaños de clusters o incluso suspensiones donde un cluster macroscopico emerge. Un objetivo importante en esta tesis es caracterizar estas fases de clusters, además de estudiar su morfología de cara a entender la fenomenología del sistema haciendo una analogía con las distribuciones de clusters y los parámetros morfológicos de los sistemas en equilibrio.

La tesis está organizada de la siguiente manera:

Nosotros primero hacemos una revisión, en el Capítulo 1, qué son los sistemas activos y las consecuencias de tener un conjunto de particulas activas. También en éste capítulo nosotros encontramos algunos ejemplos de materia activa bajo varios contextos. Aquí tambié explicamos los micro-nadadores y en particular, el movimiento de squirmer de una manera detallada.

En el Capítulo 2 explicamos la metodología numérica que usamos para simular el fluido que interactúa con los micro-nadadores. Una revisiíon completa del método está puesta aquí.

En el Capítulo 3 mostramos que las suspensiones semi-diluídas de microorganismos en 3D pueden desarrollar movimientos colectivos tales como el alineamiento polar y fluctuaciones gigante. Demostramos en éste capítulo tambiíen que tanto los movimientos colectivos como las fluctuaciones gigantes dependen de la señal hidrodinámica de las particulas; además los sistemas con fluctuaciones gigantes generan una distribución de tamaños de cluster donde el cluster macroscopico aparece. Esta notable separación de fase emerge gracias a las interacciones hidrodinamicas que re-orientan y alinean a las particulas. NO es una separación de fase debida a la reducción de velocidad cuando la densidad local crece.

Además, las suspensiones alineadas generan un movimiento super-difusivo a tiempos largos. En éste capítulo también contiene un estudio computacional completo de suspensiones de squirmers en 3D. Mostramos medidas globales de la suspensión, parámetros globales como la fluctuación en la densidad, la velocidad dependiente de la densidad o el desplazamiento cuadrático medio. Todas éstas medidas nos dan información del comportamiento general de la suspensión.

En el Capítulo 4 mostramos simulaciones de una suspension diluida de partículas esféricas auto-propulsadas atractivas, donde también se toma en cuenta la hidrodinámica. Las partículas están restringidas a moverse y orientarse paralelas a un plano constante. Para empezar, observamos que dependiendo de la razón entre atracción y propulsión, las partículas se agregan formando clusters. En seguida, analizamos su estructura, comparando el caso cuando las particulas activas se comportan como pushers o como pullers (siempre en la región donde las atracciones inter-partícula compete con la autopropulsión). Finalmente, comparamos los resultados obtenidos con un sistema que consiste de discos Brownianos autopropulsados en las mismas condiciones. Hemos encontrado que la hidrodinamica controla el nado coherente entre los nadadores, mientras que los nadadores con interacciones directas, modelados por un potencial Lennard-Jones, contribuye a que los nadadores se cohesionen.

En el Capítulo 5, desarrollamos simulaciones numéricas de suspensiones de squirmers donde las particulas fueron confinadas a moverse solamente en un plano, pero el solvente se mueve libremente en 3D. Vemos que el orden polar de la sus-

pensión depende de la señal hidrodinámica y de las colisiones de las particulas como en el caso no confinado, sin embargo debido a la restricción geometrica a moverse en el plano, vemos que dependiendo de la forma de nado (pusher/puller) estas se pueden alinear en paralelo o perpendicular al plano de nado. Cuando los squirmers solamente se pueden re-orientar y están fijos en el plano encontramos que el orden polar desaparece para todos los casos, pero el orden polar sigue presente en el plano de nado para pullers, mientras que los pushers son más estables isotrópicamente.

Este alineamiento que emerge debido a el confinamiento de particulas fijas es estudiado más sistematicamente, haciendo simulaciones para diferentes tamaños, encontrando que el alineamiento emerge completamente debido a la restricción de confinamiento y las interacciones hidrodinámicas entre particulas y no a un efecto de tamaño finito. Debido a la constricción geométrica, nosotros también mostramos el vector propio asociado a el orden nemático, para analizar si las particulas se re-orientan normal o paralelas al plano de confinamiento. Dando lugar al hecho de que pullers con posiciones fijas se alinean paralelamente al plano.

Finalmente en el Capítulo 6 las conclusiones y las perspectivas a la continuación del trabajo.

Appendix A

Identifying clusters

In order to detect the clusters in the suspension, we use the first minimum (r_{cl}) of the radial distribution function and identify particles within this distance as neighbours belonging to the same cluster.

To start with, we compute the radial distribution function of a Lennard-Jones fluid at the ϕ studied in the manuscript (for this purpose, we consider configurations in the time interval when the system is in steady state.
In practice, two particles belong to the same cluster when they are closer than a given distance r_{cl}. Although the $g(r)$ structure depend on the hydrodynamic signature and the interaction strength, in figure A.1 we show that a value of $r_{cl} = 1.8\sigma$ is compatible with all chosen values of ξ and β.

One important remark about the radial distribution function around r_{cl} is that $g(r)$ is quite constant around r_{cl}, the length of this valley in the $g(r)$ relates the distance between the first and the second shell of coordination. This bias in the value of the first minimum does not affect in the identification of clusters. In figure A.2, we show the cluster-size distribution functions for different values of β at $\xi = 1.8$, using three different values of $r_{cl} = \{1.3, 1.5, 1.8\}\,\sigma$. We can observe that CSDs have in general the same power law with an exponential tail behaviour for the three values of r_{cl}. CSDs however, get a little bit wider as r_{cl} increases. But, as long as our choice of r_{cl} is around the first minimum of the $g(r)$, the cluster size distribution does not depend on the exact value of r_{cl}.

The figure A.2 also shown that the width of the distributions are more affected for pushers than for pullers. Since pullers are more structured (longer peaks on the $g(r)$) therefore the minimum is better defined.

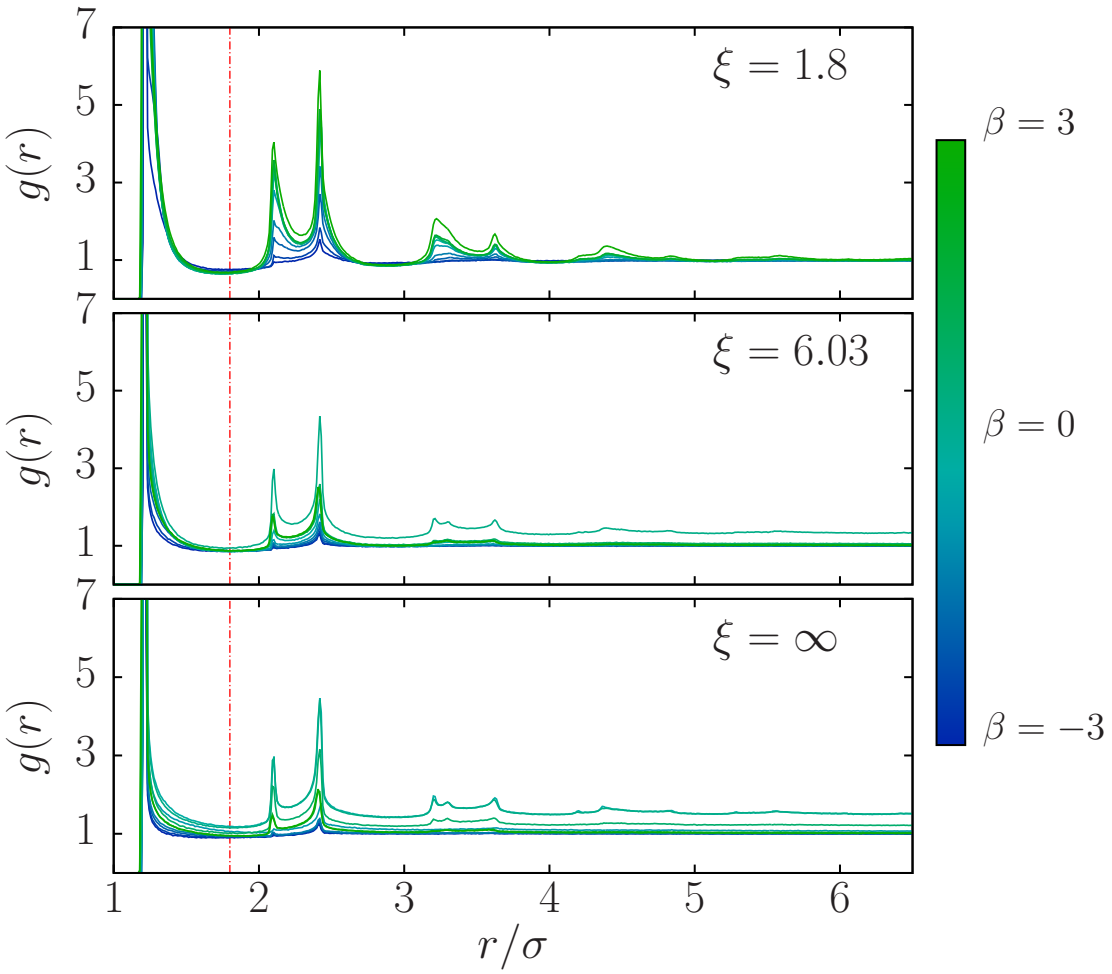

Figure A.1: Radial distribution functions $g(r)$ for three different values of $\xi = \{1.8, 6.03, \infty\}$. The color of the curves is set as a function of β the greener the curve, the more positive β value, whereas the bluer the curve, the more negative the β value. Red line represents the value of $r = r_{cl}$.

A.1 Values of Δs_i used to compute $f(s)$

As mentioned in Chap 4, when computing the cluster-size distribution in order to improve the statistics we group clusters with size within the interval $\Delta s_i = (s_{i,max} - s_{i,min})$, as in Ref. [87]. In Table A.1 we explicitly indicate all chosen Δs_i centred around s.

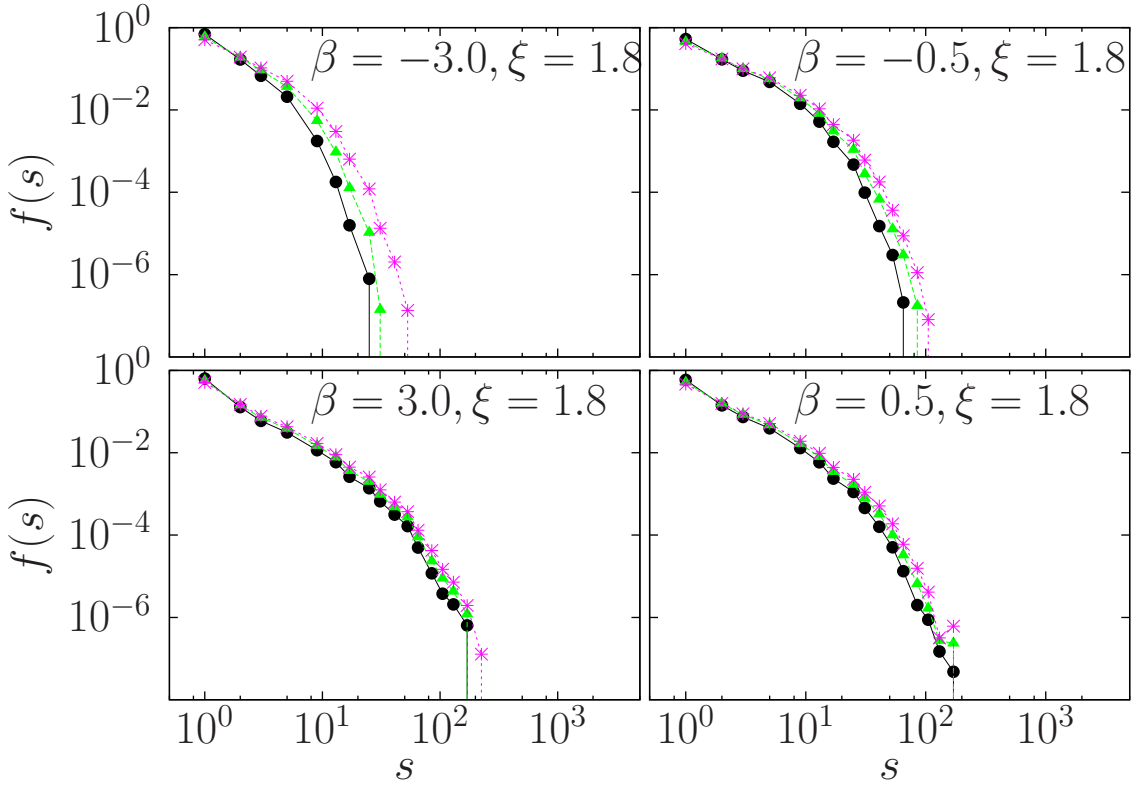

Figure A.2: Cluster-size distribution $f(s)$ for values of $\xi = 1.8$. Black circles correspond to $r_{cl} = 1.3\sigma$, green triangles to $r_{cl} = 1.5\sigma$, magenta stars to $r_{cl} = 1.8\sigma$. The chosen values for β and ξ are indicated in the legend.

Table A.1: Boundaries of the cluster-size intervals, $[s_{i,max}, s_{i,min}]$, centred around s.

$[s_{i,max}, s_{i,min}]$	s	$[s_{i,max}, s_{i,min}]$	s	$[s_{i,max}, s_{i,min}]$	s
1	1	[36,45]	41	[451,600]	526
2	2	[46,55]	51	[601,1000]	801
3	3	[76,95]	81	[1001,1300]	1151
[4,7]	5	[96,120]	109	[1301,2000]	1651
[8,11]	9	[121,140]	131	[2001,3500]	2751
[12,15]	14	[141,200]	171	[3501,5000]	4251
[16,21]	17	[201,250]	226	[5001,7000]	6001
[22,27]	25	[251,300]	276	[7001,10000]	8501
[28,35]	32	[301,450]	376		

A.2 Size effects in attractive squirmer suspensions swimming in a slab

Here we showed how size system affects to the morphology and to the cluster-size distribution of interactive squirmers in a slab. The morphology is characterized by the radius of gyration of the clusters while cluster-size distribution by the PDF of the cluster-size. All the results are presented for four different βs and three different interaction strengths.

A.2.1 Cluster-size distribution

In Figure A.3 we represent the cluster-size distribution for different values of ξs and βs for two different sizes, $N = 10^3$ with solid symbols and $N = 10^4$ with hollow symbols. Both systems with the same area fraction of $\phi = 0.1$. There are not finite size effects in the cluster-size distributions for $\xi = 1.8$ as we observe in the top-left side of figure A.3 where the CSD's for small systems matched with the correspondent CSD for large systems, a similar behaviour can be found when $\xi = 6.03$. However, for $\xi = \infty$ CSD's match perfectly for small clusters but, for big clusters CSDs for small systems are above the CSDs for big systems, as we show in the bottom side of figure A.3. The mismatch at big clusters is clearly due to finite size effects, since the formation of big clusters is mostly driven by the hydrodynamic interactions, thus long range interactions.

A.2.2 Radius of gyration

In order to find structural differences among clusters for two different system sizes, we start with analysing the radius of gyration. In figure A.4 we represent the radius of gyration normalized by the particle's radius for different values of ξs and βs for two different sizes, $N = 10^3$ with solid symbols and $N = 10^4$ with hollow symbols.

In general, there are not finite-size effects in the radius of gyration of the clusters despite the value of ξ. All the curves of size dependence radius of gyration match between small and large systems.

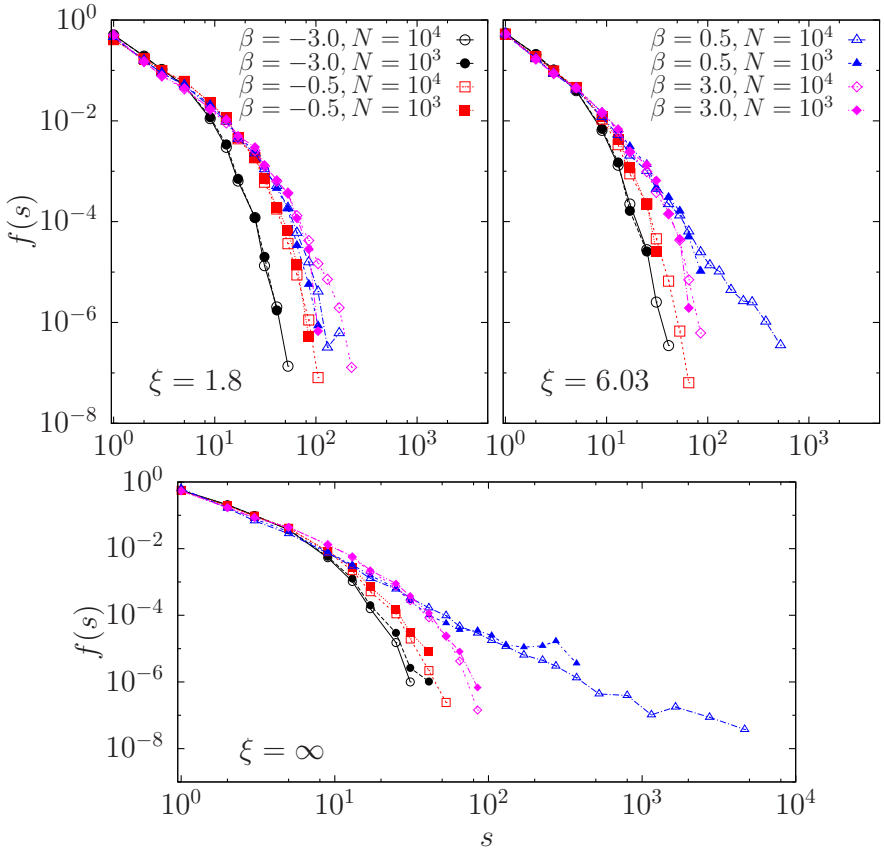

Figure A.3: Cluster-size distribution $f(s)$ for values of $\xi = \{1.8, 6.03, \infty\}$. Circles correspond to $\beta = -3$, squares to $\beta = -0.5$, triangles to $\beta = 0.5$ and diamonds to $\beta = 3$. Solid symbols are for small systems with $N = 10^3$ whereas solid symbols are for big systems with $N = 10^4$.

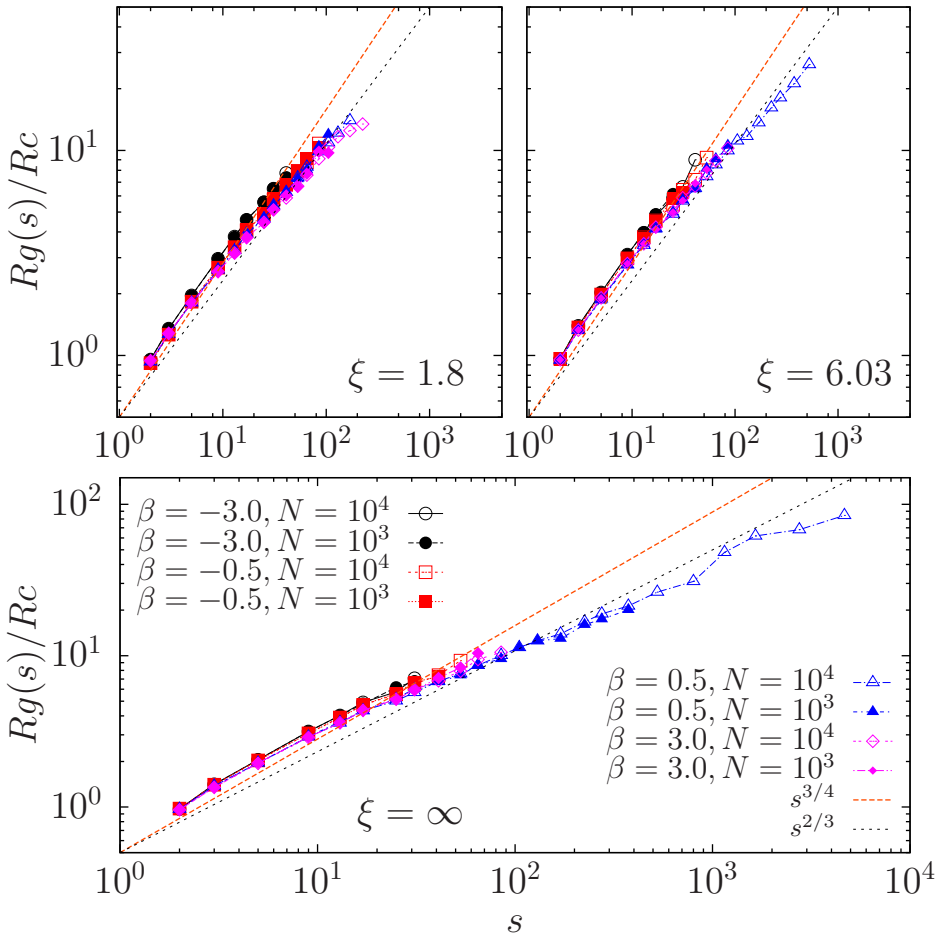

Figure A.4: Radius of gyration $R_g(s)$ (normalized by the radius of a particle) as a function of the cluster-size for values of $\xi = \{1.8, 6.03, \infty\}$.Circles correspond to $\beta = -3$, squares to $\beta = -0.5$, triangles to $\beta = 0.5$ and diamonds to $\beta = 3$. Solid symbols are for small systems with $N = 10^3$ whereas solid symbols are for big systems with $N = 10^4$. Orange dashed curve and pointed black curve are depicted as guide to the eye and represent $s^{3/4}$ and $s^{2/3}$ respectively.

Appendix B

Angular velocity

Angular velocity $\boldsymbol{\omega}_0$ of a rigid body with respect to a set of axes with origin at O is related with the inertia tensor $\mathbf{I}_0$ and the angular momentum $\mathbf{L}_0$ as [113]

$$\mathbf{L}_0 = \mathbf{I}_0 \cdot \boldsymbol{\omega}_0 \tag{B.1}$$

where the inertia tensor is defined as:

$$\mathbf{I}_0 = \sum_{k=1}^{N_p} \left(m_k r_k^2 \mathbf{1} - m_k \mathbf{r}_k \mathbf{r}_k \right). \tag{B.2}$$

Let $\mathbf{r}$ and $\mathbf{r}'$ be the position vectors of any particle P in the body relative to O and the center of mass G respectively, and let $\mathbf{R}$ be the coordinate of G relative to O, see Fig.B.1,

$$\mathbf{r}' = \mathbf{r} - \mathbf{R}. \tag{B.3}$$

Thus we can define the inertia tensor of a rigid body relative to the center of mass $\mathbf{I}_G$ as:

$$\mathbf{I}_G = \sum_{k=1}^{N_p} \left(m_k r_k'^2 \mathbf{1} - m_k \mathbf{r}'_k \mathbf{r}'_k \right); \tag{B.4}$$

and angular momentum $\mathbf{L}_g$

$$\mathbf{L}_G = \sum_{k=1}^{N_p} \mathbf{r}'_k \times m_k \mathbf{v}'_k; \tag{B.5}$$

where $\mathbf{r}'_k$ is given by eqn.(B.3) and its temporal derivative is $\mathbf{v}'_k$.

Hence, we have that angular velocity with respect to the center of mass $\boldsymbol{\omega}$ can

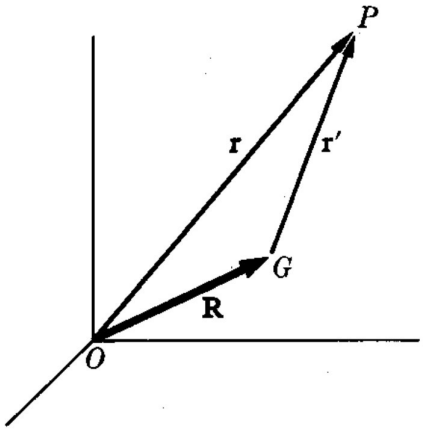

Figure B.1: Location of position P with respect to points O and G.

be written as:

$$\mathbf{L}_G = \mathbf{I}_G \cdot \boldsymbol{\omega} \tag{B.6}$$

We calculated $|\boldsymbol{\omega}|$ for every cluster at each simulation. We diagonalized the inertia tensor in eqn. (B.6) using the very well known method of Singular Value Decomposition [114].

Angular velocity on fixed clusters

As a way of verification, we show in this note the angular velocity of a single cluster for different cluster size, since we calculate the velocity of particles as $\mathbf{v}_i = \boldsymbol{\omega}_0 \times \mathbf{r}_i$ at fixed $\boldsymbol{\omega}_0 = 0.001\ \widehat{k}$ (lattice units).

We construct clusters of different sizes $N = \{2, 3, 5, 6, 8, 80, 180\}$ each clusters is constructed as "polymer" where a particle i is putted randomly $2R + \varepsilon$ far from particle $i - 1$ and all particles do not overlap each other. $\varepsilon = 0.05$(lattice units) and $R = 2.3$(lattice units) The particles $i = 0$ is placed at the center of the box, the box size is $L_x = L_y = 400$ and $L_z = 26$ as a way of simplicity we fixed $r_z = L_z/2$ for all the particles in all the cluster sizes. As we already said $\mathbf{v}_i = \boldsymbol{\omega}_0 \times \mathbf{r}_i$ with $\boldsymbol{\omega}_0 = 0.001\ \widehat{k}$. Hence, we expect as output an angular velocity $\omega = 0.001$ (lattice units), independently of the cluster size. The configuration of the clusters is depicted in Fig.B.2. As we see, cluster polymer-like were used.

Angular velocity for different cluster sizes is depicted in Fig.B.3 where we can see how $\omega = \omega_0$ for all cluster size. Hence, the angular velocity that we expected is accomplish.

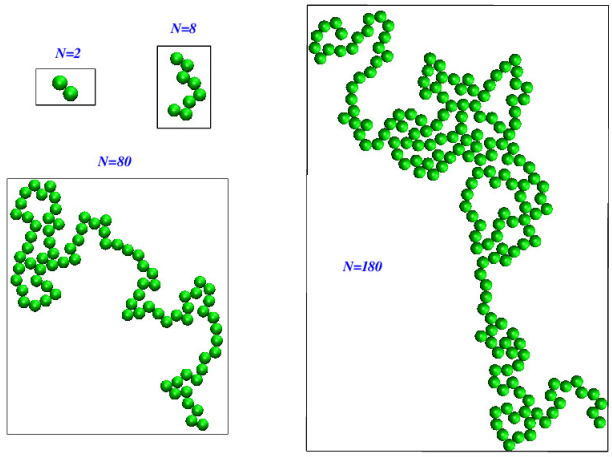

Figure B.2: Snpashots of clusters for $N = \{2, 8, 80, 180\}$.

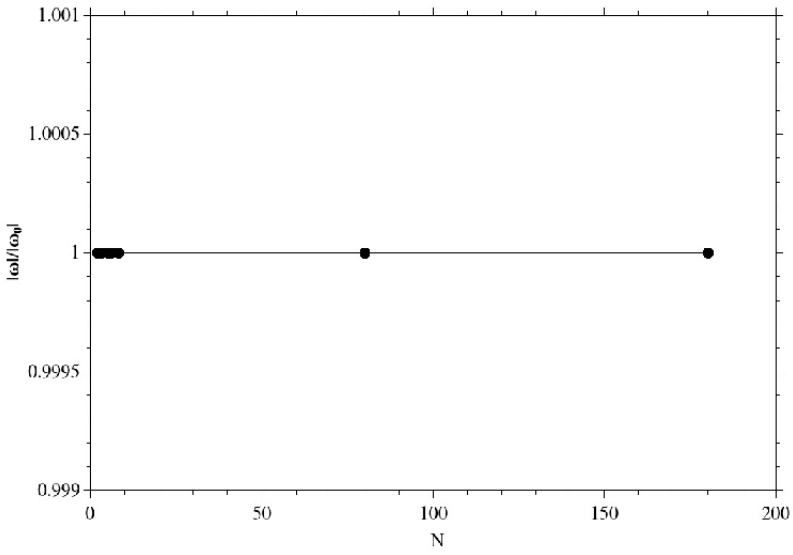

Figure B.3: Angular velocity normalized by $\omega_0 = 0.001$ is shown here. Values are exactly 1.

References

[1] S. Ramaswamy, "The mechanics and statistics of active matter," *Annual Review of Condensed Matter Physics*, **1**, (1), 323–345, 2010.

[2] T. Vicsek and A. Zafeiris, "Collective motion," *Physics Reports*, **517**, (3-4), 71 – 140, 2012.

[3] I. S. Aranson, "Collective behavior in out-of-equilibrium colloidal suspensions," *Comptes Rendus Physique*, **14**, (6), 518 – 527, 2013.

[4] M. C. Marchetti, J. F. Joanny, S. Ramaswamy, T. B. Liverpool, J. Prost, M. Rao, and R. A. Simha, "Hydrodynamics of soft active matter," *Rev. Mod. Phys.*, **85**, 1143–1189, Jul 2013.

[5] A. M. Menzel, "Tuned, driven, and active soft matter," *Physics Reports*, **554**, 1 – 45, 2015.

[6] F. Peruani, A. Deutsch, and M. Bär, "Nonequilibrium clustering of self-propelled rods," *Phys. Rev. E*, **74**, 030904, Sep 2006.

[7] F. Peruani and M. Bär, "A kinetic model and scaling properties of non-equilibrium clustering of self-propelled particles," *New Journal of Physics*, **15**, (6), 065009, 2013.

[8] I. Theurkauff, C. Cottin-Bizonne, J. Palacci, C. Ybert, and L. Bocquet, "Dynamic clustering in active colloidal suspensions with chemical signaling," *Phys. Rev. Lett.*, **108**, 268303, Jun 2012.

[9] J. Palacci, S. Sacanna, A. P. Steinberg, D. J. Pine, and P. M. Chaikin, "Living crystals of light-activated colloidal surfers," *Science*, **339**, (6122), 936–940, 2013.

[10] S. Thutupalli, R. Seemann, and S. Herminghaus, "Swarming behavior of simple model squirmers," *New Journal of Physics*, **13**, (7), 073021, 2011.

[11] A. P. Petroff, X.-L. Wu, and A. Libchaber, "Fast-moving bacteria self-organize into active two-dimensional crystals of rotating cells," *Phys. Rev. Lett.*, **114**, 158102, Apr 2015.

[12] Y. Fily and M. C. Marchetti, "Athermal phase separation of self-propelled particles with no alignment," *Phys. Rev. Lett.*, **108**, 235702, Jun 2012.

[13] G. S. Redner, M. F. Hagan, and A. Baskaran, "Structure and dynamics of a phase-separating active colloidal fluid," *Phys. Rev. Lett.*, **110**, 055701, Jan 2013.

[14] A. Wysocki, R. G. Winkler, and G. Gompper, "Cooperative motion of active brownian spheres in three-dimensional dense suspensions," *EPL (Europhysics Letters)*, **105**, (4), 48004, 2014.

[15] M. E. Cates and J. Tailleur, "Motility-induced phase separation," *Annual Review of Condensed Matter Physics*, **6**, (1), 219–244, 2015.

[16] J. Stenhammar, A. Tiribocchi, R. J. Allen, D. Marenduzzo, and M. E. Cates, "Continuum theory of phase separation kinetics for active brownian particles," *Phys. Rev. Lett.*, **111**, 145702, Oct 2013.

[17] T. Speck, J. Bialké, A. M. Menzel, and H. Löwen, "Effective cahn-hilliard equation for the phase separation of active brownian particles," *Phys. Rev. Lett.*, **112**, 218304, May 2014.

[18] S. C. Takatori, W. Yan, and J. F. Brady, "Swim pressure: Stress generation in active matter," *Phys. Rev. Lett.*, **113**, 028103, Jul 2014.

[19] S. C. Takatori and J. F. Brady, "Towards a thermodynamics of active matter," *Phys. Rev. E*, **91**, 032117, Mar 2015.

[20] A. P. Solon, J. Stenhammar, R. Wittkowski, M. Kardar, Y. Kafri, M. E. Cates, and J. Tailleur, "Pressure and phase equilibria in interacting active brownian spheres," *Phys. Rev. Lett.*, **114**, 198301, May 2015.

[21] R. G. Winkler, A. Wysocki, and G. Gompper, "Virial pressure in systems of spherical active brownian particles," *Soft Matter*, **11**, 6680–6691, 2015.

[22] A. P. Solon, Y. Fily, A. Baskaran, M. E. Cates, Y. Kafri, M. Kardar, and J. Tailleur, "Pressure is not a state function for generic active fluids," *Nat Phys*, **11**, (8), 673–678, Aug 2015.

[23] A. Tiribocchi, R. Wittkowski, D. Marenduzzo, and M. E. Cates, "Active Model H: Scalar Active Matter in a Momentum-Conserving Fluid," *ArXiv e-prints*, Apr. 2015.

[24] R. Matas-Navarro, R. Golestanian, T. B. Liverpool, and S. M. Fielding, "Hydrodynamic suppression of phase separation in active suspensions," *Phys. Rev. E*, **90**, 032304, Sep 2014.

[25] A. Zöttl and H. Stark, "Hydrodynamics determines collective motion and phase behavior of active colloids in quasi-two-dimensional confinement," *Phys. Rev. Lett.*, **112**, 118101, Mar 2014.

[26] T. Ishikawa and T. J. Pedley, "Coherent structures in monolayers of swimming particles," *Phys. Rev. Lett.*, **100**, 088103, Feb 2008.

[27] I. Llopis and I. Pagonabarraga, "Dynamic regimes of hydrodynamically coupled self-propelling particles," *EPL (Europhysics Letters)*, **75**, (6), 999, 2006.

[28] T. Ishikawa and T. J. Pedley, "Diffusion of swimming model micro-organisms in a semi-dilute suspension," *Journal of Fluid Mechanics*, **588**, 437–462, 10 2007.

[29] T. Ishikawa and T. J. Pedley, "Dispersion of model microorganisms swimming in a nonuniform suspension," *Phys. Rev. E*, **90**, 033008, Sep 2014.

[30] T. Ishikawa, J. T. Locsei, and T. J. Pedley, "Development of coherent structures in concentrated suspensions of swimming model micro-organisms," *Journal of Fluid Mechanics*, **615**, 401–431, Nov 2008.

[31] A. A. Evans, T. Ishikawa, T. Yamaguchi, and E. Lauga, "Orientational order in concentrated suspensions of spherical microswimmers," *Physics of Fluids*, **23**, (11), 111702, 2011.

[32] J. J. Molina, Y. Nakayama, and R. Yamamoto, "Hydrodynamic interactions of self-propelled swimmers," *Soft Matter*, **9**, 4923–4936, 2013.

[33] N. Oyama, J. Jairo Molina, and R. Yamamoto, "Purely hydrodynamic origin for swarming of swimming particles," *ArXiv e-prints*, Apr. 2015.

[34] F. Alarcón and I. Pagonabarraga, "Spontaneous aggregation and global polar ordering in squirmer suspensions," *Journal of Molecular Liquids*, **185**, 56 – 61, 2013.

[35] M. J. Lighthill, "On the squirming motion of nearly spherical deformable bodies through liquids at very small reynolds numbers," *Communications on Pure and Applied Mathematics*, **5**, (2), 109–118, 1952.

[36] J. R. Blake, "A spherical envelope approach to ciliary propulsion," *Journal of Fluid Mechanics*, **46**, 199–208, 3 1971.

[37] T. Ishikawa, "Suspension biomechanics of swimming microbes," *Journal of The Royal Society Interface*, **6**, (39), 815–834, 2009.

[38] J. R. Howse, R. A. L. Jones, A. J. Ryan, T. Gough, R. Vafabakhsh, and R. Golestanian, "Self-motile colloidal particles: From directed propulsion to random walk," *Phys. Rev. Lett.*, **99**, 048102, Jul 2007.

[39] S. Thutupalli, R. Seemann, and S. Herminghaus, "Swarming behavior of simple model squirmers," *New Journal of Physics*, **13**, (7), 073021, 2011.

[40] L. Zhu, E. Lauga, and L. Brandt, "Self-propulsion in viscoelastic fluids: Pushers vs. pullers," *Physics of Fluids*, **24**, (5), 2012.

[41] L. J. Fauci and R. Dillon, "Biofluidmechanics of reproduction," *Annual Review of Fluid Mechanics*, **38**, (1), 371–394, 2006.

[42] T. J. Pedley, , and J. O. Kessler, "Hydrodynamic phenomena in suspensions of swimming microorganisms," *Annual Review of Fluid Mechanics*, **24**, (1), 313–358, 1992.

[43] N. A. Hill and T. J. Pedley, "Bioconvection," *Fluid Dynamics Research*, **37**, (1-2), 1, 2005.

[44] J. W. Costerton, K. J. Cheng, G. G. Geesey, T. I. Ladd, J. C. Nickel, M. Dasgupta, , and T. J. Marrie, "Bacterial biofilms in nature and disease," *Annual Review of Microbiology*, **41**, (1), 435–464, 1987.

[45] A. Hamel, C. Fisch, L. Combettes, P. Dupuis-Williams, and C. N. Baroud, "Transitions between three swimming gaits in paramecium escape," *Proceedings of the National Academy of Sciences*, **108**, (18), 7290–7295, 2011.

[46] E. M. Purcell, "Life at low Reynolds number," *American Journal of Physics*, **45**, (1), 3–11, Jan. 1977.

[47] J. R. Blake and M. A. Sleigh, "Mechanics of ciliary locomotion," *Biological Reviews*, **49**, (1), 85–125, 1974.

[48] T. Ishikawa, M. P. Simmonds, and T. J. Pedley, "Hydrodynamic interaction of two swimming model micro-organisms," *Journal of Fluid Mechanics*, **568**, 119–160, 12 2006.

[49] I. Pagonabarraga and I. Llopis, "The structure and rheology of sheared model swimmer suspensions," *Soft Matter*, **9**, 7174–7184, 2013.

[50] E. Lauga and T. R. Powers, "The hydrodynamics of swimming microorganisms," *Reports on Progress in Physics*, **72**, (9), 096601, 2009.

[51] O. Pak and E. Lauga, "Generalized squirming motion of a sphere," *Journal of Engineering Mathematics*, **88**, (1), 1–28, 2014.

[52] S. Succi, *The Lattice Boltzmann Equation for Fluid Dynamics and Beyond*. New York: Clarendon Press, 2001.

[53] D. L. Ermak and J. A. McCammon, "Brownian dynamics with hydrodynamic interactions," *The Journal of Chemical Physics*, **69**, (4), 1978.

[54] P. J. Hoogerbrugge and J. M. V. A. Koelman, "Simulating microscopic hydrodynamic phenomena with dissipative particle dynamics," *EPL (Europhysics Letters)*, **19**, 155, Jun. 1992.

[55] R. D. Groot and P. B. Warren, "Dissipative particle dynamics: Bridging the gap between atomistic and mesoscopic simulation," *The Journal of Chemical Physics*, **107**, (11), 1997.

[56] P. Espanol and P. Warren, "Statistical mechanics of dissipative particle dynamics," *EPL (Europhysics Letters)*, **30**, (4), 191, 1995.

[57] S. Chen and G. D. Doolen, "Lattice Boltzmann Method for fluid flows," *Annu. Rev. Fluid Mech.*, **30**, (1), 329–364, 1998.

[58] D. A. Wolf-Gladrow, *Lattice-gas cellular automata and lattice Boltzmann models an introduction*, 1st ed. Springer, Mar. 2000.

[59] J. Hardy, Y. Pomeau, and O. de Pazzis, "Time evolution of a two-dimensional model system. I. Invariant states and time correlation functions," *Journal of Mathematical Physics*, **14**, 1746–1759, Dec. 1973.

[60] U. Frisch, B. Hasslacher, and Y. Pomeau, "Lattice-gas automata for the navier-stokes equation," *Phys. Rev. Lett.*, **56**, 1505–1508, Apr 1986.

[61] G. R. McNamara and G. Zanetti, "Use of the boltzmann equation to simulate lattice-gas automata," *Phys. Rev. Lett.*, **61**, 2332–2335, Nov 1988.

[62] J. D. Sterling and S. Chen, "Stability analysis of lattice boltzmann methods," *Journal of Computational Physics*, **123**, (1), 196 – 206, 1996.

[63] W. G. Vincenti and J. C. H. Kruger, *Introduction to Physical Gas Dynamics*. John Wiley and Sons,, 1965.

[64] F. J. Higuera, S. Succi, and R. Benzi, "Lattice gas dynamics with enhanced collisions," *EPL (Europhysics Letters)*, **9**, (4), 345, 1989.

[65] R. Benzi, S. Succi, and M. Vergassola, "The lattice boltzmann equation: theory and applications," *Physics Reports*, **222**, (3), 145 – 197, 1992.

[66] M. E. Cates, K. Stratford, R. Adhikari, P. Stansell, J.-C. Desplat, I. Pagonabarraga, and A. J. Wagner, "Simulating colloid hydrodynamics with lattice boltzmann methods," *Journal of Physics: Condensed Matter*, **16**, (38), S3903, 2004.

[67] Y. H. Qian, D. d'Humières, and P. Lallemand, "Lattice bgk models for navier-stokes equation," *EPL (Europhysics Letters)*, **17**, (6), 479, 1992.

[68] H. Chen, S. Chen, and W. H. Matthaeus, "Recovery of the navier-stokes equations using a lattice-gas boltzmann method," *Phys. Rev. A*, **45**, R5339–R5342, Apr 1992.

[69] M. C. Sukop and D. T. Thorne, *Lattice Boltzmann Modeling: An Introduction for Geoscientists and Engineers*, 1st ed. Springer, Jan. 2007.

[70] B. H. P. L. Y. P. U. Frisch, D. d'Humières and J.-P. Rivet, "Lattice gas hydrodynamics in two and three dimensions," *Complex Systems*, **1**, 649, 1987.

[71] M. C. Sukop and D. Or, "Lattice boltzmann method for modeling liquid-vapor interface configurations in porous media," *Water Resources Research*, **40**, (1), 2004.

[72] A. J. C. Ladd, "Numerical simulations of particulate suspensions via a discretized boltzmann equation. part 1. theoretical foundation," *Journal of Fluid Mechanics*, **271**, 285–309, 7 1994.

[73] C. P. Lowe, D. Frenkel, and A. J. Masters, "Long-time tails in angular momentum correlations," *The Journal of Chemical Physics*, **103**, (4), 1995.

[74] N.-Q. Nguyen and A. J. C. Ladd, "Lubrication corrections for lattice-boltzmann simulations of particle suspensions," *Phys. Rev. E*, **66**, 046708, Oct 2002.

[75] R. Matas-Navarro, "Hydrodynamic effects in externally and internally driven particle suspensions: fluctuation-induced forces, active settling and bacterial patterns." Doctoral Thesis, University of Barcelona, 2012.

[76] J.-C. Desplat, I. Pagonabarraga, and P. Bladon, "LUDWIG: A parallel Lattice-Boltzmann code for complex fluids," *Computer Physics Communications*, **134**, (3), 273–290, Mar. 2001.

[77] K. Stratford and I. Pagonabarraga, "Parallel simulation of particle suspensions with the lattice boltzmann method," *Computers & Mathematics with Applications*, **55**, (7), 1585 – 1593, 2008.

[78] V. M. Kendon, M. E. Cates, I. Pagonabarraga, J.-C. Desplat, and P. Bladon, "Inertial effects in three-dimensional spinodal decomposition of a symmetric binary fluid mixture: a lattice boltzmann study," *Journal of Fluid Mechanics*, **440**, 147–203, 8 2001.

[79] K. Stratford, R. Adhikari, I. Pagonabarraga, J.-C. Desplat, and M. E. Cates, "Colloidal jamming at interfaces: A route to fluid-bicontinuous gels," *Science*, **309**, (5744), 2198–2201, 2005.

[80] R. Ledesma-Aguilar, A. HernÃ¡ndez-Machado, and I. Pagonabarraga, "Three-dimensional aspects of fluid flows in channels. i. meniscus and thin film regimes," *Physics of Fluids*, **19**, (10), 2007.

[81] B. Delmotte, E. E. Keaveny, F. PlourabouÃ©, and E. Climent, "Large-scale simulation of steady and time-dependent active suspensions with the force-coupling method," *Journal of Computational Physics*, **302**, 524 – 547, 2015.

[82] R. Eppenga and D. Frenkel, "Monte carlo study of the isotropic and nematic phases of infinitely thin hard platelets," *Molecular Physics*, **52**, (6), 1303–1334, 1984.

[83] H. P. Zhang, A. Be'er, E.-L. Florin, and H. L. Swinney, "Collective motion and density fluctuations in bacterial colonies," *Proceedings of the National Academy of Sciences*, **107**, (31), 13 626–13 630, 2010.

[84] Y. Fily, S. Henkes, and M. C. Marchetti, "Freezing and phase separation of self-propelled disks," *Soft Matter*, **10**, 2132–2140, 2014.

[85] S. Ramaswamy, R. A. Simha, and J. Toner, "Active nematics on a substrate: Giant number fluctuations and long-time tails," *EPL (Europhysics Letters)*, **62**, (2), 196, 2003.

[86] H. Chaté, F. Ginelli, G. Grégoire, and F. Raynaud, "Collective motion of self-propelled particles interacting without cohesion," *Phys. Rev. E*, **77**, 046113, Apr 2008.

[87] C. Valeriani, E. Sanz, P. N. Pusey, W. C. K. Poon, M. E. Cates, and E. Zaccarelli, "From compact to fractal crystalline clusters in concentrated systems of monodisperse hard spheres," *Soft Matter*, **8**, 4960–4970, 2012.

[88] V. Narayan, S. Ramaswamy, and N. Menon, "Long-lived giant number fluctuations in a swarming granular nematic," *Science*, **317**, (5834), 105–108, 2007.

[89] J. Deseigne, O. Dauchot, and H. Chaté, "Collective motion of vibrated polar disks," *Phys. Rev. Lett.*, **105**, 098001, Aug 2010.

[90] H. H. Wensink and H. Löwen, "Emergent states in dense systems of active rods: from swarming to turbulence," *Journal of Physics: Condensed Matter*, **24**, (46), 464130, 2012.

[91] F. Schweitzer and L. Schimansky-Geier, "Clustering of "active" walkers in a two-component system," *Physica A: Statistical Mechanics and its Applications*, **206**, (3-4), 359 – 379, 1994.

[92] M. E. Cates, D. Marenduzzo, I. Pagonabarraga, and J. Tailleur, "Arrested phase separation in reproducing bacteria creates a generic route to pattern formation," *Proceedings of the National Academy of Sciences*, **107**, (26), 11 715–11 720, 2010.

[93] S. R. McCandlish, A. Baskaran, and M. F. Hagan, "Spontaneous segregation of self-propelled particles with different motilities," *Soft Matter*, **8**, 2527–2534, 2012.

[94] F. D. C. Farrell, M. C. Marchetti, D. Marenduzzo, and J. Tailleur, "Pattern formation in self-propelled particles with density-dependent motility," *Phys. Rev. Lett.*, **108**, 248101, Jun 2012.

[95] G. S. Redner, A. Baskaran, and M. F. Hagan, "Reentrant phase behavior in active colloids with attraction," *Phys. Rev. E*, **88**, 012305, Jul 2013.

[96] I. Buttinoni, J. Bialké, F. Kümmel, H. Löwen, C. Bechinger, and T. Speck, "Dynamical clustering and phase separation in suspensions of self-propelled colloidal particles," *Phys. Rev. Lett.*, **110**, 238301, Jun 2013.

[97] M. E. Cates and J. Tailleur, "When are active brownian particles and run-and-tumble particles equivalent? consequences for motility-induced phase separation," *EPL (Europhysics Letters)*, **101**, (2), 20010, 2013.

[98] J. Tailleur and M. E. Cates, "Statistical mechanics of interacting run-and-tumble bacteria," *Phys. Rev. Lett.*, **100**, 218103, May 2008.

[99] J. Schwarz-Linek, C. Valeriani, A. Cacciuto, M. E. Cates, D. Marenduzzo, A. N. Morozov, and W. C. K. Poon, "Phase separation and rotor self-assembly in active particle suspensions," *Proceedings of the National Academy of Sciences*, **109**, (11), 4052–4057, 2012.

[100] B. M. Mognetti, A. Šarić, S. Angioletti-Uberti, A. Cacciuto, C. Valeriani, and D. Frenkel, "Living clusters and crystals from low-density suspensions of active colloids," *Phys. Rev. Lett.*, **111**, 245702, Dec 2013.

[101] V. Prymidis, H. Sielcken, and L. Filion, "Self-assembly of active attractive spheres," *Soft Matter*, **11**, 4158–4166, 2015.

[102] R. M. Navarro and S. M. Fielding, "Clustering and phase behaviour of attractive active particles with hydrodynamics," *Soft Matter*, **11**, 7525–7546, 2015.

[103] A. Baskaran and M. C. Marchetti, "Statistical mechanics and hydrodynamics of bacterial suspensions," *Proceedings of the National Academy of Sciences*, **106**, (37), 15 567–15 572, 2009.

[104] R. M. Navarro, personal communication, April 2013.

[105] D. Levis and L. Berthier, "Clustering and heterogeneous dynamics in a kinetic monte carlo model of self-propelled hard disks," *Phys. Rev. E*, **89**, 062301, Jun 2014.

[106] A. A. D. Stauffer, *Introduction to Percolation Theory*, 2nd ed. UK: Taylor & Francis,, 1991.

[107] F. Alarcón and I. Pagonabarraga, "Macroscopic clusters and super-diffusion in 3d microswimmer suspensions, using large-scale simulations." In preparation, 2015.

[108] A. Dominguez, personal communication, 2014.

[109] J. Bleibel, A. Dominguez, F. Gunther, J. Harting, and M. Oettel, "Hydrodynamic interactions induce anomalous diffusion under partial confinement," *Soft Matter*, **10**, 2945–2948, 2014.

[110] M. P. Allen and D. J. Tildesley, *Computer Simulation of Liquids (Oxford Science Publications)*, reprint ed., ser. Oxford science publications. Oxford University Press, Jun. 1989.

[111] T. Vicsek, A. Czirók, E. Ben-Jacob, I. Cohen, and O. Shochet, "Novel type of phase transition in a system of self-driven particles," *Phys. Rev. Lett.*, **75**, 1226–1229, Aug 1995.

[112] F. Ginot, I. Theurkauff, D. Levis, C. Ybert, L. Bocquet, L. Berthier, and C. Cottin-Bizonne, "Nonequilibrium equation of state in suspensions of active colloids," *Phys. Rev. X*, **5**, 011004, Jan 2015.

[113] K. R. Symon, *Mechanics*, 2nd ed. Reading, Massachusetts: Addison-Wesley, 1960.

[114] W. H. Press, S. A. Teukolsky, W. T. Vetterling, and B. P. Flannery, *Numerical Recipes in C: The Art of Scientific Computing*, 3rd ed. Cambridge: Cambridge University Press, 2007.